Quantum phases and particle correlations in a honeycomb lattice

D i s s e r t a t i o n

zur Erlangung des Doktorgrades
am Fachbereich Physik der Universität Hamburg

vorgelegt von

Dipl.-Phys. Eva-Maria Richter
aus Mechernich

Hamburg
2015

Abstract

In this thesis, one- and two-component ultracold bosonic quantum gases in honey-comb optical lattices are examined. For simulations, the Bose-Hubbard model is used in concert with an exact diagonalization method, to get access to correlations, wavefunctions and energies of the discrete system.

Ultracold Bosons in two different hyperfine states, generated in an optical lattice open the possibility to investigate short ranged two-particle correlations in the Mott insulator phase. These correlations can be interpreted as next neighbor z-correlations of iso-spins, associated with the different particle sorts. A manifold phase diagram is analyzed, which shows both anti ferromagnetic and ferromagnetic correlations. In the anti-ferromagnetic regime the groundstate of the system never assumes a Néel state, which is in agreement with theoretical predictions. In the ferromagnetic Mott insulator regime, for increasing cell sizes, increasing domains can be identified, which allows for increasing ferromagnetic correlations. In the superfluid regime we can investigate two special phases, depending on the ratio of interaction between same and different kind of atoms. In the limit of small interactions between different kind of particles the iso spins build up superpositions on one lattice site to find a state where the on-site square of the in-plane (xy) component reaches maximum. For increasing interactions this superposition is transferred to a super-counter-fluid (SCF) phase. In the opposite limit of small interactions between the same kind of particles, I identify a supersolid order. In this phase, the system can be described by a nontrivial density-modulation. The corresponding superlattice is four times bigger than the primary unit cell and includes simultaneous solid and superfluid qualities, i.e. it is a supersolid. To suggest an experimental method to detect the supersolid phase, the lattice symmetry is broken by a spin-dependent lattice. This way a supersolid signal in the population imbalance from site to site is identified. The important features of the phase diagram are reproduced also for increasing cell sizes. This confirms that our small size systems develop strong fingerprints of the physics emerging in macroscopic systems.

Zusammenfassung

In der vorliegenden Arbeit werden ein- und zweikomponentige ultrakalte bosonische Gase in einem hexagonalen optischen Gitter untersucht. Das Hubbard Modell wurde verwendet, um Korrelationen, Wellenfunktionen und Energien im diskreten System mit exakten Methoden zu berechnen. Wird das System mit Bosonen unterschiedlicher Hyperfeinzustände geladen, treten kurzreichweitige Korrelationen im Mottisolatorzustand auf. Diese lassen sich interpretieren als Korrelationen der z-Komponenten des Isospins der unterschiedlichen Teilchensorten. Es zeigt sich ein vielfältiges Phasendiagramm mit anti-ferromagnetischen oder ferromagnetischen z-Korrelationen. Der Grundzustand im anti-ferromagnetischen Mottisolator-Regime nimmt, in Übereinstimmung mit der Theorie, für keine Systemgröße den Néelzustand ein. Im ferromagnetischen Mottisolatorzustand ist zu größeren Zellen hin eine klare Domänenstruktur erkennbar, die in zunehmenden Maße ferromagnetische Korrelationen liefert.

Im superfluiden Zustand bilden sich in Abhängigkeit der Wechselwirkungsparametern zwischen gleichen und unterschiedlichen Bosonen zwei besondere Phasen aus. Im antiferromagnetischen superfluiden Regime liegt im Grenzfall verschwindend kleiner Wechselwirkung zwischen verschiedenen Teilchen eine Überlagerung der Isospins an einem Gitterplatz vor. In dieser Phase ist das Quadrat der planaren Am-Platz-Komponente des Isospins maximal, diese Überlagerung geht für wachsende Wechselwirkung in einen superfluid counterflow (SCF-Phase) über. Im anderen Grenzfall können wir ein Supersolid identifizieren. In dieser Phase kann das System durch eine nichttriviale Dichtemodulation beschrieben werden. Diese Art von Übergitter hat eine vierfach größere Einheitszelle als das ursprüngliche Gitter und vereint somit superfluide sowie feste Eigenschaften zugleich, ein Supersolid. Ein spezielles spinabhängiges optisches Gitter bricht die Symmetrie für eine Teilchensorte. Dies hat im Falle des supersoliden Zustandes für beide Teilchensorten ein Besetzungsungleichgewicht benachbarter Gitterplätze zur Folge. Experimentell lässt sich dies als Supersolid-Signal verwenden. Die Korrelationen bestätigen sich für zunehmende Systemgrößen, dies ist ein deutliches Anzeichen dafür, dass unsere Ergebnisse ebenso für makroskopische Systeme qualitativ gültig sind.

Publikationen

Im Rahmen der vorliegenden Arbeit ist die folgende wissenschaftliche Veröffentlichung entstanden.

[63] M.Prada* und E.-M.Richter* and D. Pfannkuche, *Isospin Correlations in two-partite Hexagonal Optical Lattices*,Phys. Rev. A 90, 013613 (2014)

* M. Prada and E.-M. Richter contributed equally to this work.

Contents

Chapter 1

Introduction

Since the experimental realization of Bose-Einstein condensates (BEC) in 1995 [3, 19], the investigation of BEC has become a fascinating field of research. This quantum phase has been theoretical predicted in 1925 by A. Einstein and S. Bose [12, 23]. The macroscopic wavefunction of a BEC, its superfluid behaviour, and the possibility to observe a special quantum state provides a connection between the quantum system and our macroscopic world. In case of a big and homogeneous system, this quantum state is well described by an effective single particle wavefunction. By considering the interaction between particles the Gross Pitaevskii Equation, a nonlinear Schrödinger equation [32, 60] is derived. Today, the theoretical and experimental investigations concerning Bose-Einstein condensates have become manifold. One important field of research related to BEC is the investigation of Bose condensed atoms in an optical lattice. An optical lattice is generated by counter propagating laser beams, which interferences build a *crystal of light*. The tunneling strength, which depends on the lattice depth, can be controlled by the laser intensity and the particle interaction can be controlled by using Feshbach resonances [17, 40]. Thereby the most important system parameters can be tuned very well. For an increasing lattice depth, the system performs a quantum phase transition from the superfluid to the Mott insulator phase. For a deep optical lattice the description of the system by an collective particle wavefunction is not valid any more, the strong correlated regime is entered. Whereas ultracold atoms in an optical lattice are well described by the Bose-Hubbard-Modell [26, 41] in every regime, in the superfluid as well as in the Mott insulator phase. The first experimental realization of superfluid to Mott insulator phase transition in an optical lattice in 2002 [30] opened an interesting field of research with various applications in different areas of science. By arranging laser beams in a special geometric order, different lattice symmetries can be realized [42, 46, 59, 67, 73], even spin-dependent lattices can be generated by using polarized laser beams [71]. By loading multicomponent Bose gases [2, 36, 39], Fermi gases [24, 29, 43] or even Bose-Fermi mixtures [35, 56, 75], manifold quantum phases and extraordinary phenomena have been explored. This all opens many new opportunities to inves-

tigate the quantum behavior of many body systems in condensed matter physics under ideal circumstances [4, 9, 10, 53]. Particularly with regard to the question of magnetic ordering [15, 68], ultracold quantum gases represent a high grade model system for strongly interacting many body systems. The investigation of iso magnetic ordering of a two component quantum gas in an optical lattice will be one of the main focuses of this work in the regime of strong interactions. The second main focus is the investigation of a striking supersolid and a supercounterfluid phase in the superfluid regime.

In this thesis, an extended phasediagram of a two component gas in a honeycomb optical lattices is explored. Until now approximative methods are used mostly in theoretical studies to investigate whether the Mott insulator regime [22, 36, 37, 48] or the superfluid regime [62]. In contrast, in this work one single method was employed to generate a full phase diagram, the exact diagonalization method. This opens the possibility to compute many particles correlationfunctions and investigate their evolution exactly from weak to strong coupling. These many body correlation functions are not accessible by using approximative methods.

In Chapter 2, the basic information about atoms in optical lattices, the Bose-Hubbard Hamiltonian for two component gases, and their corresponding iso magnetism is given.

In Chapter 3, a short overview of the algorithms used in the simulation program is given and the basic features of the system are studied in order to investigate the crossover between the superfluid and the Mott insulator state.

In Chapter 4, iso magnetic correlations in the strong coupling regime are investigated, in order to distinguish different ordered phases. By changing atomic and lattice properties, the relative strength of the interactions can be changed and the corresponding groundstate of the system can be described as 'ferromagnetic' or 'anti ferromagnetic'. Calculations have been performed for different sized unit cells in order to determine finite size effects.

In Chapter 5, the investigations of in- and out-of plane correlation functions for the n-th nearest neighbor and higher order correlations allow even to explore the superfluid regime. In this regime a conspicuous supersolid [44, 51, 57, 64, 75] and a highly entangled in-plane iso magnetic state is found, which is transferred to a super-counter-fluid phase (SCF) [37, 38, 48].

Chapter 2

Basics

In this chapter the basic background on one- and two-component Bose gases in honeycomb optical lattices are given, to support the understanding of the following work. Since we deal with bosons in laser fields, the atom-photon interaction for an multilevel atom is explained. Further, a description of periodic optical potentials is obtained, especially for the honeycomb (spindependent) lattice on which this work focuses. The atom-atom interaction is discussed and reduced to the s-wave scattering length. In the following the theoretical background for exact diagonalization is elucidated in case of the finite system, a honeycomb lattice with four, six, eight and ten sites. We derive the Bose Hubbard Hamiltonian for a two component bosonic system. An introduction of the superfluid to Mott insulator transition is given, to understand the behavior of atoms in flat lattices, which behave superfluid, and in deep lattices, where all atoms are pinned at lattice sites (Mott insulator). As the system is examined with respect to iso magnetic correlations, we will also focus on site depended pair-correlation functions. A short introduction to the supersolid phase is given, which is characterized by a superfluid order and a coexisting spacial density modulation. For experts who are experienced in this area I would advice to skip this chapter and start with the first results in chapter 3.

2.1 Atom-photon interaction

To generate a Bose-Einstein condensate, atoms are trapped and cooled by laser light. The colling requires absorption and spontaneous emission of photons [58]. This spontaneous force is connected to the imaginary part of the polarizability of the atom α. The trapping is effected by the interaction of the light induced dipole moment of the atom and the electric light field itself and it depends on the real part of the polarizability α. If ω_L is the frequency of the laser and ω_A the atomic resonance frequency, the detuning is given by $\Delta = \omega_A - \omega_L$. If the resonance frequency of the atom is bigger than the laser frequency, the induced dipole moment oscillates out of phase and the atom is pushed out of the region

with the higher laser intensity. If the resonance frequency is smaller, the induced dipole oscillates in phase with the electric field and the atom is guided in direction of higher field intensity by the dipole force. Using a spacial inhomogeneous laser field $I(r)$, atoms can be trapped in the region of highest intensity with $\Delta < 0$ which is called red detuned. In a blue detuned laser beam ($\Delta > 0$) with a spatial inhomogeneous laser beam the atoms are pressed out of the intensity maxima [7]. In the following the dressed atom approach is introduced, let me refer the reader to [31] for a more detailed discussion. In case of multi-level atoms, we have to implement a fully quantized model, also known as the dressed atom approach [13]. In the ideal case, the laser field consists of one single mode ω_L, which is coupled to the atom. This coupling is given by the dipole approximation. Although the laser field is time dependent, thus we can treat this coupling time independently using the Floquet theory [72]. This allows a time independent description of a periodically time dependent field. The Hilbert space of the atomic subsystem is given by the ground state $|g\rangle$ and the exited state $|e\rangle$, with a transition energy of $\hbar\omega_A$. The sub space of the laser field is given by the fock basis $|N\rangle$, which corresponds to N photons in the mode ω_L of the laser. With $\hat{H}_L$ being the Hamiltonian of the laser field and $\hat{H}_A$ being the Hamiltonian of the atom, the Hamiltonian of the atom and the laser field is given by $\hat{H}_A + \hat{H}_L$. Therefore the basis of the combined, noninteracting system, is given by $|g,0\rangle, |e,0\rangle, ..., |g,N\rangle, |e,N\rangle$. Without an interaction, the energy eigenvalues are given by the combination of the two eigenvalues for the laser and the atom

$$\hat{H}_A + \hat{H}_L \,|g, N+1\rangle \;=\; (N+1)\hbar\omega_L \,|g, N+1\rangle, \qquad (2.1)$$

$$\hat{H}_A + \hat{H}_L \,|e, N\rangle \;=\; N\hbar\omega_L + \hbar\omega_A \,|g, N+1\rangle. \qquad (2.2)$$

The dressed states are given by considering the atom-laser interaction in the dipole approximation. Absorption and stimulated emission are considered in this way. Denoting $\hat{p}$ the dipole moment operator and $\vec{E}(\vec{r})$ the electric field, the coupling is given by [13],[31]

$$\hat{H}_{AL} \;=\; -\hat{d}\vec{E}_L \qquad (2.3)$$

$$\text{stimulated emission}: \qquad \hat{H}_{AL}\,|e, N\rangle \;=\; \frac{\hbar}{2}\Omega_{ge}e^{i\phi}\,|g, N+1\rangle \qquad (2.4)$$

$$\text{absorption}: \qquad \hat{H}_{AL}\,|g, N+1\rangle \;=\; \frac{\hbar}{2}\Omega_{ge}e^{-i\phi}\,|e, N\rangle \qquad (2.5)$$

$$\text{with}: \qquad \Omega_{ge} \;=\; \frac{\vec{E}(\vec{r})}{\hbar}\left\langle g|\hat{d}|e\right\rangle \qquad (2.6)$$

Ω_{ge} is the Rabi frequency which gives the strength of the coupling between $|g\rangle$ and $|e\rangle$. The coupling strength is huge if the detuning between laser and atom $\Delta = \omega_A - \omega_L$ is small. Neglecting the energy non conserving matrix elements, the corresponding Hamiltonian is given by

$$H = \begin{pmatrix} \ldots & 0 & 0 & 0 \\ 0 & \hbar\omega_A + N\hbar\omega_L & \frac{\hbar}{2}\Omega_{ge}e^{i\phi} & 0 \\ 0 & \frac{\hbar}{2}\Omega_{ge}e^{-i\phi} & (N+1)\hbar\omega_L & 0 \\ 0 & 0 & 0 & \ldots \end{pmatrix}. \tag{2.7}$$

Therefore, the eigenvalues of the coupled system are given by

$$E(N) = N\hbar\omega_L + \frac{\hbar}{2}(\omega_A + \omega L) \pm \frac{\hbar\sqrt{\Delta^2 + \Omega_{ge}^2}}{2}. \tag{2.8}$$

The new eigenstates of the coupled system are superpositions of the unperturbed states

$$|1, N\rangle = sin\theta\, |g, N+1\rangle + cos\theta\, |e, N\rangle \tag{2.9}$$

$$|2, N\rangle = cos\theta\, |g, N+1\rangle - sin\theta\, |e, N\rangle. \tag{2.10}$$

The angle θ is defined as $\tan 2\theta = -\Omega_{ge}/\Delta$ with $0 \leq 2\theta \leq \pi$. Fig. 2.1 shows the
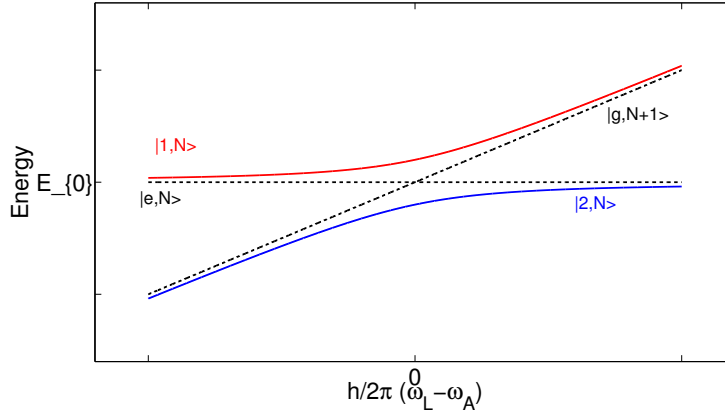
Figure 2.1: The energies of the unperturbed states and the new coupled states. The dashed lines show the energies of the unperturbed states $|g, N+1\rangle$ and $|e, N\rangle$, the solid lines present the energy of the dressed states.

energy levels of the dressed states in dependence of $\hbar\omega_L$. The dashed lines show the energies of the unperturbed states $|g, N+1\rangle$ and $|e, N\rangle$ and the solid lines present the energy of the dressed states. Far from the resonance, an asymptotic behavior can be observed, i.e. the eigenstates of the coupled system change into the unperturbed eigenstates because the coupling is very small, $\Delta^2 \gg \Omega_{ge}^2$. For resonant coupling ($\omega_L = \omega_A$) the eigenstates are superpositions and they are separated by an energy difference of $\hbar\omega_{ge}$. As the Rabi frequency is a function of the electric field $E(\vec{r})$ the energy eigenvalues lead to a spatially varying potential for

an atom at position $\vec{r}$. In case of large detuning the potential can be approximated in a tailor series

$$E(N) = \frac{\hbar}{2}\left(\omega_A + \omega_L + 2N\omega_L \pm |\Delta|\right) \pm \frac{\hbar\Omega_{ge}^2}{2\Delta}. \tag{2.11}$$

Neglecting the constant terms and focusing to red detuning we obtain

$$V(\vec{r}) = -\frac{\hbar\Omega_{ge}^2}{2\Delta} = -\frac{\vec{E}^2(\vec{r})}{2\Delta\hbar}|\left\langle g|\hat{d}|e\right\rangle|^2. \tag{2.12}$$

The potential therefore depends quadratically on the electric field and the dipole matrix element.

2.2 Periodic optical Potentials

As real atoms are presented by a multi level system, the dipole matrix element in (2.12) can be derived by the Wigner-Eckart-Theorem

$$\left\langle j|\vec{d}\hat{e}|i\right\rangle = c_{ij}||d||. \tag{2.13}$$

Summing up the contributions of all coupled exited states by considering the corresponding coupling strengths c_{ij} and detuning Δ_{ij}, the energy shift of an electronic ground state is given by

$$\Delta E_i = \frac{3\pi c^2\Gamma}{2\omega_0^3}I \times \sum_j \frac{c_{ij}}{\Delta_{ij}}, \tag{2.14}$$

which also gives the dipole potential. In case of Rb_{87} respectively for alkali atoms with nuclear spin $I = \frac{3}{2}$, only the D-line doublet has to be considered $^2S_{1/2} \rightarrow$ $^2P_{3/2}, ^2P_{1/2}$. The quantum numbers $m_F = -1, 0, 1$ are the hyperfine levels and $\mathcal{P}$ denotes the laser polarization π, σ^+, σ^-. As the detuning is huge compared to the hyperfine splitting of the exited states, equation (2.14) can be reduced to

$$U_{dip}(\vec{r}) = \frac{\pi c^2\Gamma}{2\omega_0^3}\left(\frac{2 + \mathcal{P}g_F m_F}{\Delta_{2,F}} + \frac{1 - \mathcal{P}g_F m_F}{\Delta_{1,F}}\right)I(\vec{r}). \tag{2.15}$$

Further, if the fine-splitting of the exited states Δ'_{FS} is very small compared to the detuning $\Delta_{1,F}, \Delta_{F,2}$, the U_{dip} can, with expansion in terms of $\frac{\Delta'_{FS}}{\Delta}$ till the first order, further be reduced to

$$U_{dip}(\vec{r}) = \frac{3\pi c^2\Gamma}{2\omega_0^3}\left(1 + \frac{1}{3}\mathcal{P}g_F m_F \frac{\Delta'_{FS}}{\Delta}\right)I(\vec{r}). \tag{2.16}$$

Where Δ is the detuning to the center of the D line doublet. The zeroth order gives the well known potential of a simple two level system. The first order contains the dependence of the Polarization $\mathcal{P}$ and the m_f-hyperfine-state.

2.2.1 Hexagonal lattices potential

In the following, an optical lattice will be generated by a set of monochromatic laser beams. Our simulations focus on honeycomb lattices partially with a triangular sub lattice structure. Those lattices have a six fold rotational symmetry and give rise to multiple interesting features, which are discussed in this work. Fig. 2.2 a shows how laser beams have to be arranged to create those lattice structures. We consider an ordering where the three laser beams and their polarizations both are situated in the xy-plane (Fig. 2.2 b). The wave vectors and polarizations are chosen as

$$
\vec{k}_1 = \begin{pmatrix} 0 \\ 1 \end{pmatrix}, \qquad \vec{k}_2 = \begin{pmatrix} \frac{\sqrt{3}}{2} \\ -\frac{1}{2} \end{pmatrix}, \qquad \vec{k}_3 = \begin{pmatrix} -\frac{\sqrt{3}}{2}, \\ -\frac{1}{2} \end{pmatrix} \tag{2.17}
$$

$$
\vec{e}_1 = \begin{pmatrix} 1 \\ 0 \end{pmatrix}, \qquad \vec{e}_2 = \begin{pmatrix} -\frac{1}{2} \\ \frac{\sqrt{3}}{2} \end{pmatrix}, \qquad \vec{e}_3 = \begin{pmatrix} -\frac{1}{2}. \\ \frac{\sqrt{3}}{2} \end{pmatrix} \tag{2.18}
$$

Therefore, the electric field of this configuration is given by

$$
\vec{E} = \begin{pmatrix} e^{i(yk-\omega t)} - \frac{1}{2}e^{i((\frac{\sqrt{3}}{2}x-\frac{1}{2}y)k-\omega t)} - \frac{1}{2}e^{i((\frac{-\sqrt{3}}{2}x-\frac{1}{2}y)k-\omega t)} \\ \frac{\sqrt{3}}{2}e^{i((\frac{\sqrt{3}}{2}x-\frac{1}{2}y)k-\omega t)} - \frac{\sqrt{3}}{2}e^{i((\frac{-\sqrt{3}}{2}x-\frac{1}{2}y)k-\omega t)} \end{pmatrix}. \tag{2.19}
$$

As we pointed out in the previous section, the dipole potential obeys 2.16 in our case, with intensity

$$
\begin{aligned}
I(\vec{r}) &= 2c\epsilon_0 |\vec{E}(\vec{r},t)|^2 \\
&= |E_0|^2 2c\epsilon_0 \left(3 - \cos(\sqrt{3}kx)) - \cos(\frac{\sqrt{3}}{2}kx - \frac{3}{2}ky) - \cos(\frac{\sqrt{3}}{2}kx + \frac{3}{2}ky) \right).
\end{aligned} \tag{2.20}
$$

The polarization $\mathcal{P}$, well discussed in [20], where $\sigma\pm$ are the Jones vectors for right- and left-hand polarization. For a wave propagating in z-direction, they are given by

$$
\sigma_+ = \frac{1}{\sqrt{2}} \begin{pmatrix} 1 \\ i \end{pmatrix}, \tag{2.21}
$$

$$
\sigma_- = \frac{1}{\sqrt{2}} \begin{pmatrix} 1 \\ -i \end{pmatrix}. \tag{2.22}
$$

The Polarization is shown in (Fig.2.2b)

$$
\begin{aligned}
\mathcal{P} &= \frac{|\vec{E}\vec{\sigma}_+|^2 - |\vec{E}\vec{\sigma}_-|^2}{|\vec{E}\vec{\sigma}_+|^2 + |\vec{E}\vec{\sigma}_-|^2} \\
&= \frac{-\sqrt{3}\sin(\sqrt{3}kx) + \sqrt{3}\sin(\frac{\sqrt{3}}{2}kx - \frac{3}{2}ky) + \sqrt{3}\sin(\frac{\sqrt{3}}{2}kx - \frac{3}{2}ky)}{3 - \cos(\sqrt{3}kx) - \cos(\frac{\sqrt{3}}{2}kx - \frac{3}{2}ky) - \cos(\frac{\sqrt{3}}{2}kx + \frac{3}{2}ky)}.
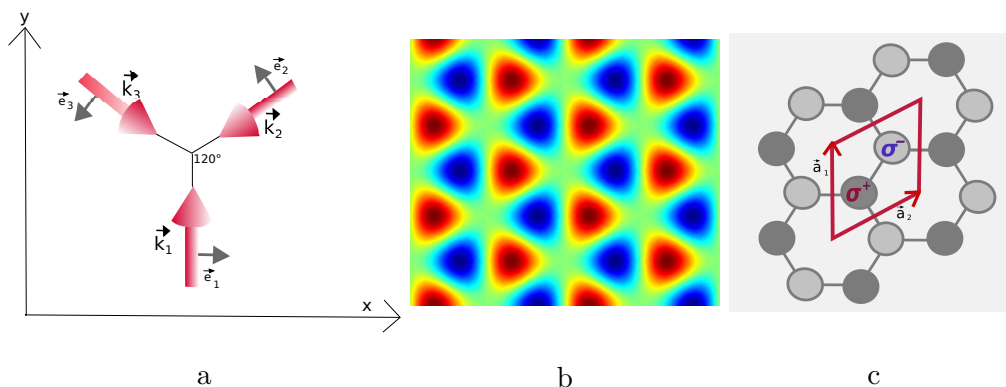\end{aligned} \tag{2.23}
$$

a

b

c

Figure 2.2: a) The laser configuration to create a spin-dependent hexagonal optical lattice b) The polarization of the laser-field with σ^+ (red) and σ^--(blue)-polarization c) The unit cell of the spin dependent honeycomb lattice

2.2.2 Spin dependent lattice potential

Using the described laser beam configuration, a spin dependent optical lattice is created and equation (2.14) gives the corresponding dipole potential for the different m_f-states. Those are shown in Fig. 2.3. The unit vectors of the honeycomb

a

b

c
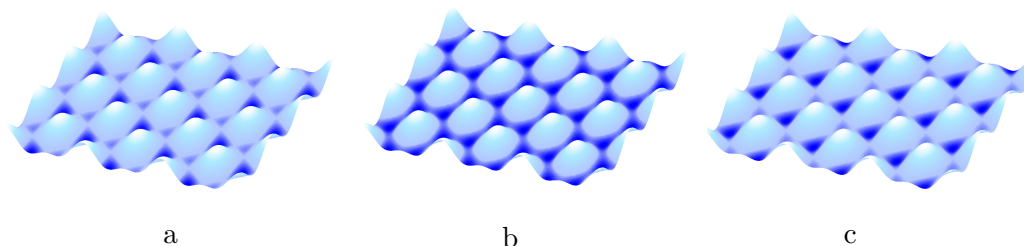
Figure 2.3: The hexagonal lattice potential for bosons in different hyperfine-states m_f a) $m_f = -1$ b) $m_f = 0$ c) $m_f = 1$.

lattice are

$$\vec{a}_1 = \frac{2}{3}\lambda_L \begin{pmatrix} 0 \\ 1 \end{pmatrix}, \qquad \vec{a}_2 = \frac{2}{3}\lambda_L \begin{pmatrix} \frac{\sqrt{3}}{2} \\ \frac{1}{2} \end{pmatrix}. \qquad (2.24)$$

The unit cell consists of a two component basis, one basis point with $\sigma+$-polarization and one with $\sigma-$-polarization, see Fig. 2.2 c. They are situated at

$$\vec{a}_{\sigma+} = \frac{1}{3}(\vec{a}_1 + \vec{a}_2) \qquad \text{and} \qquad \vec{a}_{\sigma-} = \frac{2}{3}(\vec{a}_1 + \vec{a}_2). \qquad (2.25)$$

in case of $m_f = 1$. In case of $m_f = -1$, it is the other way round. For $m_f = 0$, the polarization is zero for both basis points (see Fig. 2.3 b and a homogeneous

honeycomb lattice is created. With adding multiplies of the unitary cell, one can build up several sized supercells, like the four, six, eight and ten sited sized cell. Since my interest also focused on finite size effect, I investigated the groundstate in the superfluid and Mott insulator for different sized supercells. See Chapter 2.4.5 for a detailed discussion.

2.3   Atom-atom interaction

As the groundstate of a many particle state has to be investigated, the scattering of neutral atoms is introduced, [14]. The scattering of two particles can be described by the sum of an incoming plane wave (e.g. for the propagation direction z) and an outgoing scattered wave. The latter is spherical and depends on the angle between the propagation directions of the atoms before the scattering event. For large r the wave function is given by

$$\Psi = e^{ikz} + f(\theta)\frac{e^{ikr}}{r}, \tag{2.26}$$

where $f(\theta)$ is the scattering amplitude. The energy of the state in case of two particles with the same mass $(m_r = \frac{m}{2})$ is given by

$$E = \frac{\hbar^2 k^2}{m}. \tag{2.27}$$

While in dilute ultra-cold gases the atoms only have very low energies, in the limit for $k \to 0$ the wave function becomes

$$\Psi = 1 - \frac{a}{r} \tag{2.28}$$

[14]. The scattering amplitude a is constant and called s-wave scattering length. In the first order, (also known as Born approximation), the s-wave scattering length is given by

$$a_{born} = \frac{m}{\pi\hbar^2}U(0), \tag{2.29}$$

where U is the Fourier transform of the bare atom-atom interaction and $|\vec{k}-\vec{k'}| = 0$. In the case of low momentum $k \to 0$, U can be treated as effective two particles interaction

$$a_{born} = \frac{m}{\pi\hbar^2}\int d\vec{r}\, U_{eff}(\vec{r}), \tag{2.30}$$

$$\int d\vec{r}\, U_{eff}(\vec{r}) = \frac{4\pi\hbar^2 a}{m}. \tag{2.31}$$

In the coordinate space, as the two particle are situated at $\vec{r}$ and $\vec{r'}$, this interaction is very short ranged, which means it has the contact form, given by the δ-function;

$$U(\vec{r}, \vec{r'}) = \frac{4\pi\hbar^2 a}{m}\delta(\vec{r} - \vec{r'}). \tag{2.32}$$

In case of low energies, this effective interaction provides good results and describes the properties at the relevant densities sufficiently well, although the true inter-atomic potential has a much more complicated structure.

2.4 Hamiltonian for multicomponent bosonic system

In this section, the Bose-Hubbard Hamiltonian for a two-component bosonic system, is derived. First, i will consider the many particle formalism in case of one and two particle operators. Subsequently in case of an optical lattice the Hamiltonian can be written as a Bose-Hubbard Hamiltonian, where the behavior of the system is described in terms of inter-site tunneling of particles and the interaction of particles at one site. I briefly introduce the reader to the exact diagonalization method, the finite lattice structure of my system and its consequences for product states and matrix elements of the Bose-Hubbard Hamiltonian.

2.4.1 Many particle formalism

In a quantum system of n particles a state is characterized by an n-tuple of occupied states

$$A = (\alpha_1, \alpha_2, ..., \alpha_n). \tag{2.33}$$

Considering the indistinguishability of the particles, all permutations must be contained in the wave function; for bosons fully symmetric and for fermions anti-symmetric

$$\psi^B_{(\alpha_1,...,\alpha_n)}(x_1, ..., x_n) = \frac{1}{\sqrt{N!}} \sum_P \phi_{\alpha_{p1}}(x_1)...\phi_{\alpha_{pn}}(x_n) \tag{2.34}$$

$$\psi^F_{(\alpha_1,...,\alpha_n)}(x_1, ..., x_n) = \frac{1}{\sqrt{N!}} \sum_P (-1)^P \phi_{\alpha_{p1}}(x_1)...\phi_{\alpha_{pn}}(x_n). \tag{2.35}$$

In the particle number representation, a state with n particles in state α is represented by

$$|n_1, n_2, ..., n_n\rangle. \tag{2.36}$$

The creation operator $a^\dagger_\alpha$ increases the particle number in state α by one particle

$$a^\dagger_\alpha |n_1, n_2, ..., n_\alpha, ..., n_n\rangle = \sqrt{n_\alpha + 1} |n_1, n_2, ..., n_\alpha + 1, ..., n_n\rangle \tag{2.37}$$

correspondingly, the anhillation operator a_α decreases the particle number in state α by one particle

$$a_\alpha |n_1, n_2, ..., n_\alpha, ..., n_n\rangle = \sqrt{n_\alpha} |n_1, n_2, ..., n_\alpha - 1, ..., n_n\rangle \tag{2.38}$$

and

$$a_\alpha^\dagger a_\alpha \left| n_1, n_2, ..., n_\alpha, ..., n_n \right\rangle = n_\alpha \left| n_1, n_2, ..., n_\alpha, ..., n_n \right\rangle. \tag{2.39}$$

The hermitian operator $a_\alpha^\dagger a_\alpha$ is called the particle number operator because of his eigenvector $\left| n_1, n_2, ..., n_\alpha, ..., n_n \right\rangle$ and the corresponding eigenvalue n_α. The vacuum state is given by $\left| 0 \right\rangle$ and

$$a_\alpha \left| 0 \right\rangle = 0 \tag{2.40}$$

for all α. By successively applying the creation operator on the vacuum state, any state of indistinguishable particles can be obtained

$$\left| n_1, n_2, ..., n_n \right\rangle = \frac{1}{\sqrt{n_1! n_2! ... n_n!}} (a_1^\dagger)^{n_1} (a_2^\dagger)^{n_2} ... (a_n^\dagger)^{n_n} \left| 0 \right\rangle. \tag{2.41}$$

The following commutation relations are obtained for bosons

$$[a_\alpha^\dagger, a_\beta^\dagger] = a_\alpha^\dagger a_\beta^\dagger - a_\beta^\dagger a_\alpha^\dagger = 0 \tag{2.42}$$

$$[a_\alpha, a_\beta] = a_\alpha a_\beta - a_\beta a_\alpha = 0 \tag{2.43}$$

$$[a_\alpha, a_\beta^\dagger] = \delta_{\alpha\beta} \tag{2.44}$$

In the framework of second quantization, the field operator $\Psi^\dagger(x)$ can be derived by

$$\hat{\Psi}^\dagger(x) = \sum_\alpha \phi_\alpha^*(x) a_\alpha^\dagger \tag{2.45}$$

$$\hat{\Psi}(x) = \sum_\alpha \phi_\alpha(x) a_\alpha \tag{2.46}$$

where $\phi_\alpha(x)$ is a solution of the Schrödinger equation. $\Psi^\dagger(x)$ creates a particle in the state $\hat{\phi}_\alpha(x)$ and $\hat{\Psi}(x)$ annihilates a particle in the state $\hat{\phi}_\alpha(x)$. An operator in second quantization can be obtained by field operators and it depends on the number of particles the operator acts on. For a one particle operator we have

$$\hat{\mathcal{O}}^1(x) \to \int d^3x \Psi_\sigma^\dagger(x) \mathcal{O}(x) \Psi_\sigma(x) = \tag{2.47}$$

$$\sum_{\nu,\nu'} \int d^3x \phi_\nu^*(x) \mathcal{O}(x) \phi_\nu(x) a_\nu^\dagger a_{\nu'} =$$

$$\sum_{\nu',\nu} O_{\nu',\nu} a_\nu^\dagger a_{\nu'},$$

where $O_{\nu',\nu}$ is given by the scalar matrix element of the operator:

$$O_{\nu',\nu} = \int d^3x \phi_\nu^*(x) \mathcal{O}(x) \phi_\nu \tag{2.48}$$

Therefore, the expectation values can be obtained by

$$\langle \mathcal{O} \rangle = \langle n_1, ..., n_n | \mathcal{O} | n_1, ..., n_n \rangle = \tag{2.49}$$

$$\sum_{\nu,\nu'} O_{\nu',\nu} \underbrace{\left\langle n_1, ..., n_n | a_\nu^\dagger a_{\nu',\sigma} | n_1, ..., n_n \right\rangle}_{n_\nu \delta_{\nu\nu'}} =$$

$$\sum_\nu O_\nu n_\nu.$$

A two particle operator $\mathcal{O}^{(2)}$ can be correspondingly obtained by

$$\mathcal{O}^{(2)}(x,x') \rightarrow \sum_{\sigma,\sigma'} \int d^3x d^3x' \Psi_\sigma^\dagger(x) \Psi_{\sigma'}^\dagger(x') \mathcal{O}^{(2)}(x,x') \Psi_\sigma(x) \Psi_{\sigma'}(x') =$$

$$\tag{2.50}$$

$$\sum_{\sigma,\sigma',\nu_i} \int d^3x d^3x' \phi_{\nu_1}^*(x) \phi_{\nu_2}^*(x') \mathcal{O}^{(2)}(x,x') \phi_{\nu_3}(x') \phi_{\nu_4}(x) a_{\nu_1,\sigma}^\dagger a_{\nu_2,\sigma'}^\dagger a_{\nu_3,\sigma'} a_{\nu_4,\sigma} =$$

$$\tag{2.51}$$

$$\sum_{\nu_i,\sigma,\sigma'} O_{\nu_1,\nu_2,\nu_3,\nu_4} a_{\nu_1,\sigma}^\dagger a_{\nu_2,\sigma'}^\dagger a_{\nu_3,\sigma'} a_{\nu_4,\sigma} \tag{2.52}$$

with

$$O_{\nu_1,\nu_2,\nu_3,\nu_4} = \int d^3x d^3x' \phi_{\nu_1}^*(x) \phi_{\nu_2}^*(x') \mathcal{O}^{(2)}(x,x') \phi_{\nu_3}(x') \phi_{\nu_4}(x) \tag{2.53}$$

and the expectation values are

$$\left\langle \mathcal{O}^{(2)} \right\rangle = \langle n_1, ..., n_n | \mathcal{O}^2 | n_1, ..., n_n \rangle = \tag{2.54}$$

$$\sum_{\sigma,\sigma',\nu_i} O_{\nu_1,\nu_2,\nu_3,\nu_4} \left\langle n_1, ..., n_n | a_{\nu_1,\sigma}^\dagger a_{\nu_2,\sigma'}^\dagger a_{\nu_3,\sigma'} a_{\nu_4,\sigma} | n_1, ..., n_n \right\rangle. \tag{2.55}$$

Since two basis states are equal or orthonormal, the last part in equation 2.55 only gives a non-vanishing result if the operation

$$a_{\nu_1,\sigma}^\dagger a_{\nu_2,\sigma'}^\dagger a_{\nu_3,\sigma'} a_{\nu_4,\sigma} \tag{2.56}$$

results in the same state as before. For instance, in case of $\sigma = \sigma'$ this means the operation only acts on the boson A subspace, thus non-vanishing expectation values only occur for

$$\nu_1 = \nu_4 \text{ and } \nu_2 = \nu_3, \tag{2.57}$$
$$\text{or } \nu_1 = \nu_3 \text{ and } \nu_2 = \nu_4. \tag{2.58}$$

Since bosons can occupy the same state also

$$\nu_1 = \nu_2 = \nu_3 = \nu_4 \tag{2.59}$$

is a possible solution. In the case of $\sigma \neq \sigma'$, we only get a result unequal to zero if

$$\nu_1 = \nu_4 \text{ and } \nu_2 = \nu_3. \tag{2.60}$$

2.4.2 Hamiltonian

In this section, the Hamiltonian for a two-component bosonic system, is derived. Previously, I derived the bosonic field operator $\Psi_A^\dagger$ which creates a boson of type A at r. Respectively, $\Psi_A(r)$ annihilates a boson of type A at location r. For bosons of type B, corresponding field operators are $\hat{\Psi}_B^\dagger(\vec{r})$ and $\hat{\Psi}_B(\vec{r})$.
The Hamiltonian consists of the sum of the kinetic energies for the two bosons

$$H_{kin} = \frac{\hat{p}^2}{2m_{B/A}}, \tag{2.61}$$

the single particle potential V_{dip} of the optical lattice which is the spin dependent honeycomb potential (2.16) in our case, and the interaction energy U. The two particle-interacting potential is well approximated by

$$U(\vec{r}, \vec{r'}) = \frac{4\pi\hbar^2 a}{2m_r}\delta(\vec{r} - \vec{r'}) = \frac{g}{2}\delta(\vec{r} - \vec{r'}), \tag{2.62}$$

as discussed in section 2.2.1. In case of two different kind of bosons we usually have to consider three different scattering possibilities: The scattering of two A-bosons, the scattering of two B-bosons, and an A-B-scattering. These lead to three corresponding scattering lengths. The interaction energy for two particles of the same kind, one in $\vec{r}$ and one in $\vec{r'}$ is then given by

$$H_{AA} = \int d^3(r)d^3(r')\hat{\Psi}_A^\dagger(\vec{r})\hat{\Psi}_A^\dagger(\vec{r'})\frac{g_A}{2}\delta(\vec{r} - \vec{r'})\hat{\Psi}_A(\vec{r'})\hat{\Psi}_A(\vec{r}) \tag{2.63}$$

and respectively

$$H_{BB} = \int d^3(r)d^3(r')\hat{\Psi}_B^\dagger(\vec{r})\hat{\Psi}_B^\dagger(\vec{r'})\frac{g_B}{2}\delta(\vec{r} - \vec{r'})\hat{\Psi}_B(\vec{r'})\hat{\Psi}_B(\vec{r}).$$

The part of the Hamiltonian for one bosonic species (e.g. A) is therefore given by

$$H_A = \int d^3r\hat{\Psi}_A^\dagger(\vec{r})[\frac{\hat{p}^2}{2m_A} + U_{dip}(\vec{r}) + \hat{\Psi}_A^\dagger(\vec{r'})\frac{g_A}{2}\hat{\Psi}_A(\vec{r'})\hat{\Psi}_A(\vec{r}). \tag{2.64}$$

An additional part arises from the scattering of the two different bosonic species

$$H_{AB} = \int d^3(r)d^3(r')\hat{\Psi}_A^\dagger(\vec{r})\hat{\Psi}_B^\dagger(\vec{r'})\frac{g_{AB}}{2}\delta(\vec{r} - \vec{r'})\hat{\Psi}_B(\vec{r'})\hat{\Psi}_A(\vec{r}). \tag{2.65}$$

Thus the complete Hamiltonian is given by the sum:

$$H = H_A + H_B + H_{AB}. \tag{2.66}$$

Now the field operators $\hat{\Psi}_A^\dagger(\vec{r})$ and $\hat{\Psi}_B^\dagger(\vec{r})$ can be expanded in a spatial part and in the (creation)- and annihilation-operators for the A-bosons

$$\hat{\Psi}_A^\dagger(\vec{r}) = \sum_i \phi_{A,i}(\vec{r})\hat{a}_i^\dagger \tag{2.67}$$

and for the B-bosons.

$$\hat{\Psi}_B^\dagger(\vec{r}) = \sum_i \phi_{B,i}(\vec{r})\hat{b}_i^\dagger. \tag{2.68}$$

2.4.3 Bose-Hubbard Hamiltonian

In presence of an optical lattice the behaviour of the system can be described in terms of inter-site tunneling of particles, from site to site and the interaction of particles at the same site. The basis functions, which fulfill the condition to be localized at the lattice site best, are the Wannier functions. Therefore, the Wannier basis is chosen to derive the corresponding field operators and to expand the full Hamiltonian derived in the last section. If $\xi_q^{(n)}(z)$ are the Bloch functions, the well localized Wannier-functions can be defined by

$$w^{(n)}(x - x_j) = \frac{1}{\sqrt{N_S}} \sum_0^n e^{iqx_j} \xi_q^{(n)}(x), \tag{2.69}$$

[1]. For the lowest band with $q \approx 0$ one can write the Hamiltonian within the Wannier basis

$$H = -\sum_{ij} J_{A,ij}\hat{a}_i^\dagger \hat{a}_i - \sum_{ij} J_{B,ij}\hat{b}_i^\dagger \hat{b}_i + \sum_{i,j,k,l} \frac{U_{A,ijkl}}{2}\hat{a}_i^\dagger \hat{a}_j^\dagger \hat{a}_k \hat{a}_l + \tag{2.70}$$

$$\sum_{i,j,k,l} \frac{U_{B,ijkl}}{2}\hat{b}_i^\dagger \hat{b}_j^\dagger \hat{b}_k \hat{b}_l + \sum_{i,j,k,l} V_{AB,ijkl}\hat{a}_i^\dagger \hat{b}_j^\dagger \hat{b}_k \hat{a}_l,$$

with

$$U_{A/B,ijkl} = g \int d^3r w_{A/B}^{(0)}(r - r_i)^* w_{A/B}^{(0)}(r - r_j)^* w_{A/B}^{(0)}(r - r_k) w_{A/B}^{(0)}(r - r_l), \tag{2.71}$$

$$V_{AB,ijkl} = g \int d^3r w_A^{(0)}(r - r_i)^* w_B^{(0)}(r - r_j)^* w_B^{(0)}(r - r_k) w_A^{(0)}(r - r_l). \tag{2.72}$$

and

$$J_{A/B,ij} = \int d^3 w^{(0)}(r - r_i)[\frac{\hat{p}^2}{2m_{A/B}} + U_{dip}]w^{(0)}(r - r_j). \tag{2.73}$$

If the lattice is sufficiently deep, the hopping of non-nearest neighbors is small enough to be neglected. Also, the next neighbor interaction for different site U_{ijkl} is much smaller than U_{iiii} and therefore the sums only contains hopping for next neighbors and the on-site interaction U_i. With the particle number operator $\hat{n}_i = a_i^\dagger a_i$ for boson A and $\hat{m}_i = b^\dagger b$ for boson B the Bose-Hubbard Hamiltonian can be written as

$$\mathbf{H}_{BH} = -J_A \sum_{i,j} (\hat{a}_{i,}^\dagger \hat{a}_j + cc) - J_B \sum_{i,j} (\hat{b}_i^\dagger \hat{b}_j + cc)$$

$$+ \frac{U_A}{2} \sum_i \hat{n}_i (\hat{n}_i, -1) + \frac{U_B}{2} \sum_i \hat{m}_i (\hat{m}_i - 1) \qquad (2.74)$$

$$+ V_{AB} \sum_i \hat{n}_i \hat{m}_i + \epsilon_A \sum_i \hat{n}_i + \epsilon_B \sum_i .\hat{m}_i$$

J_A (J_B) is the hopping for the A-Bose component (B-Bose component). The operators $\hat{b}$ and $\hat{a}$ are the annihilation operators for the B-boson and the A-boson, $\hat{b}^\dagger$ and $\hat{a}^\dagger$ are the creation operators accordingly. The energy-shift $\epsilon_{A/B}$ for A and B bosons can occur due to a confining or a spin-dependent potential which gives a sublattice structure. The expectation values of the particles number operators $\hat{n}_i = a^\dagger a$ and $\hat{m}_i = b^\dagger b$ give the numbers of A- respectively B-bosons at site i.

2.4.4 Exact diagonalization

Since the simulations are performed in the framework of exact diagonalization, we are able to compute the complete wave functions and eigenvalues. All correlation functions and expectation values can be calculated, even for the exited states in every regime. In contrast to a meanfield approach, which only results in densities and occupations of the groundstate. But unfortunately, performing exact diagonalization only allows to deal with small systems, due to the numerical effort. If a supercell with n=8 sites and half filling for every kind of atom is choosen, the dimension of the many particle basis amounts to the number of $d = 108900$. In the case of twelve sites filled with six A- and six B-bosons the basis size increases to $d = 153165376$, which exceeded my calculation capabilities. Therefore finite size effects have to be considered, but they will be discussed in detail later in Chapter 4.3. In the following, a short recall of the method of exact diagonalization is given. The time dependent Schrödinger equation in any basis is given by

$$i\hbar \frac{d}{dt} |\Psi(t)\rangle = H(t) |\psi(t)\rangle. \qquad (2.75)$$

If H is time independent, the wave function can be factorized as

$$|\Psi_i(t)\rangle = e^{\frac{iE_i t}{\hbar}} |\Psi_i\rangle \qquad (2.76)$$

and the eigenvalue problem

$$\langle n| \hat{H} \sum_{n'} n'\rangle \langle n'|\Psi\rangle = E \langle n|\Psi\rangle \qquad (2.77)$$

can be solved in any basis $|n\rangle$ of our Hilbert space. This leads to a system of n equations for coefficients and eigenvalues

$$\sum_{n'}(H)_{nn'}c_{n'} = Ec_n, \tag{2.78}$$

where $(H)_{nn'}$ is the matrix element $\left\langle n|\hat{H}|n'\right\rangle$. Due to the hermiticity of H, the matrix (H) can be diagonalized to D_A. In the basis of its eigenvectors, H becomes a diagonal matrix of eigenvalues. A matrix P exist for hermitian matrices, which is invertible and solves the equation:

$$D_A = P^{-1}DP. \tag{2.79}$$

In the columns the eigenvectors are inscribed. Thus, by diagonalizing (H), the eigenvectors and eigenvalues are calculated. The Hamiltonian is constructed by one- and two-particle operators. Since on-site interaction and nearest neighbor tunneling is just considered, most matrix elements vanish and the sparse-matrix-representation can be used [54]. The numerical diagonalization is done with the Arnoldi package, which has been developed at the Rice University in Houston, Texas [65]. Like mentioned in the beginning of this section, as the numerical diagonalization is associated with a high computational effort, i.e. the systems have to be small enough. In case of two different sorts of bosons, the calculations have been performed for supercells up to ten lattice sites. In case of a one component system, the calculation have been done for a supercell with twelve sites filled with twelve bosons. The different supercells and their periodicity will be discussed in the following section.

2.4.5 Finite lattice structure and product states

Like described above, small systems only can be considered because of the huge calculation effort in exact diagonalization of system with periodic boundary conditions. In the honeycomb lattice, every lattice site has three next nearest neighbors. If the system is filled with two different kinds of atoms, the smallest size of a supercell is the four sited cell. Also six-, eight- and ten-sited supercell are examined to reduce and investigating finite size effects. In every case, the entire lattice can be generated by tiling one supercell beneath another. The resulting wavefunction is of course restricted to the chosen supercell, which is disscussed in Chapter 4. In case of a six-sited supercell the site **3** has the nearest neighbors **0**, **2** and **4** (see Fig. 2.4 a). The boundary conditions are considered such that the particles which tunnels out of the unit cell, tunnels in again at the other side. As the first example, the six-sited lattice cell is shown in Fig. 2.4. If the particle tunnels from site **2** to site **5**, it tunnels into the next cell, the upper left. In this case the periodic boundary conditions make sure that it tunnels into the same cell again at the lower right. To implement the tunneling in the program, the 2-dimensional structure has been transferred in a one dimensional chain, see Fig. 2.4 b. The
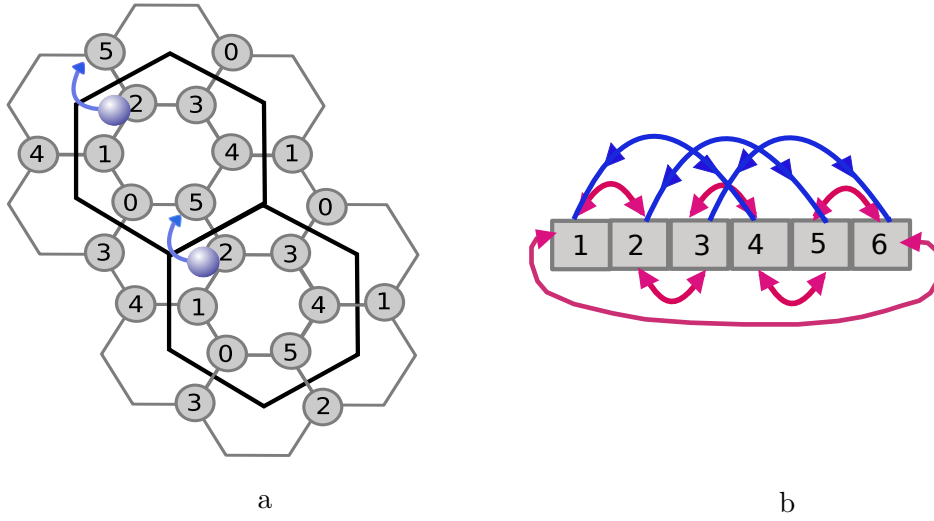
Figure 2.4: The periodic boundary condition for the six sited cell in the hexagonal lattice structure (a) and transfered in a chain with additional tunneling terms. This can be considered as the Fockbasis (b). Where for example a state $|2, 0, 0, 1, 0, 0\rangle$ would f.i. mean: two particles on site **0** and one particle on site **3** and the other sites are empty.

third nearest neighbor easily can be considered by the additional tunneling terms, like it is depicted with different colors in Fig. 2.4 b. The red arrows denote the neighbors inside the cell, and the blue arrows denote the tunneling which leads to the next unit cell. In this way, the Fock states easily can be build. For instance, the state $|2, 0, 0, 1, 0, 0\rangle$ would mean two particles on site **0** and one particle on site **3** and the other sites are empty. As we want to investigate the behavior of two sorts of bosons we have to build up a product space of the Fock basis of the two bosonic species $|n\rangle = |n_A\rangle \otimes |n_B\rangle$, where $|n_A\rangle$ and $|n_B\rangle$ are the A- and B-boson subspace. Figure 2.5 illustrates this with a simple example. The dimension of the basis therefore equals the number of product states

$$D_{(n_{AB})} = D_{(n_A)} \times D_{(n_B)}, \tag{2.80}$$

with the dimension of the separated fockstates of the A, respectively B-bosonic subspaces

$$D_{A,B} = \frac{(N_{A,B} + N_s - 1)!}{N_{A,B}!(N_s - 1)!}, \tag{2.81}$$

where N_s is the number of lattice sites and $N_{A,B}$ is the number of A- respectively B-bosons [54]. Therefore the size of the Hamiltonian matrix is $D_{n_{AB}}^2$.
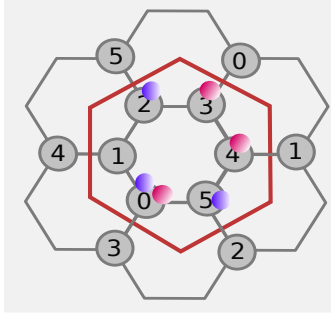
Figure 2.5: A state like depicted here consists of parts of the two bosonic subspaces $|n_{blue}\rangle$ and $|n_{red}\rangle$ this state e.g. can be written as $|n_{blue,red}\rangle = |1,0,1,0,0,1\rangle\,|1,0,0,1,1,0\rangle$.

2.4.6   Matrixelements

To diagonalize the Hamilton matrix, the elements must be calculated, as discussed in section 2.4.3. By using the Bose-Hubbard model, just one and two-particle operators have to be calculated. As for the expectation values, most of the matrix elements are zero. For the one particle operator

$$\langle n_1, ..., n_n|\mathcal{O}|n_1', ..., n_n'\rangle =$$
$$\sum_{\nu,\nu',\sigma} O_{\nu',\nu} \left\langle n_1, ..., n_n|a_{\nu,\sigma}^\dagger a_{\nu',\sigma}|n_1', ..., n_n'\right\rangle \tag{2.82}$$

with

$$O_{\nu',\nu} = \int d^3x \phi_\nu^*(x)\mathcal{O}(x)\phi_\nu \tag{2.83}$$

the expression gives a result unequal to zero if

$$|n\rangle = |n'\rangle$$

or if

$$|n\rangle = |....,n_{\nu_1}, ..., n_{\nu_2}, ...\rangle$$

and

$$|n'\rangle = |....,n_{\nu_1}+1, ..., n_{\nu_2}-1, ...\rangle .$$

The two-particle number operator gives matrix elements like:

$$\langle n_1, ..., n_n|\mathcal{O}^2|n_1', ..., n_n'\rangle =$$
$$\sum_{\sigma,\sigma',\nu_i} O_{\nu_1,\nu_2,\nu_3,\nu_4} \left\langle n_1, ..., n_n|a_{\nu_1,\sigma}^\dagger a_{\nu_2,\sigma'}^\dagger a_{\nu_3,\sigma'} a_{\nu_4,\sigma}|n_1', ..., n_n'\right\rangle \tag{2.84}$$

with

$$O_{\nu_1,\nu_2,\nu_3,\nu_4} = \int d^3x d^3x' \phi_{\nu_1}^*(x)\phi_{\nu_2}^*(x')\mathcal{O}^{(2)}(x,x')\phi_{\nu_3}(x')\phi_{\nu_4}(x). \tag{2.85}$$

For the two particle operator only the matrix elements of following states give non-vanishing result:

$$|n\rangle = a_{\nu_1}^\dagger a_{\nu_1}^\dagger a_{\nu_1} a_{\nu_1} |n'\rangle$$
$$|n\rangle = a_{\nu_3}^\dagger a_{\nu_1}^\dagger a_{\nu_1} a_{\nu_2} |...., n_{\nu_2} + 1, ..., n_{\nu_3} - 1, ...\rangle$$
$$|n\rangle = a_{\nu_2}^\dagger a_{\nu_2}^\dagger a_{\nu_1} a_{\nu_1} |...., n_{\nu_1} + 2, ..., n_{\nu_2} - 2, ...\rangle$$
$$|n\rangle = a_{\nu_1}^\dagger a_{\nu_2}^\dagger a_{\nu_3} a_{\nu_3} |...., n_{\nu_1} - 1, ..., n_{\nu_2} - 1, .., n_{\nu_3} + 2, ...\rangle$$
$$|n\rangle = a_{\nu_3}^\dagger a_{\nu_3}^\dagger a_{\nu_1} a_{\nu_2} |...., n_{\nu_1} + 1, ..., n_{\nu_2} + 1, ..., n_{\nu_3} - 2, ...\rangle$$
$$|n\rangle = a_{\nu_4}^\dagger a_{\nu_2}^\dagger a_{\nu_3} a_{\nu_1} |...., n_{\nu_1} + 1, ..., n_{\nu_2} - 1, .., n_{\nu_3} + 1, ..., n_{\nu_4} - 1, ..\rangle$$

The algorithm therefore has to check if a pair of states correspond to these above, in this case the matrix element has to be evaluated and added up.

2.5 Iso-Magnetism

A large part of this work deals with the investigation of isomagnetism. As our lattice cell is filled with two kind of bosons, the question arises how do the atoms arrange each other for a given ratio of interaction V_{AB} (interaction between different kind of atoms) and interaction $U_{AA/BB}$ (interaction between the same kind of atoms). The ordering in the anti-ferromagnetic regime is expected to be a state where boson A prefers to sit on a site next to a B-boson. In the ferromagnetic case a ground-state is preferred where the same sort of atoms occupy adjoining sites. This is due to the energy cost for virtual tunneling (see Fig. 2.8). Figuratively spoken, in case of $V_{AB} > U_{AA,BB}$, a virtual tunnel process to the next neighbored site which also is occupied by a particle, it energetically convenient for the system, if the considered particles are of a same kind. In contrast, if $U_{AA,BB} > V_{AB}$ it would be better if the next neighbor site is occupied by the other kind. Our system contains n particles by n sites, both $n/2$ for A- and B-bosons. Then, in the localized phase, where the atoms are pinned at the lattice sites, one would expect two different ordered groundstates depending on the ratio of interaction. These two possibilities are depicted in Fig. 2.6 in case of a square lattice, the corresponding ground-state of the system can be described as 'ferromagnetic' or 'anti-ferromagnetic'. By computing different correlation-functions, we can read out the quantum magnetic ordering, even in the superfluid regime..

2.5.1 Iso-spin Hamiltonian

In limit of $t \ll V_{AB}, U_{AA}, U_{BB}$, i.e. in the localized phase, an effective spin-Hamiltonian can be derived in second order perturbation theory. The hopping term can be mapped onto an effective isospin Hamiltonian [22, 48]. If we have a two level system, like bosons in two hyperfine states, they can be mapped on an
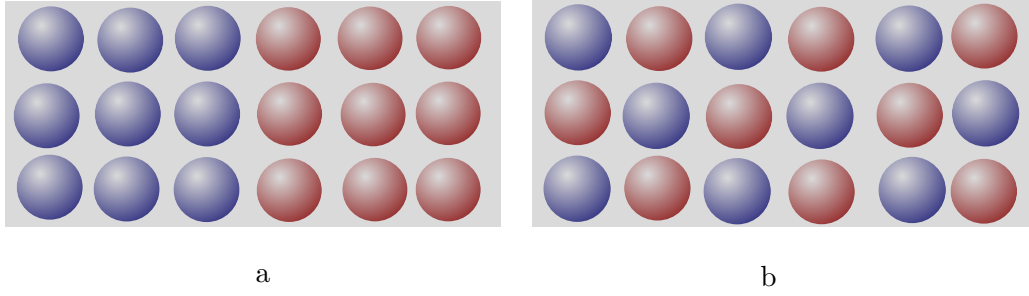
Figure 2.6: (a) A 'ferromagnetic' groundstate which is dominant for the case, that $U_{AA,BB} < V_{AB}$. Due to virtual tunneling, the same sort of atoms are expected to occupy adjoining sites. (b) In case of $U_{AA,BB} < V_{AB}$, the atoms prefer to sit on a site next the other sort of atoms. This would end up in a state where the staggered order is predominant.

iso spin system where boson A corresponds to spin-up ($|A\rangle \rightarrow |\uparrow\rangle$), and boson B corresponds to spin down ($|B\rangle \rightarrow |\downarrow\rangle$). The on-site part of the Bose Hubbard Hamiltonian is chosen to be the unperturbed H_0 and the hoping term to be the perturbation H_1. The ground state in the Mott insulator is given by the state where every single atom occupies one lattice site. The first exited state is given by one double occupied state, the energy difference is U in case of two atoms of the same kind. For atoms of different sorts it is given by V_{AB}, see Fig. 2.7.
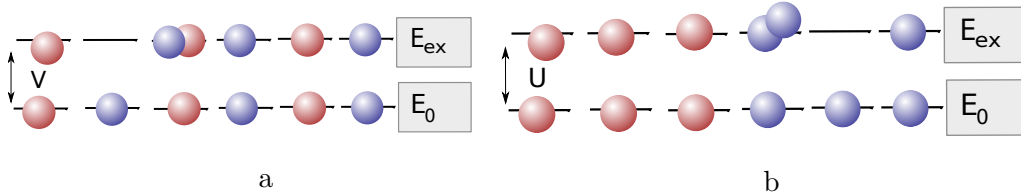

Figure 2.7: Shown here is the energy spectrum in the Mott insulator phase. The state of single occupations is the groundstate (bottom), whereas the state with one double occupation is the first excited state (top). The energy difference between these states is U in case of atoms of the same kind (b) and V_{AB} in case of different atoms (a).

$$\mathbf{H}_{BH} = H_0 + H_{hop}, \tag{2.86}$$

with

$$H_0 = \sum_i \left[\frac{U}{2}(\hat{n}_i(\hat{n}_i - 1) + \hat{m}_i(\hat{m}_i - 1)) + V_{AB}\hat{n}_i\hat{m}_i \right], \tag{2.87}$$

and

$$H_{hop} = -J \sum_{i,j} \left[(\hat{a}_i^\dagger \hat{a}_j + cc) + (\hat{b}_i^\dagger \hat{b}_j + cc) \right]. \tag{2.88}$$

In second order perturbation theory the energy shift compared to the groundstate is by

$$E_0^2 = \sum_{e \neq 0} \frac{|\langle e^0 | H_1 | 0 \rangle|^2}{E_0^0 - E_e^0}, \tag{2.89}$$

where $\langle e^0 |$ is the exited state and $\langle 0 |$ is the ground state. If higher excitations are negligible and only double occupations are considered as virtual tunnel processes, the two possibilities for the exited energy E_e^0 are U, in case of a AA-or BB-double occupation (see Fig.2.7 b), and V_{AB}, in case of AB-double occupation (see Fig. 2.7 a). Therefore

$$E_0^2 = -\sum_{e \neq 0} \frac{\langle 0 | H_1 | e^0 \rangle \langle e^0 | H_1 | 0 \rangle}{U} - \sum_{e \neq 0} \frac{\langle 0 | H_1 | e^0 \rangle \langle e^0 | H_1 | 0 \rangle}{V}. \tag{2.90}$$

is obtained. The expression $\langle e^0 | H_1 | 0 \rangle$ ($\langle 0 | H_1 | e^0 \rangle$) means virtual tunneling in to (out of) the excited state. We can add $m = 0$ to the sum, because the matrix element $\langle 0 | H_1 | 0 \rangle$ is equal to zero. Therefore we obtain:

$$E_0^2 = -\sum_e \frac{< 0 | H_1 | \overbrace{e^0 >< e^0}^{1} | H_1 | 0 >}{U} - \sum_e \frac{< 0 | H_1 | \overbrace{e^0 >< e^0}^{1} | H_1 | 0 >}{V}. \tag{2.91}$$

Inserting the H_1 hopping term, we obtain

$$E_0^2 = -\frac{J^2}{U} \sum_{ijkl} (\hat{a}_i^\dagger \hat{a}_j + cc) + (\hat{b}_i^\dagger \hat{b}_j + cc) - \frac{J^2}{V_{AB}} \sum_{ijkl} (\hat{a}_k^\dagger \hat{a}_l + cc) - (\hat{b}_k^\dagger \hat{b}_l + cc). \tag{2.92}$$

Using the isospin $\hat{S}_{i,z} = \frac{n_{i,A} - n_{i,B}}{2}$, the commutation relations and the Swinger-Boson representation [5]

$$S^+ = a^\dagger b \qquad \text{and} \qquad S^- = b^\dagger a, \tag{2.93}$$

Equation (2.92) results in the anisotropic Heisenberg-spin-1/2 model [18]:

$$H_{int} = -\frac{J^2}{2} \left(\frac{1}{U} - \frac{1}{V_{AB}} \right) (\sigma_z^i \sigma_z^j - \sigma_-^i \sigma_+^j - \sigma_+^i \sigma_-^j). \tag{2.94}$$

Depending on the ratio of interaction V_{AB} and interaction U the energy is minimized for the ferro- or anti-ferromagnetic ordering. I expect a ferromagnetic order in the limit $V > U >> t$, since the prefactor of $\sigma_z^i \sigma_z^j$ is positive whereas in the regime of $U > V >> t$ in contrast I expect an antiferromagnetic ordering, (staggered order) because the prefactor changed its sign.
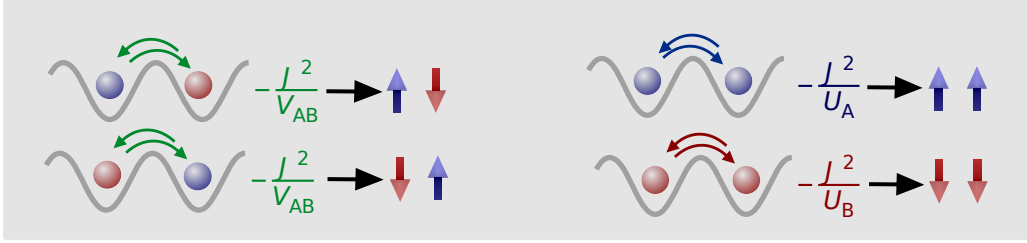
Figure 2.8: Depicted here are the different contributions for the energy difference of the tunnel processes for different situations

2.5.2 Correlation functions

By diagonalizing the Bose Hubbard Hamiltonian exactly we obtain all eigenvalues and eigenvectors. The eigenvectors $|\Psi\rangle = \sum_N c_N |N\rangle$ contain a large number of contributions and do not enable us to get asses to the physical properties of the system easily. One possibility to characterize the system is computing expectation values like the fluctuations on a site i $\langle \Delta n_i \rangle$ or the particle occupation number $\langle n_i \rangle$. But the most powerfull quantity, is computing several correlation functions since they allow insight into the behavior of the system. A correlation function can be developed by the general pair-correlation function:

$$g_{i,j}^{\alpha\beta} = \left\langle \Psi | a_{i,\alpha}^\dagger a_{j,\beta}^\dagger a_{j,\beta} a_{i,\alpha} | \Psi \right\rangle. \tag{2.95}$$

The lattice indices are i and j and α and β are the particle sorts. As I want to investigate 'ferromagnetic' or 'antiferromagnetic' ordering for different parameter regimes, I have to design different correlation functions which give a quantity to measure 'ferromagnetic' and 'anti-ferromagnetic' ordering. In general ferromagnetism means a long range phenomena which occurs even for two different points being separated from each other by a long distance. In the Mott insulator phase a ferromagnetic ordering especially considers the next neighbors, i.e. the interaction is short range. As our model only considers nearest neighbor hopping and on-site-interaction the 'magnetic' behavior is certainly destined by virtual tunneling (see section 2.5.1) between nearest neighbors. The correlation function $g_{i,j} = \langle \hat{S}_{i,z} \hat{S}_{j,z} \rangle$ distinguishes between ferro- or anti-ferromagnetic behavior. If $g_{ij} \leq 0$, an anti-ferromagnetic ordering is dominant, for $g_{ij} \geq 0$ a ferromagnetic behavior is dominant. In case of two bosons, the corresponding iso spin operator $\hat{S}_{i,z}$ can be derived by $\hat{S}_{i,z} = \frac{1}{2}(n_{i,A} - n_{i,B})$, which would result in $\hat{S}_{i,z} = \frac{1}{2}$ when site i is occupied with boson A and $\hat{S}_{i,z} = -\frac{1}{2}$ when site i is occupied with boson B. Therefore g_{ij} is given by:

$$\begin{aligned} \langle \hat{S}_{i,z} \hat{S}_{i+1,z} \rangle &= \langle \psi | (\hat{n}_{i,A} \hat{n}_{i+1,A} + \hat{n}_{i,B} n_{i+1,B} \\ &\quad - \hat{n}_{i,A} \hat{n}_{i+1,B} - \hat{n}_{i,B} \hat{n}_{i+1,A}) | \psi \rangle \\ &= \text{FM-AF} \end{aligned} \tag{2.96}$$

with AF being the anti-ferromagnetic part and FM the ferromagnetic.

$$|\psi\rangle = \sum_N |c_N|N\rangle$$

$$\text{AF} = \sum_N |c_N|^2 (n_{i,A} n_{i+1,B} + n_{i,B} n_{i+1,A}) \tag{2.97}$$

$$\text{FM} = \sum_N |c_N|^2 (n_{i,A} n_{i+1,A} + n_{i,B} n_{i+1,B}).$$

As our system is finite, we have to consider finite size effects, which result from small particle numbers and small lattice cells. So, if a particle of sort A occupy site i, there are only (n_A-1) A-particles of the total $(2n-1)$ particles left to contribute for ferromagnetic correlations. In contrast to the anti ferromagnetic case, if boson A occupy site i there are n B-particles of the total $(2n-1)$ particles left to allow for anti-ferromagnetic correlations. Therefore, the normalized correlation functions for small systems and small particle numbers are given by

$$g = \sum_{<i,j>} \frac{(\frac{2n-1}{n-1}FM - \frac{2n-1}{n}AF)}{2 \times (FM + AF)}, . \tag{2.98}$$

here, $< i,j >$ stands for all next neighbored pairs. In the limit of an infinite number of sites and particles ($< i,j > \rightarrow \infty$) this equation leads to the result in equation (2.96). In the superfluid regime, the wave function broadens over the entire lattice.

By computing the distance-correlation functions, which depend on the distance Δ between the considered sites, I can do statements about long-range correlations. To consider weights, the correlation functions are normalized. N is the number of sites in the cell, N_A (N_B) gives the number of A-(B)-particles in the cell. For different particles and different lattice sites, the pair correlation-function

$$g_{i,j}^{\alpha\beta} = \left\langle \Psi | a_{i,\alpha}^\dagger a_{i,\alpha} a_{j,\beta}^\dagger a_{j,\beta} | \Psi \right\rangle = \left\langle n_i^\alpha n_j^\beta \right\rangle \tag{2.99}$$

$$g_{i,i+\Delta}^{AB} = \frac{N^2}{N_A N_B} \left\langle n_i^A n_{i+\Delta}^B \right\rangle \tag{2.100}$$

can be derived, as well as

$$g_{i,i+\Delta}^{AA} = \frac{N^2}{N_A(N_A - 1)} \left\langle n_i^A n_{i+\Delta}^A \right\rangle \tag{2.101}$$

in case of same kind of particles and different lattice sites. I discuss these in more detail in Chapter 5. Since in the superfluid regime, also high on-site occupations

are possible and probable, the on-site correlation functions play an important role, they can be derived by

$$g_{i,i}^{AA} = \frac{N^2}{N_A(N_A - 1)} \left\langle n_i^A(\langle n_i^A \rangle - 1)\right.$$

$$g_{i,i}^{AB} = \frac{N^2}{N_A(N_A - 1)} \left\langle n_i^A n_i^B \right\rangle.$$

(2.102)

This will also be discussed in Chapter 5 together with the nontrivial multiple operator correlations. Those play an important role when considering the supersolid order.

2.6 Superfluid to Mott insulator transition

The superfluid to the Mott insulator transition is one of the most famous events in the field of quantum optics [27, 28, 30]. Considering the Bose-Hubbard model (2.12), only the ratio between the on-site interaction U and the hopping constant J (kinetic energy) is responsible for the quantum phase of the system. Although it is not an exactly solvable model, the superfluid Mott insulator transition is a well understood feature. By changing the ratio U/J the system is driven to the superfluid to Mott insulator transition. Next, I will briefly introduce the two limiting regimes of vanishing on-site interaction U/J, and vanishing hopping constant J, for a more detailed discussion see [10]. In the regime of vanishing on-site interaction U/J, which means a flat lattice, the particles are delocalized and all atoms are in the single particle ground state. This is the lowest Bloch state with quasimomentum $q = 0$. The spatial particle distribution is completely disordered, because of the Heisenberg's uncertainty relation and the exact quasimomentum. Therefore, this state is characterized by high particle fluctuations, gap less excitations, and long-range order. The latter will play an important role in Chapter 5, which deals with distance depending correlation functions. For $N, N_S \to \infty$ the superfluid state corresponds to a coherent state and is similar to the Bose-Einstein-condensate ground state in 3D. For N bosons in a lattice with N_s sites i the superfluid wavefunction can be written as

$$|\Psi_{SF}\rangle = \frac{1}{\sqrt{N!}} \left(\frac{1}{\sqrt{N_s}} \sum_i \hat{a}_i^\dagger \right)^N |0\rangle.$$

(2.103)

To get an idea of the multiple occupation, for example in the case of $\eta = \frac{N}{N_S} = 1$, one will find more than one atom per site with the probability of $1 - \frac{2}{e} = 0.27$, because every atom wants to occupy all lattice sites with the same probability [10]. For increasing U/J, the system underlies a phase transition to the other limiting case, the Mott insulator. This state occurs for $J \to 0$ which is equivalent to a deep

optical lattice. This can be reached easily in experiments and in case of integer filling this state can be written as

$$|\psi_{MI}\rangle = \left(\prod_i a_i^{\dagger \frac{N}{N_s}}\right)|0\rangle. \tag{2.104}$$

It is a pure product of local Fock states, characterized by bosons localized at single lattice sites. Low (for small J) or even no particle fluctuations ($J = 0$) occur in this phase and the on site correlation is equal to zero. This is investigated in Chapter 3 in case of my system. One double occupied site (e.g. for integer filling $\eta = 1$) costs the additional energy U. Therefore the Mott insulator is characterized by gapped excitations. This means, for a given U, an energy gap occurs between the ground and the first exited state. If one particle enters a site occupied by another one (first excited state, see Fig. 2.7), this energy gap equals U, [30, 41]. This state is characterized by the loss of the long-range coherence, therefore the nearest neighbor correlation function is usefull to characterize the isomagnetic ground state in this regime, this will be carried out in Chapter 4. With increasing $J > 0$, the atoms start hopping and double occupations occur, however they still cost the double occupation energy U. The Mott insulating state will be reduced, double occupancy occur. In case of $J \approx U$ the profit in kinetic energy dominate the cost of double occupancy. Further decreasing U the system undergoes the Mott insulator to superfluid transition. The atoms are delocalized over the whole lattice. The phase transition from the superfluid to the MI-state can be described by a mean-field approach [76] where the critical value of U/J for the occurrence of phase transition can be obtained by

$$(U/zJ)_c = 2\eta + 1 + \sqrt{(2\eta + 1)^2 - 1} \tag{2.105}$$

with the number of nearest neighbors z and η the number of atoms per lattice site. With the Gutzwiller ansatz [77] similar values can be derived. Both approaches are valid for infinite sytems. For a hexagonal lattice, the best prediction for the critical value for U/J is achieved by Teichmann et $all.$ [73] using the process-chain approach, which gives

$$(U/J)_c = 11.6. \tag{2.106}$$

Due to the finiteness of our system and the exact diagonalization method the parameters to estimate the crossing regime from Superfluid to Mott insulator in this work are the particle fluctuations, the on site correlations, and the energy gap between the ground and the first exited state (see section 3.1). The resulting superfluid state will be characterized by high fluctuations and high on-site correlations and a long range order. The Mott insulator is characterized by vanishing particle fluctuations, low on-site correlations and a loss of the long range order. This will be examined in detail in Chapter 3. I find the criteria for the Mott insulator and the superfluid regime related to our finite system. It remains to be noted, that the value $(U/J)_c = 11.6$, is very close to our calculations.

2.7 Supersolid order

A special quantum state, also known from the condensed matter physic, is the supersolid state [25, 33, 34, 52]. A good introduction and overview is given by [6, 11, 51]. The supersolid state is characterized by a superfluid order and a coexisting spacial density modulation. Although the wave-function of the particles is extended over the whole lattice, the density is not uniformly distributed. Its density is modulated for a simple case schematically depicted in Fig. 2.9. The famous
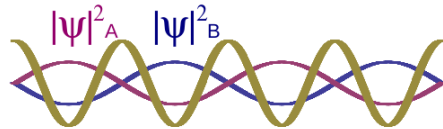

Figure 2.9: Shown here is a simple case of a density modulation in a superfluid regime, which indicates a supersolid. The density modulation lowers the symmetry of the system, this is characteristic for a supersolid state.

experiment which demonstrate this phenomena is described in [45], where a "Non-Classical Rotational Inertia" of solid helium has been observed. This experiment is still highly competitive, as it is not evidenced if the decrease of the inertia for very low temperature really has been a proof of a supersolid structure [66]. The increasing tunability of optical lattices and multiple atomic properties opens up new opportunities to investigate quantum phases, for example the supersolid state. Theoretically the occurance of a supersolid state has been investigated in multiple ways. In case of one boson component by considering the offsite interaction in an extended Bose-Hubbard Hamiltonian [69] or below Bose-Hubbard [21]. The supersolid phase has been examined theoretically by addressing bipolar particles [16] and in Bose-Fermi-mixtures [75]. A supersolid of two bosonic species with a filling imbalance has been demonstrated by [44]. Since a supersolid state is hard to imagine, a short introduction, is depicted here [11].

solid order

The solid order, like atoms in a crystalline structure, is characterized by a spatial arrangement in ordered configurations; it does not even have to be periodic. With the local density $\rho(\vec{r})$ of the particles in the crystal, the average density in the crystal of the volume Γ can be written as:

$$\bar{\rho} = \frac{1}{\Gamma} \int d^3 r \rho(\vec{r}) \qquad \text{and} \qquad \delta\rho(\vec{r}) = \rho(\vec{r}) - \bar{\rho} \qquad (2.107)$$

expressing the deviation of ρ at $\vec{r}$. In a liquid or a gas $\rho(\vec{r}) = \hat{\rho}$ and $\delta\rho = 0$. In a crystal, the translational symmetry is broken, therefore $\delta\rho$ does not vanish. In

the crystal order the density deviation is proceeded by

$$\delta\rho(\vec{r}) = \delta\rho(\vec{r} + \vec{T}) \qquad \text{with} \qquad \vec{T} = c_1\vec{a}_1 + c_2\vec{a}_2 + c_3\vec{a}_3 \qquad c_i = 0, \pm 1, \pm 2, ...$$

$\vec{a}_i$ are the lattice vectors and therefore $\vec{T}$ reaches any point of the lattice. For the reciprocal lattice the lattice vector $\vec{G}$ fulfills the condition

$$\vec{T} * \vec{G} = 2\pi n \qquad \text{with} \qquad n \in \mathbb{N} \tag{2.108}$$

and the density in the k-space is given by the Fourier transform of $\delta\rho(\vec{r})$

$$\tilde{\rho}(\vec{k}) = \frac{1}{\Omega} \int d^3 r \delta\rho(\vec{r}) e^{i\vec{k}\vec{r}}. \tag{2.109}$$

$S(\vec{k}) = |\tilde{\rho}(\vec{k})|^2$ is known as the static structure factor. In a solid, $S(\vec{k})$ peaks periodically in the dependence of the wave vector G. Experimentally it is reflected by intensity of Bragg peaks. This order is also called long range order (LRO).

superfluid order
The superfluid order is characterized by a density including two different parts, one is the superfluid ρ_s and the other is the normal fraction ρ_n [74].

$$\rho(\vec{r}) = \rho_s(\vec{r}) + \rho_n(\vec{r}). \tag{2.110}$$

Where the superfluid fractions is neither subjected to dissipation nor has entropy in contrast to the normal component. For a translational invariant system, like a fluid or a gas, the densities are not spacial variant

$$\rho_n = \rho_n(\vec{r}) \qquad \text{and} \qquad \rho_s = \rho_s(\vec{r}). \tag{2.111}$$

Below a critical temperature T_c, the transition to the superfluid starts. The superfluid part becomes nonzero and increases, until the whole system is in the superfluid fraction at $T = 0$ and the density of the superfluid fraction becomes the average density

$$\rho_s(T = 0) = \bar{\rho}. \tag{2.112}$$

The macroscopic wavefunction of the condensate fraction has the meaning of a complex order parameter, which indicates the phase transition. The one-particle density matrix can be derived by

$$n(\vec{r}, \vec{r'}) = \left\langle \hat{\Psi}^\dagger(\vec{r})\hat{\Psi}(\vec{r'}) \right\rangle. \tag{2.113}$$

In the case of superfluidity, where all boson are delocalized and the wavefunction is extended over the whole system, the probability to detect a boson at a special position $\vec{r}$ is equal at every position $\vec{r}$, even for $r \to \infty$. That implies

$$n(\vec{r}, \vec{r'}) = n(\vec{r} - \vec{r'}) = n_0 \qquad \text{as} \qquad r \to \infty. \tag{2.114}$$

This means, because two indistinguishable particles can change places with each other over a arbitrary large distance, each particle can be considered as delocalized throughout the whole system. This order is called *off diagonal long range order* (ODLRO) [47, 52].

supersolid order

For a superfluid system, which breaks translational symmetry, the density of the superfluid fraction at $T = 0$ is smaller than the average density

$$\rho_s(T = 0) < \bar{\rho}, \tag{2.115}$$

because of the existence of the normal fraction [52]. This means, the superfluid fraction $\frac{\rho_s}{\bar{\rho}}$ never reaches unity in a supersolid, not even at $T = 0$. The supersolid order is then characterized by the combination of the LRO and the ODLRO, which occur simultaneously and for the same species of particles. The system is superfluid, what means, that the particles are delocalized all over the whole system (ODLRO) and additionally there is a non-vanishing density deviation $\delta\rho(\vec{r}) \neq 0$ which depends on the position $\vec{r}$ and lowers the translational symmetry. Considering this work I found a phase where the system is described by a nontrivial density-modulation. The corresponding superlattice period is two times bigger than the primary unit cell and includes simultaneous solid and superfluid qualities. This is discussed in Chapter 5.

Chapter 3

Ultracold bosons in honeycomb lattices

In this chapter I give a short overview of the algorithm used in the simulation program. I study the basic features of an one component system in order to determine whether the system is superfluid or it is in the Mott insulator state. To characterize the crossover regime, the particle fluctuations, the on-site correlation function, and the first excitation energy is studied. The combined results caused the crossover regime very well. Next, a one-component system in a honeycomb lattice with a triangular lattice structure is described. The triangular sub-lattice is shifted by an energy ϵ, which I discuss for varying lattice-depths and for different particle numbers, generating several particle-distributions and crossovers between superfluid and Mott insulator states in the different sub-lattices.

3.1 Algorithm and system

As mentioned above, this work has been done in the framework of exact diagonalization with periodic boundary conditions, using the Bose-Hubbard model for a one- and two-component bosonic systems. It is based on an algorithm developed by Dr. Dirk-Sören Lühman [54] and was primarily designed to simulate Bose-Fermi mixtures. For this project it was rebuild for a one- and two-component Bose gas. I start by describing basic features to introduce the system in more detail. Fig. 4.2 shows the cells we used for calculations (red areas) and their next neighbors. Due to the periodic boundary conditions, atoms leaving the cell by tunneling, automatically reenter the cell at the opposing side. To investigate the crossover between the superfluid and the Mott insulator state in our system we have to consider fluctuations, on-site correlation, as well as the energy eigenvalues. The Fock basis set $|N\rangle$ is generated by successively filling the states to the maximum particle number. Then, only non-vanishing matrix elements have to be
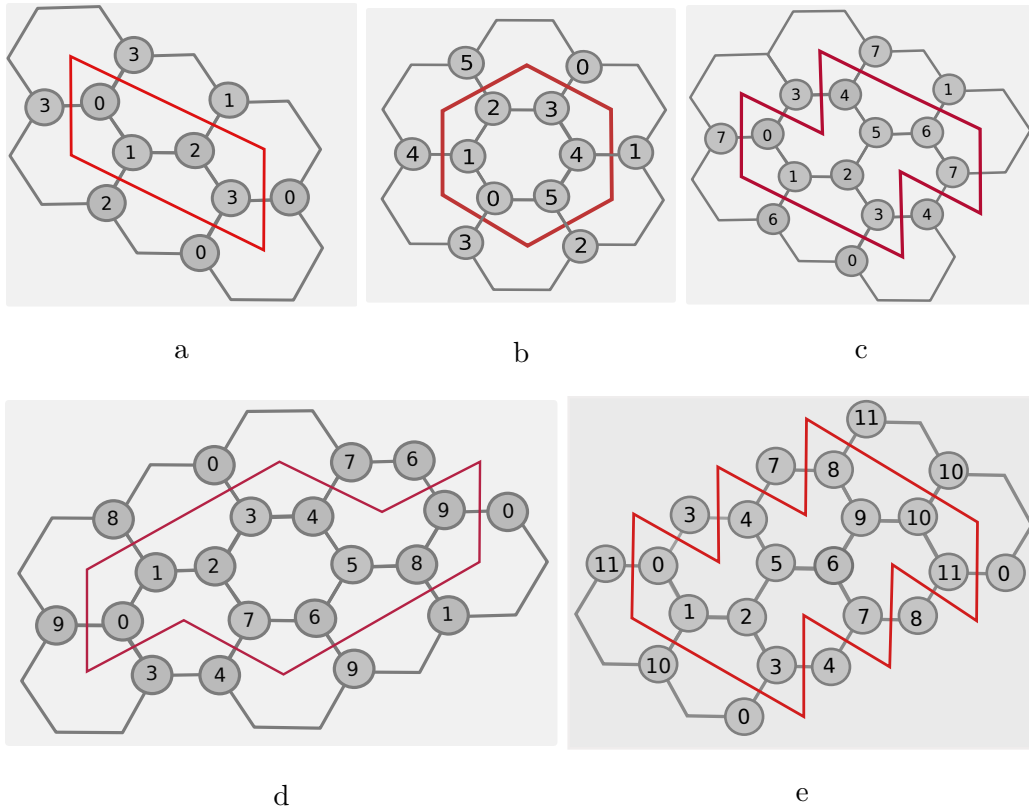
Figure 3.1: Visualization of the honeycomb unit cells used for calculations in this work. a) The four-sited cell b) The six-sited cell c) The eight-sited sized cell d) The ten-sites cell e) The twelve-sited sized cell

calculated

$$\langle N'|H|N\rangle. \tag{3.1}$$

have to be evaluated (see 2.4.6). After obtaining the eigenvalues and eigenvectors of the Hamiltonian

$$E_i \qquad \text{and} \qquad |\psi_i\rangle = \sum_n c_n^i |N\rangle, \tag{3.2}$$

the system can be described completely. Particle occupations $\langle \hat{n}_{i,n}\rangle$

$$\langle \hat{n}_i\rangle = \langle \psi_i|\hat{n}_i|\psi_i\rangle \tag{3.3}$$

and fluctuation $\langle \Delta n\rangle$ can be calculated for the ground and the exited states

$$\langle \Delta n\rangle^2 = \langle \hat{n}^2\rangle - \langle \hat{n}\rangle^2. \tag{3.4}$$

Specific correlation-function can be derived, like e.g. the g_{ij}^{AA}-correlation function, which counts all contributions to the state $|\Psi_n\rangle$ that contains a particle A at site i and a particle A at site j:

$$g_{i,j}^{AA} = \langle \hat{g}_{i,A}\hat{g}_{j,A} \rangle = \langle \Psi_n|(\hat{g}_{i,A}\hat{g}_{j,A})|\Psi_n\rangle. \tag{3.5}$$

3.1.1 Fluctuations and On-site correlations

The particle number fluctuations is defined as

$$\langle \Delta n \rangle^2 = \langle \hat{n}^2 \rangle - \langle \hat{n} \rangle^2. \tag{3.6}$$

I gives information about the system, for example whether it is an a superfluid phase (high particle fluctuations) or in a Mott insulator phase (no particle fluctuations). See Section 2.6 for more background. Due to the finiteness of the system, no critical value of U/J for the occurrence of phase transition can be obtaines, but there is a finite cross-over regime between the superfluid and the Mott insulator phase. To estimate whether the system is in the superfluid or in the Mott insulator phase, the on-site correlations have to be considered as well. In the superfluid regime, the on-site interaction is small compared to the kinetic energy. Therefore the ground state contains Fock states with high particle numbers at one lattice site, and the AA-on-site correlations are high. In the Mott insulator regime, where the bosons are pinned at the sites and the high on-site interaction prohibits a higher occupation than one particle per site, the AA-on-site correlations are low. Indeed they converge to 1 at filling $\eta = 1$, i.e. one particle per site (see Fig. 3.2 b). The AA-on-site correlation function for the ground-state is given by:

$$g_{AA} = \frac{1}{n}\sum_{i=0}^{n} \langle \Psi_0|\hat{n}_{i,A}(\hat{n}_{i,A} - 1)|\Psi_0\rangle. \tag{3.7}$$

Shown in Fig. 3.2 a are the fluctuations for different sized unit cells with $\eta = 1$. We see that the less particle fluctuations in the Mott insulating regime for increasing cell sizes. This corresponds to the fact, that in infinite systems the superfluid to Mott insulator transition is prompt and prohibits fluctuations. The AA on-site correlation functions show a similar behavior for increasing U/J ratio. The larger the cell becomes, the faster the correlations decrease (see 3.2 b). In case of the twelve-sited cell and increasing U/J, states with twelve particles at on site are avoided immediately. However, in the crossover regime, many states with similar energy contributes to the groundstate, which leads to a slow decrease of particle number fluctuations and AA-on-site correlations. Above the threshold of $U \approx 12J$, the fluctuations and the AA-on-site correlations are suppressed for increasing cell sizes. Figure 3.3 show the particle number fluctuations of an eight sided cell for fillings $\eta \in \{1, 1.5, 2\}$. First we note the high fluctuations in case of $\eta = 1.5$ and $U/J \geq 20$, i.e. the system can not be driven in the Mott insulating phase. For the example of an eight sided cell, $\eta = 1.5$ means we have 8 localized
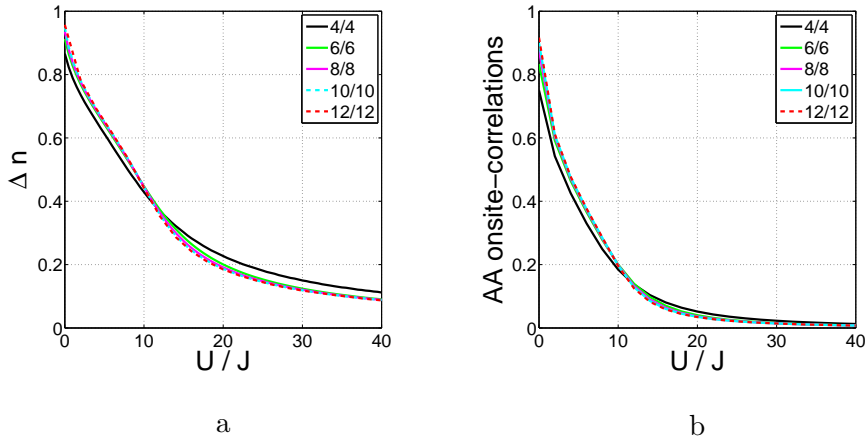
Figure 3.2: Shown here are the a) particle fluctuations and b) on-site correlations for filling $\eta = 1$ and different sized cells: -four sites, -six sites, -eight sites, -ten sites and twelve sites

atoms ($\eta = 1$) plus four extra atoms that are completely delocalized. Since all lattice sites are equal, all sites have the same probability to be occupied by one of the extra atoms. In this case four particles fluctuate between eight sites on top of the uniformly insulating background. For non commensurate filling or in disordered systems, no Mott insulator phase can be reached [55, 61].

In case of double filling ($\eta = 2$), a Mott insulating state can be formed by locating exactly two bosons on every lattice site. The fluctuations decrease fast between the superfluid and the crossover regime, but compared to $\eta = 1$ the systems reaches the Mott insulating phase at higher lattice depths. Filling the system with $\eta = 2$ effectively causes a lowering of the lattice height and enables the particles to tunnel even in deeper lattices. In the crossover regime many states with the same energy occur (much more than for a system with $\eta = 1$). The transition to the Mott state is reached for increasing U/J. Then basis states with many particles at one site do not contribute to the ground state because of the additional cost of energy. According to mean-field calculations [26, 76] the transition occurs at $(U/J)_c \approx z \times 9.9$ for filling $\eta = 2$ and at $(U/J)_c \approx z \times 5.83$ for filling $\eta = 1$. The quantity z is the number of next neighbors. In case of $U = 0$, the fluctuations increase with the filling, they show a square root dependency on the filling factor η (see Fig 3.3 b). Figure 3.4 shows the influence of the lattice cell size to the fluctuations. For an eight sited cell filled with eight bosons (cyan dashed line), the decrease of the fluctuations is more significant compared to six sites with six particles (magenta dashed line). In the limit of an infinite lattice this would result in a clear superfluid to Mott insulater transition at a certain $(\frac{U}{J})_c$. For filling
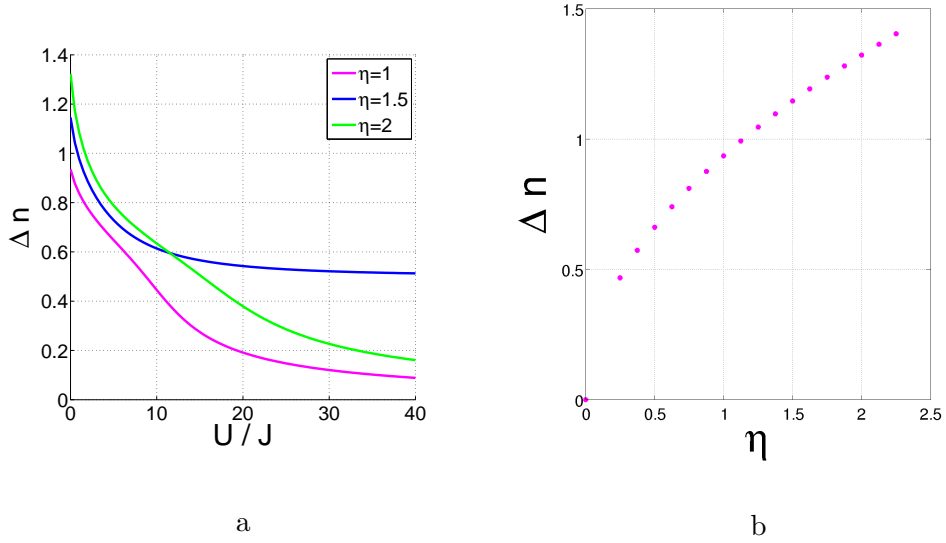
Figure 3.3: Shown a) are the Particle fluctuations for different fillings of the eight sited cell. The eight sited cell is filled with eight bosons (magenta line), with twelve bosons (blue line) and with 16 bosons (green line) for increasing U. Shown in b) are the fluctuations for $U/J = 0$ which show a square root dependency of the filling factor η in case of an eight sited cell.

$\eta = 2$ (e.g. twelve particles in a six sited cell or sixteen particles in an eight sited cell) we see a similar behavior as for $\eta = 1$. The fluctuations are decreasing for increasing cell sizes. In case of incommensurate filling $\eta = 1.5$ no difference can be seen above the threshold of $U \approx 3J$ between the blue dashed line (nine particles by six sites) and the green dashed line (twelve particles by eight sites). In the superfluid regime the fluctuations are higher for the eight sited cell, than for the six sited cell. For increasing cell sizes the fluctuations increase and in the limit of an infinite system it is expected to converge to 1 in case of $U/J = 0$ and filling $\eta = 1$. Increasing the filling factor η also increases the particle fluctuations.

3.1.2 Energy gap

Another reference point for the phase transition from superfluid to Mott insulator is the energy gap between the ground and the first exited state [30]. In the Mott insulator phase, the excitations are discrete. Given a Mott insulator ground state, a first excited state can be created by moving one atom to an already occupied site. For example $|11111102\rangle$ is a lowest excitation state, separated by U from the ground state $|11111111\rangle$. Therefore, the energy gap grows linearly with U in the Mott phase. But since dealing with finite systems, there is always an
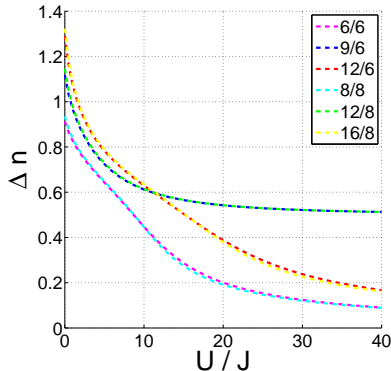
Figure 3.4: The particle fluctuations for a six-sited cell (magenta, blue and red dashed lines) and for an eight sited cell (cyan, green and yellow dashed lines) in case of different filling $\eta = 1$, $\eta = 1.5$ and $\eta = 2$. The two more sites cause already an decreasing effect on the fluctuations in the Mott insulator regime for commensurate filling.

energy gap, also deep in the superfluid regime, even for small on site interaction U. This is a consequence of the finite number of possible excitations. The energy quantization can be estimated by $\frac{1}{L^2}$ with L being the cell length, i.e. the energy gaps become smaller for increasing sample size. Then, the excitations become continuous in case of macroscopic samples in the superfluid regime. In Fig 3.5 a, the energy gap is shown for different cell sizes. For the six, the eight, and the ten sited cell I find a particular kink around $U/J \approx 10$. As shown in Fig. 3.5b, the derivative of the energy gap is discontinuous for cells of more than 4 sites. The four sited cell is simply too small to give reliable results. Another important fact is that all derivatives reach a constant value, namely 1, this means a linear increase with U, around $U/J \approx 20$. For increasing cell sizes the linear regime is reached at smaller values of U. The derivative of the energy gap in case of the ten sited cell converge faster to the value 1 than the one corresponding to the eight and the one corresponding to the six sited cell, see Fig. 3.5 b. So although we only can investigate finite sized systems and therefore are not able to identify a clear superfluid to Mott insulator transition, we have good reasons to get to the conclusion that a system beyond $U/J \approx 20$ with six or more sites and filling of $\eta = 1$ is in the Mott insulator phase. Since we noticed the jump of the derivative for all cell sized except for the 4 sited cell, we will focus the discussion on the eight sited cell filled with eight particles from now. We already mentioned above that the energy spectrum is discrete for finite sized systems, even in the superfluid regime. Shown in Figure 3.6 a are the ground state energy E_0 (blue line) and the four lowest exited energies E_1 (green), E_4 (red), E_7 (cyan), and E_8 (magenta), with increasing on-site interaction U. It has to be noted, that the energy eigenvalues E_2 and E_3 (E_5 and E_6) are degenerated to the energy eigenvalue E_1 (E_4). The kink in the energy gap results from the fact, that at a certain value U/J the forth exited energy eigenvalue crosses the first exited energy eigenvalue. Even the higher energy eigenvalues cross each other for smaller on-site interaction. In Fig. 3.6 b this can be evaluated further by following the Mott characteristic $|11111111\rangle$-
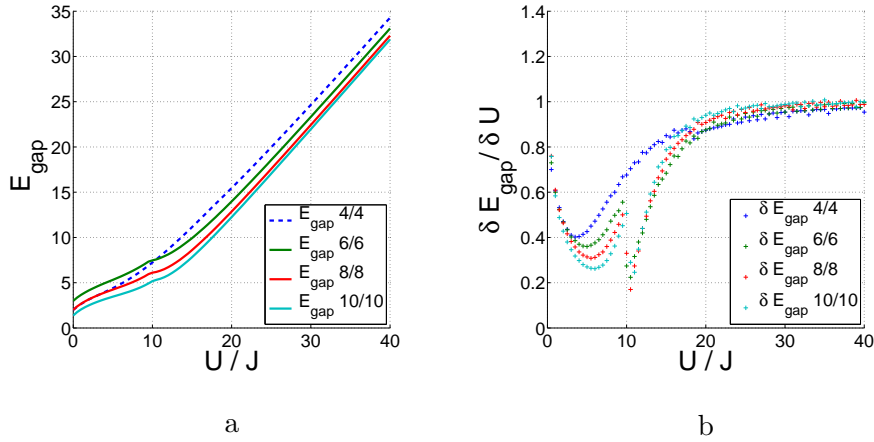
Figure 3.5: a) The energy gap for filling $\eta = 1$ and different sized cells and b)the derivatives dE_{gap}/dU

contribution to the different eigenstates, where $|11111111\rangle$ means a state where every lattice site is occupied with one single atom. As it can be identified in Fig. 3.6 b the $|11111111\rangle$-contribution to the groundstate Ψ_{E_0} increases for increasing on-site interaction (blue line). The contribution of the Mott characteristic state to the higher eigenstates increases first till $U \approx 8J$ and then it decreases. In the regime $5 \leq U/J \leq 6$ it contributes to Ψ_{E_8} (magenta line), in the regime $6 \leq U/J \leq 7$ it contributes to Ψ_{E_7} (cyan line), in the regime $7 \leq U/J \leq 10$ to Ψ_{E_4} (red line), and in the regime $U/J \geq 10$ it contributes to Ψ_{E_1} (green line). At the crossing point of the energy E_4 and E_1 the energy gap shows the kink and for further increasing U/J the contribution of the Mott characteristic state to the groundstate dominates the contribution of the Mott characteristic state to the first exited state. In the regime of $U/J \geq 20$ it amounts to 90%, that denotes the crossover to the Mott insulator. For increasing number of sites, the gap discontinuity becomes significantly smaller; considering that for growing system sizes the energy splitting gets more and more finely graduated and ends up in a continuous spectrum for infinite systems in the superfluid regime. Entering the Mott insulater, the energy gap is given by U. In case of incommensurate filling, the energy gap in dependence of U/J is depicted in Fig. 3.7 a for a filling of $\eta = 1.5$. It is striking, that there is no kink and after a fast increase of the energy gap, after $U \approx 10J$ it remains nearly the same; this means, the derivative is zero (see Fig. 3.7b). Both is not astonishing, no Mott characteristic state can occur. The dominating contribution in the Mott insulator is given by the superposition of $|121212\rangle$ and $|212121\rangle$. It is clear, that the linear increase of the energy gap in the Mott insulator regime does not occur because the system stays in the described
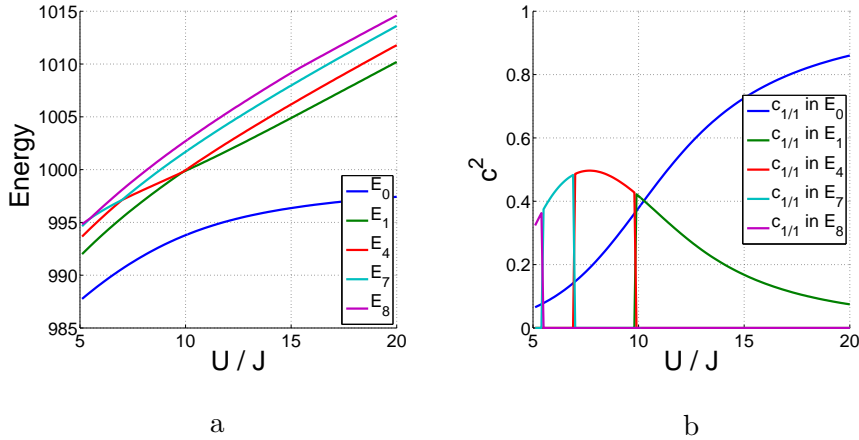
Figure 3.6: a) The energy eigenvalues E_0 (blue), E_1 (green), E_4 (red), E_7 (cyan), and E_8 (magenta) for the eight sited cell filled with eight bosons. E_2 and E_3 (E_5 and E_6) are degenerated to the energy eigenvalue E_1 (E_4). At the crossing point of E_4 and E_1 the energy gap shows the kink.
b) The contribution of the Mott characteristic $|11111111\rangle$-state to the different eigenstates. Whereas the superfluid regime is characterized by a "Mott"-characteristic state with high energy ($E_8 \rightarrow E_1$), in the Mott insulator this state becomes the groundstate.

state with eight by eight and four additional particles which fluctuate between the sites, regardless of the on-site-interaction. Notice, that it is the energy difference, which is examined, therefore it does not depend on onsite U. Another interesting case presents the double filled lattice $\eta = 2$, Fig. 3.8 displays (a) the energy gap between the first exited state and the groundstate and (b) the derivative for the case of twelve particles on six sites. As expected, the crossover regime from the superfluid to the Mott insulator state starts, compared to the case $\eta = 1$, for larger on-site-interaction. The $|222222\rangle$-state provides its largest contribution to the exited states until $U \approx 16J$. For increasing U the $|222222\rangle$-state heavily contributes to the energy ground state, this denoted a macroscopic occupation of the $|222222\rangle$-groundstate beyond $U \approx 17J$. This can be identified directly in Fig. 3.8 , where the energygap denotes this transition. Furthermore, it is obvious that the derivative reaches the constant value **1** for increasing lattice depth at $U \approx 40J$. In case of a double filled lattice, the density of states is much larger and therefore more fluctuations occur even for increasing U/J, causing the shift of the crossover to higher lattice depths. In mean-field calculations [26, 76] for a honeycomb lattice ($z = 3$) at filling $\eta = 2$, the superfluid to Mott insulator transition would emerge at $(U/J)_c \approx 30$.
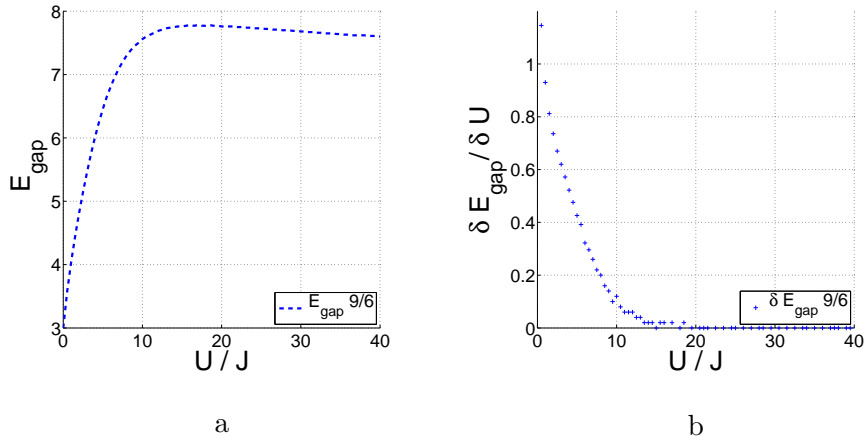
Figure 3.7: a) The energy gap for nine particles on six sites and b)the derivative dE_{gap}/dU. In case of incommensurate filling the system can not reach the Mott insulating phase.
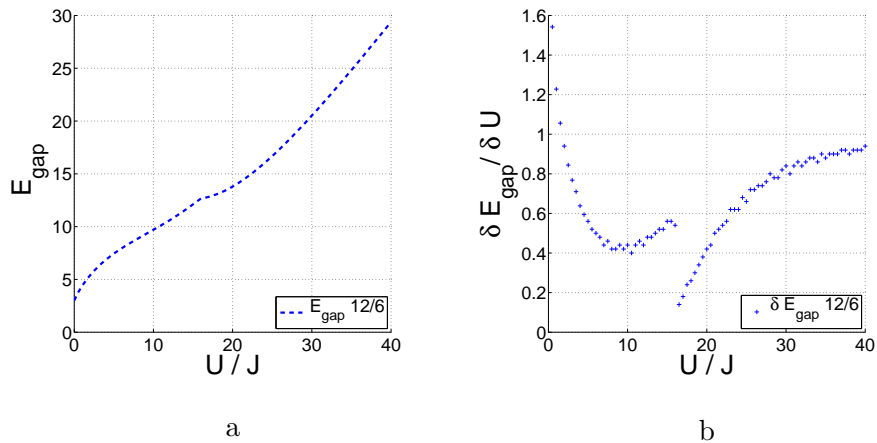

Figure 3.8: a) The energy gap for twelve particles on six sites and b)the derivative dE_{gap}/dU. Since for an increasing filling factor, the Mott insulator is reached for increasing values of U/J, the kink in the energy gap occurs also for increasing values of U/J.

3.2 Ultracold bosons in honeycomb lattices with sub-lattices structure

After investigating the basic features of our system, we study the groundstate of a bipartite honeycomb lattice with a triangular sub-lattice structure and a

variable shift ϵ between the two sub-lattices (see Fig 3.9 a). This energyshift can be implemented by a spin depending lattice potential as discussed in Chapter 2.2.2. In this section we use a unit cell of six sites. We only discuss filling with one kind of bosons and we focus on fillings between $\eta = 0.5$ (three bosons) and $\eta = 2$ (twelve bosons). The sub-lattice structure is depicted in Fig. 3.9 b, due to an energy-shift of ϵ between the sub-lattices the bosons prefer the energetically lower sub-lattice in general, until the on-site-interaction U/J is in the order of ϵ. At this point an occupation of the energetically higher sub-lattice becomes also convenient for the system, to avoid on-site interaction. The corresponding Bose-Hubbard-Hamiltonian can be written as

$$\mathbf{H}_{BH} = - \quad J_A \sum_{i,j} (\hat{a}_{i,}^\dagger \hat{a}_j + cc) + \frac{U_A}{2} \sum_i \hat{n}_i (\hat{n}_{i,} - 1) + \epsilon \sum_i \hat{n}_i, \qquad (3.8)$$

where J_A is the hopping, U_A is the on-site interaction, and ϵ is the energy shift between the sub-lattices, see Fig. 3.9 b. The particle number fluctuations in
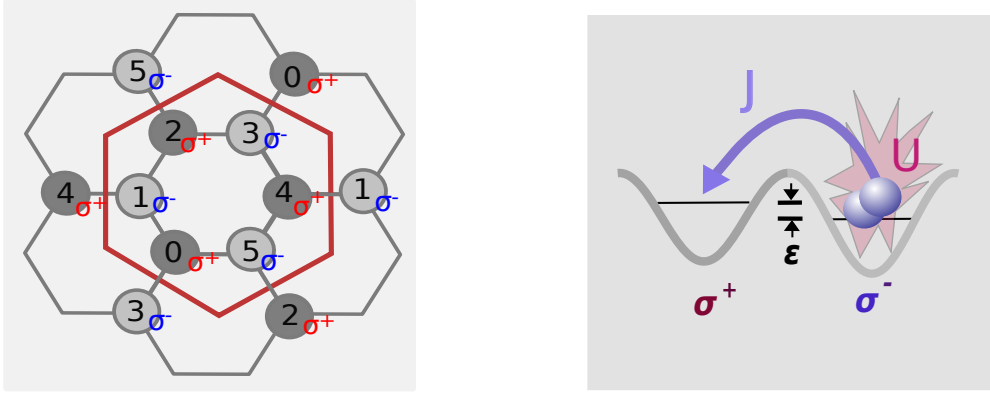

Figure 3.9: Shown here is (a) the six site unit cell with σ^+ and σ^- polarized sites of the sublattice structure and (b) The Potential of the sub-lattice structure with an energyshift ϵ.

the different sub-lattices are a a quantity to measure the localization of the particles and therefore allows for observing the superfluid to Mott insulator transition (3.1.1):

$$\langle \Delta \hat{n} \rangle^2 = \langle \hat{n}^2 \rangle - \langle \hat{n} \rangle^2. \qquad (3.9)$$

The Figures 3.10-3.17 display the particle fluctuations and the occupation number per lattice site of a one-component Bose gas in a bipartite honeycomb lattice for different filling factors. On the left side of each figure is the data of the energetically higher sub-lattice (H-sub-lattice) and on the right side is the energetically lower sub-lattice (L-sub-lattice) displayed. The x-axis denotes U/J, the interaction strength relative to the lattice depth, and the y-axis denotes the energy-shift ϵ between the two sub-lattices. Figure 3.10 shows the fluctuations in case of $\eta = 0.5$,

i.e. three particles in a lattice of six sites. As discussed in section 3.1.1, such a system can not form a homogeneous Mott insulator phase. The red area in the lower left corner indicates a homogeneous superfluid phase over the whole lattice. For high energy differences and small on-site interaction we note a depopulation of the higher sublattice and a superfluid phase with $\eta_L = 1$, in the energetically lower sub-lattice. For on-site interaction $U/J \geq 20$ and a high energy-shift ϵ the energetically lower sub-lattice reaches the Mott insulator phase. For low energy difference ϵ and increasing on-site interaction U the particles are delocalized due to non-integer filling $\eta = 0.5$. This understanding is confirmed by the occupation number, displayed in Figure 3.11. In case of vanishing energy difference the filling is $\eta = 0.5$ in both sublattices. In case of high energy difference, the H-sublattice is depleted, whereas in the L-sublattice emerge a filling $\eta = 1$. Figure 3.12 shows the particle number fluctuations for a six sited cell at filling $\eta = 1$ (six particles per cell). In both sub-lattices superfluid phase emerge at small energy shifts ϵ and small on-site interactions U, the occupation number equals to 1 (see Fig. 3.13. For an increasing energyshift the H-sublattice is depleted, the occupation number converge zero. Moreover, a superfluid phase in the energetically lower sub-lattice with filling $\eta_L = 2$, meaning six particles on three sites, can be observed. Increasing U/J at large sub-lattice splitting leads to a superfluid to Mott insulator transition in the energetically lower sub-lattice with $\eta_L = 2$. The energetically higher sub-lattice remains empty in this parameter area. For $\epsilon \approx U$, a crossover regime can be identified where the energetically higher sub-lattice is re-populated with $\eta_H = 0.5$ and $\eta_L = 1.5$ in the energetically lower sub-lattice. For $U/J >> \epsilon$ and $\epsilon = 0$ we observe both sub-lattices in a homogeneous Mott insulator phase with $\eta_H = \eta_L = \eta = 1$ (one particle per site).
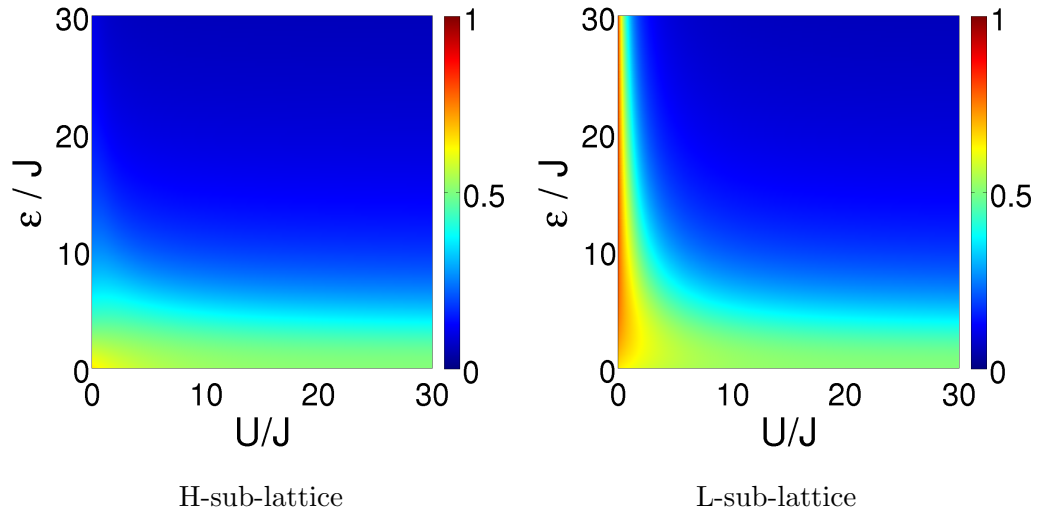
H-sub-lattice   L-sub-lattice

Figure 3.10: Fluctuations of a one component Bosegas in a bipartite honeycomb optical lattice for filling-factor $\eta = 0.5$. For high energy difference and small U/J a superfluid phase in the L-sublattice occurred, this is driven to the Mott insulator with $\eta_L = 1$ in the L-lattice for increasing values of U/J. In case of a small energy difference, no Mott insulator can be reached, due to half filling.
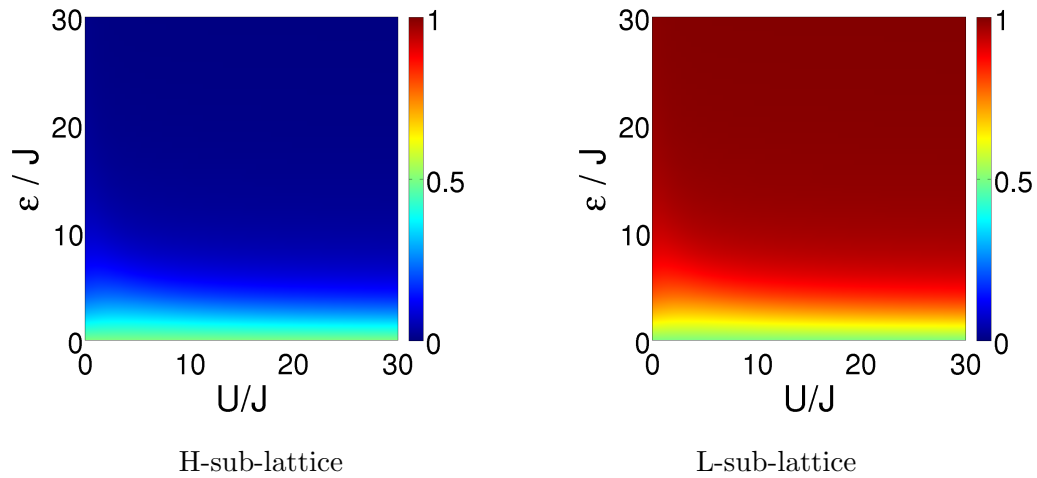

H-sub-lattice   L-sub-lattice

Figure 3.11: Occupation of a one component Bosegas in a bipartite honeycomb optical lattice for filling-factor $\eta = 0.5$. In case of high energy difference, the H-sublattice is depleted. For small on-site interaction a superfluid occurs in the L-sublattice, that is transferred to the Mott insulator in case of increasing U/J with filling $\eta = 1$. In case of vanishing energy difference the filling is $\eta = 0.5$ in both sublattices.
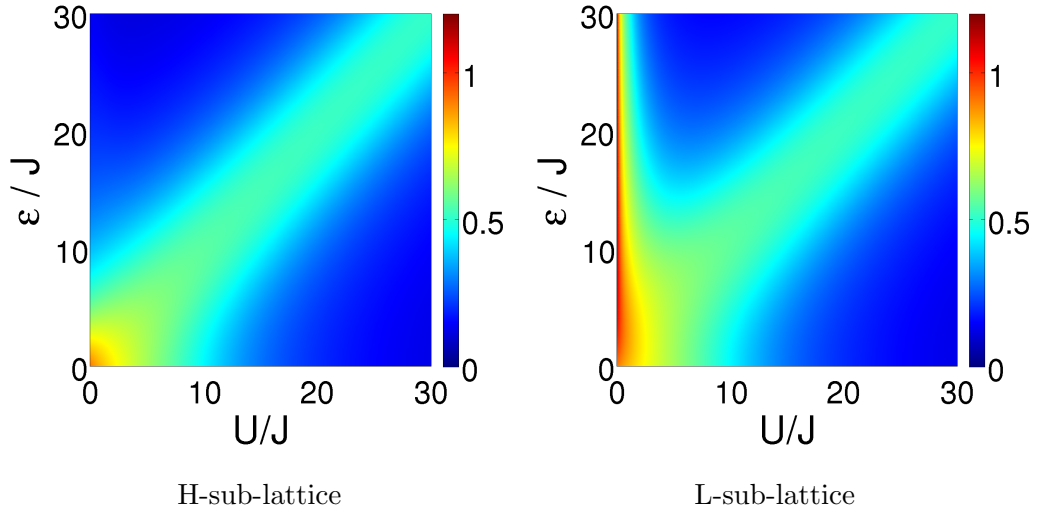
H-sub-lattice   L-sub-lattice

Figure 3.12: Fluctuations of a one component Bosegas for fillingfactor $\eta=1$. For high energy difference and small U/J a superfluid phase in the L-sublattice occurred, this is driven to the Mott insulator in the L-lattice for increasing values of U/J. For high energy difference the Mott insulator occurs in the L- sublattice and with filling $\eta = 2$. In case of a vanishing energy difference, a Mott insulator with filling $\eta = 1$ emerge in the homogenous lattice.
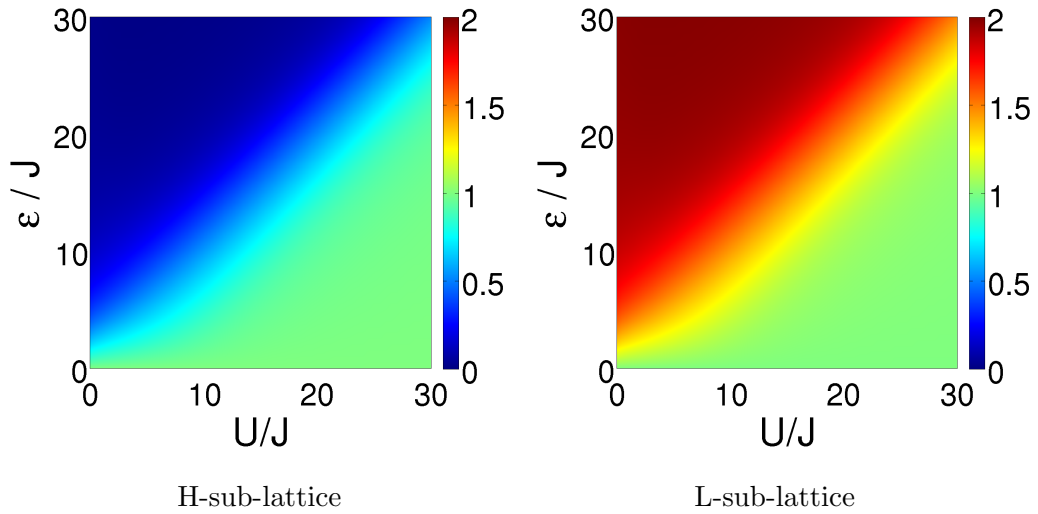

H-sub-lattice   L-sub-lattice

Figure 3.13: The corresponding occupations are shown here for filling-factor $\eta=1$. In case of high energy difference, the H-sublattice is depleted. For small on-site interaction a superfluid occurs in the L-sublattice, that is transferred to the Mott insulator in case of increasing U/J with filling $\eta_L = 2$. In case of vanishing energy difference the filling is $\eta = 1$ in both sublattices. In this case, for small on-site U/J a superfluid emerge, this is transferred to the Mott insulator for increasing U/J.
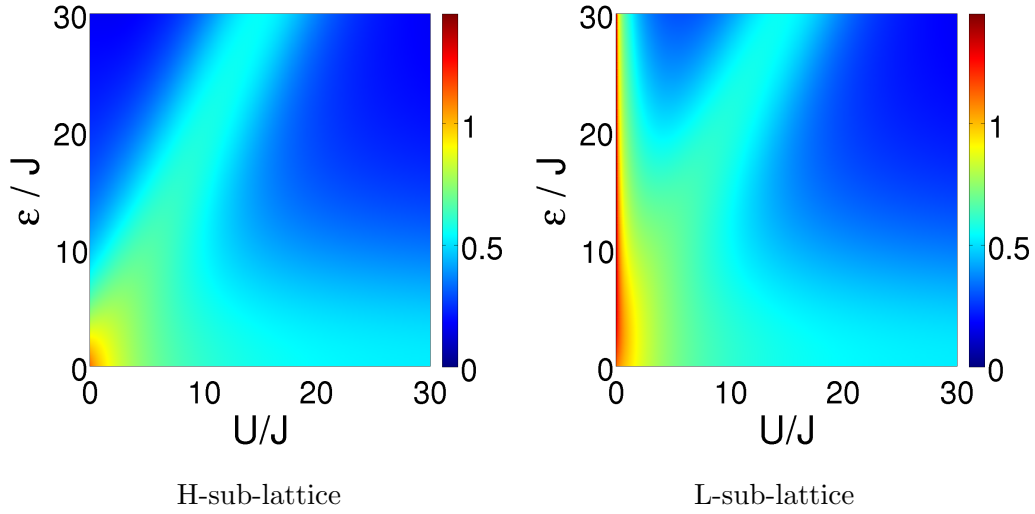
H-sub-lattice

L-sub-lattice

Figure 3.14: Fluctuations of a one component Bosegas in a bipartite honeycomb optical lattice for filling factor $\eta = 1.5$. For high energy difference and small U/J a superfluid phase in the L-sublattice occurred, this is driven to the Mott insulator in the L-lattice with $\eta_L = 3$ for increasing values of U/J. By lowering the energy difference and high U/J the H-sublattice is repopulated, a Mott insulator occurs in the H-sublattice with $\eta_H = 1$, three particles on three sites, and in the L-sublattice with $\eta_L = 2$, six particles on three sites. In case of a small energy difference, no Mott insulator can be reached, due incommensurate filling.
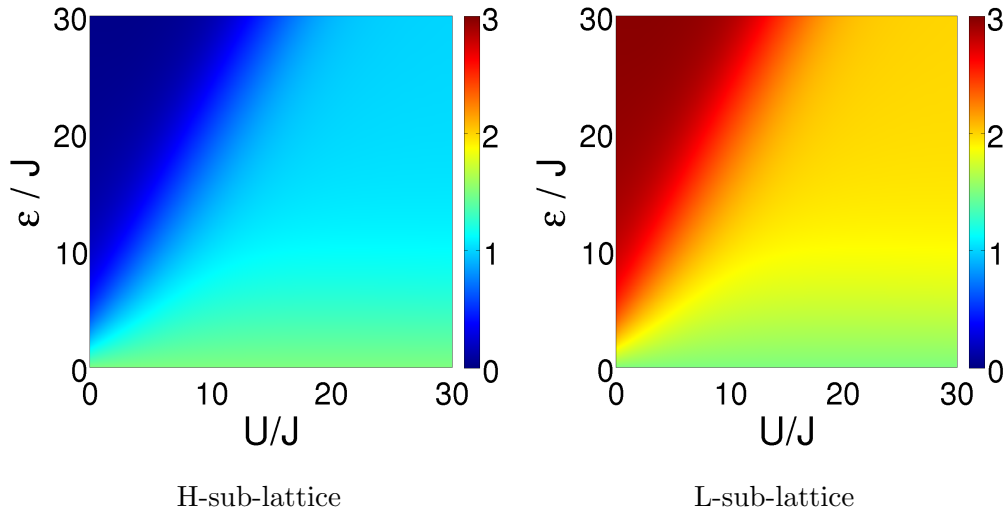

H-sub-lattice

L-sub-lattice

Figure 3.15: The corresponding occupations are shown here. For high energy difference the H-sublattice is depleted and in the L-sublattice every site is in average occupied by three bosons $\eta_L = 3$. Lowering the energy difference, the H-sublattice is repopulated, two different Mott insulators occur with $\eta_H = 1$, and $\eta_L = 2$. In case of a small energy difference, the filling is $\eta = 1.5$ in the homogeneous lattice.
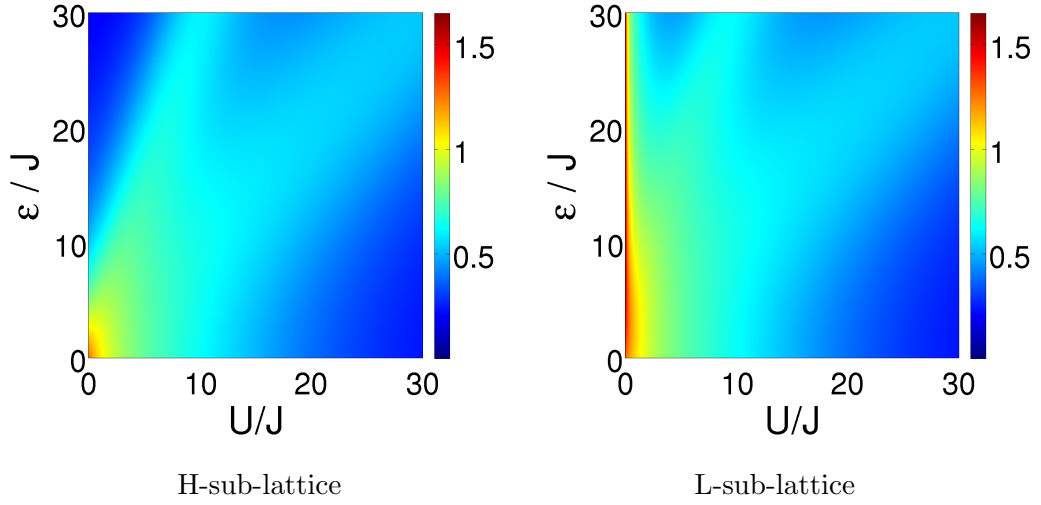
H-sub-lattice

L-sub-lattice

Figure 3.16: Fluctuations of a one component Bosegas in a bipartite honeycomb optical lattice for filling-factor η=2. For high energy difference and small U/J a superfluid phase in the L-sublattice occurred, this is driven to the Mott insulator with $\eta_L = 4$ for increasing values of U/J, the H-sublattice is empty. Increasing U/J leads to a repopulation of the H-sublattice with $\eta_H = 1$, and a Mott insulator in the L-lattice with $\eta_L = 3$. In case of a vanishing energy difference, a Mott insulator with filling $\eta = 2$ emerge in the homogenous lattice.
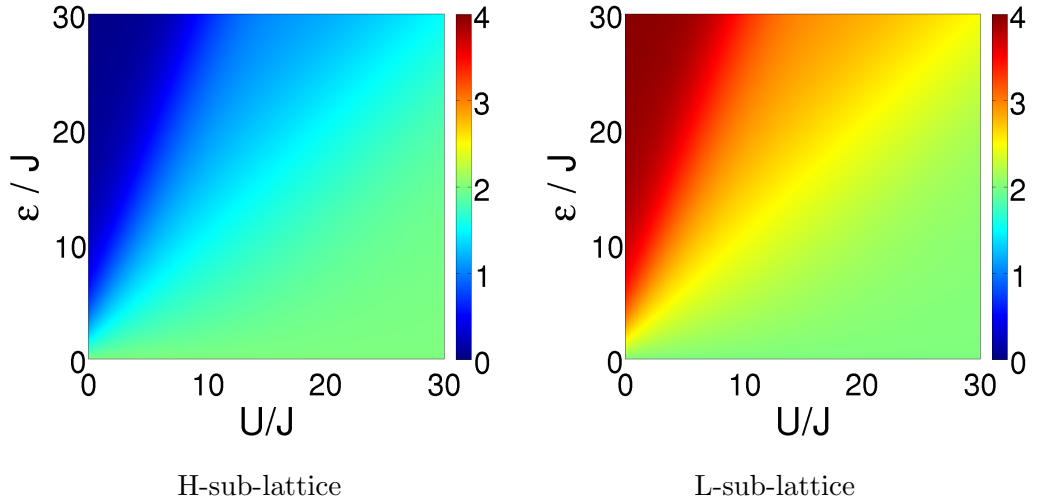

H-sub-lattice

L-sub-lattice

Figure 3.17: The corresponding occupations are shown here. In case of high energy difference, the H-sublattice is depleted and the L-sublattice is populated by 12 bosons, $\eta_L = 4$. For small on-site interaction a superfluid occurs in the L-sublattice, that is transferred to the Mott insulator in case of increasing U/J with filling $\eta = 4$. Increasing U/J leads to a repopulation of the H-sublattice with $\eta_H = 1$, and $\eta_L = 3$. In case of vanishing energy difference the filling is $\eta = 2$ in both sublattices.

The non-integer filling of $\eta = 1.5$ in Figure 3.14 does not allow a homogeneous Mott insulator phase of the homogeneous honeycomb lattice. By increasing the energy difference, the particles move to the energetically lower sub-lattice and depopulate the energetically higher lattice. For high energy differences and increasing U/J ratios, the L-lattice does a superfluid to Mott insulator transition, which results in a filling of $\eta_L = 3$. Then, all nine particles have moved to the three sites of the L-sub-lattice. For further increasing values of U/J a crossover regime is reached, where the energetically higher sub-lattice is re-populated with $\eta_H = 0.5$ and the filling of the energetically lower lattice reduces to $\eta_L = 2.5$. In case of an increased U/J ratio a crossover to a Mott insulator phase with $\eta_L = 2$ (six particles on three sites) in the energetically lower sub-lattice and $\eta_H = 1$ (three particles on three sites) in the energetically higher sub-lattice can be observed. For small energy differences we get a delocalization with $\eta = 1.5$ in both sub-lattices due to non integer fillings. Figure 3.15 shows the occupation number of the L- and the H-sublattice for a better understanding.

In Fig. 3.16 the filling is double, $\eta = 2$. In the lower left corner a superfluid on the whole honeycomb lattice occurs with $\eta = 2$, which means twelve particles on six sites. With an increasing energy difference ϵ between the sub-lattices, a depletion of the energetically higher sub-lattice is emerged and a superfluid phase with $\eta_L = 4$ (twelve particles on three sites) occurs in the energetically lower sub-lattice, which is driven to the Mott insulator phase for increasing on-site interaction. Further increasing the U/J ratio leads to a crossover regime with a repopulation of the energetically higher sub-lattice. Then, the energetically higher lattice has filling of $\eta_H = 0.5$ and the filling of the energetically lower sub-lattice is reduced to $\eta_L = 3.5$, see Fig. 3.17. For increasing U/J, the system is driven to a Mott-insulating phase with $\eta_L = 3$ and $\eta_H = 1$, i.e. nine particles are on the three sites of the L-sub-lattice and three particles are on the three sites of the H-sub-lattice. After crossing the regime with $\eta_L = 2.5$ in the energetically lower and $\eta_H = 1.5$ in the energetically higher sub-lattice, the system changes to a homogeneous Mott insulator with $\eta = 2$, which means twelve particles are equally distributed on six sites.

3.3   Conclusion

The first part of this chapter focused on basic features of the homogeneous honeycomb lattice with special attention to particle fluctuations, on-site correlations, and energy gaps, for commensurate and incommensurate fillings. Furthermore, we investigated the behavior of a system with a triangular sub-lattice structure for different filling factors. We discussed five different cell sizes at filling $\eta = 1$ in terms of particle fluctuations, on-site correlations and energies. The particle number fluctuations show a sharper step at the Mott insulator transition regime when increasing the cell size (see Fig. 3.2 a). This observation is in agreement with meanfield approximations of the superfluid to Mott insulator transition, which

show a prompt transition at the crossover point and vanishing particle fluctuations. Likewise the particle fluctuations, the on-site correlation are reduced more strongly, the bigger the corresponding cell is, see Fig. 3.2 b. In doubly filled systems (for example 16 particles in a eight sited cell), the superfluid to Mott insulator crossing is shifted to higher values of U/J in agreement with mean-field calculations [26, 76]. We also investigated the case of incommensurate filling with $\eta = 1.5$, where the redundant particles fluctuate on top of a uniformly insulating background (see Fig. 3.3). Furthermore, we studied the states of lowest energies in our finite systems and showed the decrease of the energy gap as the cell becomes bigger. A clear indication for the superfluid to Mott insulator crossing is the level crossing of the first exited state and the second exited state around $U/J \approx 10$, where the energy of the "Mott" characteristic $|11111111\rangle$-state decreases. This can be identified as a kink in the energygap. Simultaneously, the contribution of the $|11111111\rangle$-state in the groundstate increases by more than 50% at $U/J \approx 12$. This could be examined in detail for the eight sited cell. Additionally, we could identify a regime beyond $U/J \approx 20$ where the derivative of the energy gap arrives a constant value **1**, which corresponds to a linear increase with U. This denotes that we can expect our finite system to be in a Mott insulating phase at $U/J \approx 20$. Thus I am able to characterize the superfluid and the Mott insulating phase. A superfluid phase implies high particle fluctuations ($\Delta n \geq 0.6$), high on-site correlations (AA-on-site correlations ≥ 0.5), and a "Mott" characteristic $|11111111\rangle$-state with high energy. The Mott insulater phase implies low particle fluctuations ($\Delta n \leq 0.2$), low on-site correlations (AA-on-site correlations ≤ 0.1), and a "Mott" characteristic $|11111111\rangle$-groundstate with exitations linear in U. In case of the eight sited cell, this criteria leads to the conclusion, that we can assume a superfluid regime for $0 \leq U/J \leq 5$, a crossover regime for $5 \leq U/J \leq 20$, and a deep Mott insulater for $U/J \geq 20$. We will use these limit in the following chapters. In case of a sub-lattice structure like described in section 3.2, rich phase-diagrams are derived (see Fig 3.10- Fig 3.17). By changing the ratio of U/ϵ the system can be driven in the Mott insulator phase even for incommensurate filling. In the limit of high a energy difference ϵ all particles occupy the energetically lower sublattice with $n/2$ sites (n being the number of sites) and a filling of 2η. The other sublattice is empty due to the energyshift, however it will be repopulated in the case of increasing U/J, since the rate of repopulation depends on U/ϵ. We could even archive two different Mott insulators in the lattice simultaneously: In the energetically lower sublattice a Mott insulator with three bosons per site and in the energetically higher sublattice a Mott insulator with one boson per site.

Chapter 4

Isomagnetism for bosonic atoms in the Mott insulator regime

While I investigated the groundstates and the superfluid to Mott insulator crossover of a one-component Bose gas in a honeycomb lattice with and without sublattice structure, in the last chapter, my interest is now focused on a mixture of two bosonic species, which both are only subjected to the simple honeycomb structure. This would be valid for two bosons in the $m_f = 0$ state, but in differing F-states. The situation is shown in Fig. 4.1, where $V = V_{AB}$ denotes the interaction between the different kinds of bosons, U denotes the interaction between two bosons of the same kind, whereas $U = U_{AA} = U_{BB}$ is chosen to be equal. Also the hopping J is chosen to be equal ($J = J_A = J_B$) for both boson types. This describe a system, where the scattering amplitude between same kind of atoms is very similar for both atom sorts, whereas the scattering amplitude between different kind of atoms can differ. To investigate finite size effects the system properties
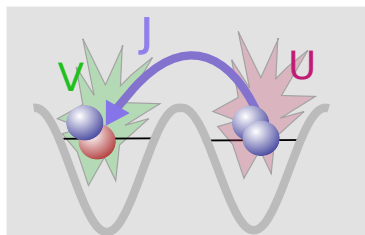

Figure 4.1: Shown here is the above mentioned situation, two different kinds of atoms in a simple honeycomb structure with the hopping $J = J_A = J_B$, the interaction $U = U_{AA} = U_{BB}$ and the interaction $V = V_{AB}$.

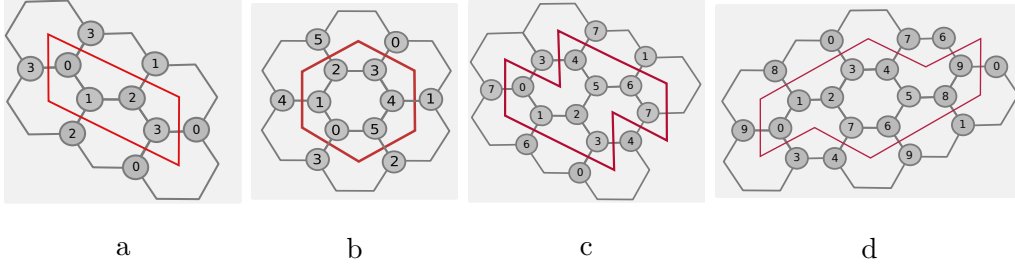have been calculated on the four, the six, the eight, and the ten sited cell.

Figure 4.2: Depicted here are the cells on which the calculations in this chapter have been performed: a) the four-sited cell b) the six-sited cell c) the eight-sited cell d) the ten-sited cell. The twelve-sited cell has not been considered in the two component case, because of the length of the two component basis with 153.165.376 states.

The two-component basis is obtained as a product basis of the basis set for A and B-bosons:

$$|N_i\rangle = |N_{i,A}\rangle \otimes |N_{i,B}\rangle. \tag{4.1}$$

Accordingly the Hamilton matrix has the dimension

$$D_{(n_{AB})} = D_{(n_A)} \times D_{(n_B)}, \tag{4.2}$$

which causes a high numerical effort to evaluate the matrix elements and find the eigensystem. The following quantities characterize the two-component system: The different particle occupations

$$\langle \hat{n}_{i,A} \rangle = \langle \Psi | \hat{n}_{A,i} | \Psi \rangle \tag{4.3}$$

and

$$\langle \hat{n}_{i,B} \rangle = \langle \Psi | \hat{n}_{B,i} | \Psi \rangle \tag{4.4}$$

as well as the density fluctuations,

$$\langle \Delta \hat{n}_{A,B} \rangle = \sqrt{\langle (\hat{n}_A + \hat{n}_B)^2 \rangle - \langle \hat{n}_A + \hat{n}_B \rangle^2} \tag{4.5}$$

which will be evaluated in Section 4.1. In case of a two component Bosegas in a honeycomb structure, it is also an interesting question of how the atoms arrange themselves in the lattice; is there a special order, in particular is it possible to identify quantum magnetic phases, like a ferro- or antiferro-magnetic ordering? A quantum-magnetic correlation function $g_{i,i+1}$ will be developed to study the next neighbor ordering in detail in the Mott insulator as well as in the superfluid phase. In the localized phase with half filling, the atoms are pinned at lattice sites

and one can e.g. distinguish different ordered phases, as depicted in Fig. 4.3, two atoms in two hyperfine-states in an optical lattice can be mapped onto an effective spin-system [22, 48]. Boson A corresponds to spin-up ($|A\rangle \rightarrow |\uparrow\rangle$), whereas boson B corresponds to spin down ($|B\rangle \rightarrow |\downarrow\rangle$). This has been introduced in Section 2.5.1 and is taken up again in Section 4.2. In section 4.2, the magnetic correlations will be calculated for differing cell sizes by evaluating the respective ground states derived from the exact diagonalization of the Bose-Hubbard matrix. I will also discuss the corresponding phase diagram. In section 4.3, the results for different cell sizes are compared to apprehend finite size effects. By computing different correlation functions, we can also, get access to the states and correlations and therefore read out the quantum magnetic ordering, in the superfluid regime. See chapter 5.
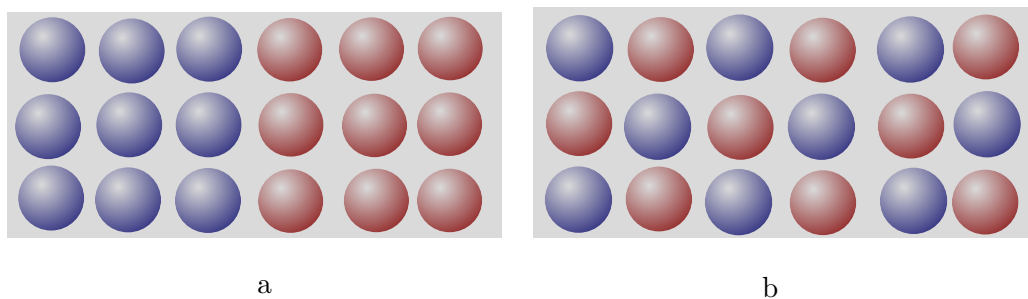

a   b

Figure 4.3: (a) A 'ferromagnetic' groundstate is preferred in case that $U_{AA,BB} < V_{AB}$. Due to virtual tunneling, the atoms would, end up in a state where the same kind of atoms occupy adjoining sites. (b) An antiferromagnetic order evolves, in case of $U_{AA,BB} > V_{AB}$. The atoms preferentially occupy on a site next to the other kind of atoms.

Quantum antiferromagnets are well known and thoroughly investigated also in condensed matter physics. One can reach the classical ground state of an anti ferromagnetic phase by dividing the lattice into two sublattices, so that every site is only neighbored by sites of the other sublattice, this is called *bipartite lattice*. The classical ground state would mean all spins with orientation "up" are arranged in one sublattice and all spins with orientation "down" are arranged in the other sublattice. This classical ground state is also called the "Néel"-state [53]. Consider that it is not an eigenstate of the Quantum Hamiltonian, like we will see in the following.
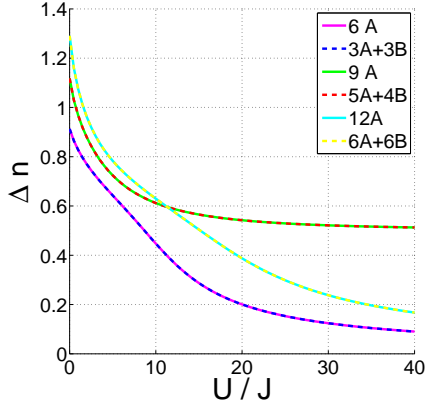
Figure 4.4: To compare the particle fluctuations, in case of $V_{AB} = U_A = U_B$:

- six A-bosons (magenta) or three A- and three B-bosons (blue dashed)

- nine A-bosons (green) or five A- and four B-bosons (red dashed)

- twelve A-bosons (cyan) or six A- and six B-bosons (yellow dashed)

4.1 Fluctuations of a two component Bose-mixture in a honeycomb lattice

To evaluating the behavior of a mixture of two kinds of bosons and investigate, (for example the iso-quantum-magnetism in the superfluid and the Mott insulating phase), we have to modify our operators for the two component case. Due to the incommensurable filling of one boson sort, the single fluctuations are an insufficient indicator for the superfluid to Mott insulator crossover. For a two component Bose gas with half filling for both sorts, the particle fluctuations for each kind of bosons never fall below $\Delta n = 0.5$. As it is possible to reach an insulating phase by distributing $4 + 4$ particles on eight sites one has to consider a more appropriate quantity. The density fluctuations can be determined by

$$\langle \Delta \hat{n}_{A,B} \rangle = \sqrt{\langle (\hat{n}_A + \hat{n}_B)^2 \rangle - \langle \hat{n}_A + \hat{n}_B \rangle^2}. \tag{4.6}$$

This expression counts the fluctuations of each sort, the fluctuations with the same kind and the ones with the other kind. In Fig. 4.4, the fluctuations for the six sited cell are evaluated by comparing a one component filling of six A-bosons with a two component filling of 3 A and 3 B bosons. Obviously, the fluctuations in both cases are the same, if $V_{AB} = U_A = U_B$ and $J_A = J_B$. Since the basis for a two-component mixture is a product basis, consisting of the two basis sets for A- and B- bosons, the number of basis states is much higher. Nevertheless, the count of the particles is equal and with $U = V$ they can be considered as the same sort, producing same energies. With respect to the different particles, no ordering is expected. Quantum magnetism, as described above, requires the distinguishability of the two kinds of atoms. We choose $J_A = J_B = J$ and $U_{AA} = U_{BB} = U$ but $V_{AB} \neq U$ to investigate the occurrence of ferro or anti-ferromagnetic regimes in the superfluid and the Mott insulator phase. These two phases, the superfluid and the Mott insulator, can, even in case of a multicomponent Bose-mixture, be distinguished by their fluctuations (see 3.1.1). In Fig. 4.5, the density fluctuations

Δn_{AB} are shown for the eight sited sized cell, filled with four A- and four B-bosons for the parameter regime $0 \le U \le 60J$ and $0 \le V_{AB} \le 60J$. The density fluctuations vary from 1 (superfluid regime) to zero (Mott insulator regime). For $U \ge 7J$ and $V_{AB} \ge 7J$ the fluctuations reach less than 50 % which means that the crossing to the Mott insulator phase is reached. For small values of U and an increasing $V/$, it strikes that the fluctuations are significantly higher than in the regime for small values of V/J and an increasing U/J. This asymmetry is caused by the different possibilities to build up states in the two limiting regimes. For small values of U/J and increasing values of V/J states can be build with up to four A- or B-particles per site. Only the configurations with AB-combinations are avoided. For small values of V/J and an increasing U/J all configurations which contain more than one A- (B-) particle per site are obviated. The AB-combinations are enhanced, but finally there are much more configurations in case of small U/J and increasing V/J, which effects more fluctuations in this regime. And something else is standing out: For very small values of U and V/J around the origin of the graph, very high fluctuations occur in the groundstate. For an increasing U/J and small values of V/J, the fluctuations decrease, like explained above, and gradually, all multi AA- or BB-occupied configurations are avoided. But for small U/J and increasing V/J, the fluctuations are reduced around $V_{AB} \approx 5J$ and then they become stronger again. This is astonishing because an increase of the interaction normally causes a reduction of the fluctuations. But as we will further investigate in chapter 5. This regime is characterized by a special behavior. For a certain value of V/J the reduction of the AB-occupations enhances the AA- and BB-fluctuations again, the states with four or three A-bosons (B-bosons) per site are found incrementally in the groundstate, which causes the re-rise of the density fluctuation for small values of U/J and an increasing V/J.

4.2 Magnetic correlations

In Section 2.5.1, we derived an effective spin-Hamiltonian in second order perturbation theory in the tunneling in the localized phase ($J \ll V_{AB}, U_A, U_B$) [22, 48]. It is given by

$$H_{int} = -\frac{J^2}{2}(\frac{1}{U} - \frac{1}{V_{AB}})(\sigma_z^i \sigma_z^j - \sigma_-^i \sigma_+^j - \sigma_+^i \sigma_-^j) \tag{4.7}$$

In this chapter, we focus on the z- correlations (out of plane correlations), which are induced by the first part of the effective Spin Hamiltonian. In the regime $U > V \gg J$, the prefactor is positive and an anti ferromagnetic ordering is expected to minimize the energy. In the regime $V > U \gg J$, the prefactor is negative and we expect ferromagnetic ordering to minimize the energy. Since this is only valid in case of $J \ll V_{AB}, U_A, U_B$ it could not be used in the superfluid and in the crossover regime. Since my focus is to examine the whole parameter regime from weak to strong coupling with one single method, I introduced site depending
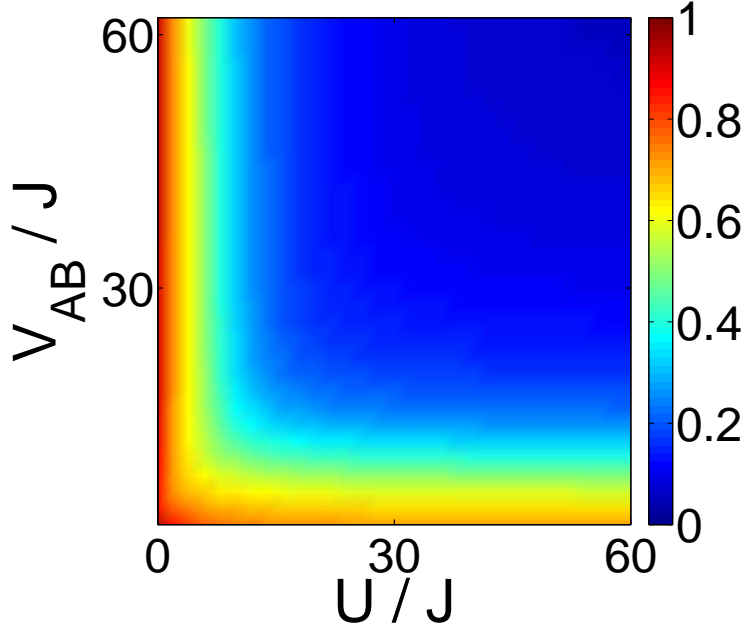
Figure 4.5: The density fluctuations of the system $\Delta n_{A,B}$. If the fluctuations are suppressed, the system is in the Mott insulator phase (blue regime). High fluctuations advert to a superfluid (rainbow colored regime) for small on-site interaction V/J or U/J.

correlation functions in 2.5.2, which allow insight into the behavior of the system in the Mott insulator, as well as in the superfluid phase. The normalized correlation functions for small systems and small particle numbers are given by

$$g_{i,j}^z = \sum_{<i,j>} \frac{(\frac{2n-1}{n-1}FM - \frac{2n-1}{n}AF)}{2 \times (FM + AF)}. \tag{4.8}$$

With AF being the anti-ferromagnetic part and FM being the ferromagnetic part

$$|\psi\rangle = \sum_N c_N |N\rangle$$
$$AF = \sum_N |c_N|^2 (n_{i,A,N} n_{j,B,N} + n_{i,B,N} n_{j,A,N}), \tag{4.9}$$
$$FM = \sum_N |c_N|^2 (n_{i,A,N} n_{j,A,N} + n_{i,B,N} n_{j,B,N})$$

here, $< i,j >$ stands for all next-neighbor-pairs. Fig. 4.6 shows the phase diagram obtained from the 'magnetic' correlations and the density fluctuations for

the eight sited cell (see Fig. 4.6), filled with four A- and four B-bosons. The corresponding ground states are explained accurately in the next section considering also the finite-size effects. It is obvious, that we can distinguish several 'magnetically' ordered states: In the upper left, a regime with ferromagnetic correlations occur, connected with high density fluctuations. Here we find a supersolid phase which is investigated further in chapter 5. In the lower right, high particle fluctuations occur too, but the corresponding correlation function shows rather anti ferromagnetic behavior. This will be also discussed in chapter 5. In the upper middle, deep in the Mott insulator phase, the correlations are ferromagnetic and it will be shown within the next section, that this regime is really characterized by a ferromagnetic ground state. Although the state is influenced by finite size effects the ferromagnetic correlations can clearly be identified. In contrast, the regime in the middle right represents the anti-ferromagnetic Mott insulator which, against all intuition, never reaches a pure Néel state like the one depicted in Fig. 4.3 b. Next neighbor correlations together with density fluctuations are able to distinguish different regimes in the interaction phase diagram. Properties of the different "phases" will be discussed in detail in subsequent sections.
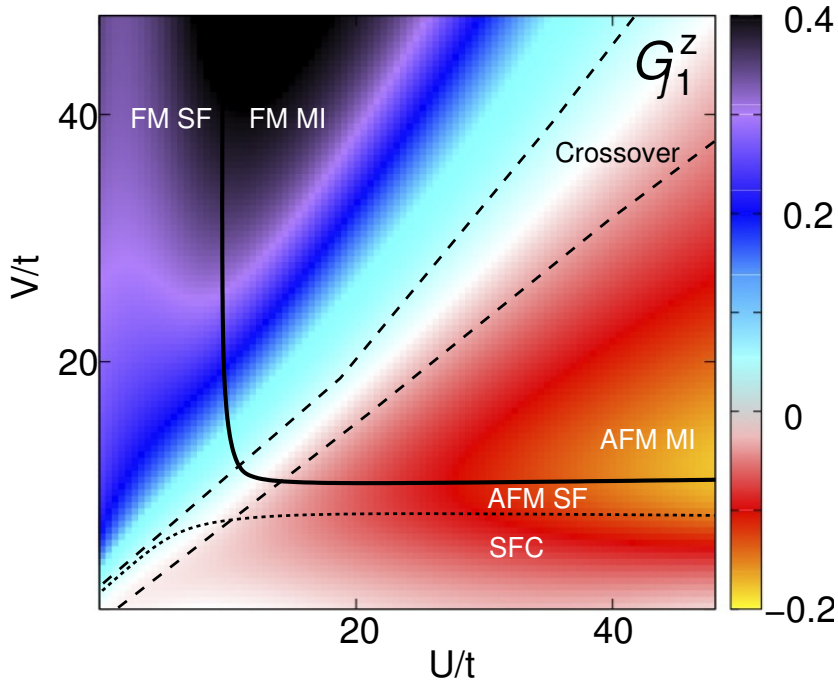
Figure 4.6: The numerical results of the iso-magnetic z-correlations as a function of U and V. The sign of $g^z_{i,j}$ determine the magnetic phases, blue, purple, and black denote ferromagnetic ordering and red and yellow denote anti ferromagnetic ordering. The different phases like FM MI (ferromagnetic ordered Mott insulator), AFM MI (anti ferromagnetic ordered Mott insulator), FM SF (ferromagnetic ordered superfluid), AFM SF (antiferromagnetic ordered superfluid), and SCF (supercounterflow) will be discussed in detail in the the next sections.

4.3 Finite size effects

Since my calculations are restricted to small systems, due to the exact diagonalization method, finite size effects are unpreventable. In the following section I will evaluate these finite size effects for different sized unit-cells with four, six, eight, and ten sites in detail. In all cases we examine a half filling for each bosonic species. Generally speaking, for $V_{AB} < U$ a order is favored, where different atom sorts sitting at adjoining sites, the $g_{i,i+1}$-correlation function has negative values. For $U < V_{AB}$ a ferromagnetic ordering is favored. Then the $g_{i,i+1}$-function has positive values and the groundstate is dominated by an ordering where adjoined sites are occupied by the same sort of atoms. It will be shown, that the ferromagnetic ground state order is explicitly dependent on the size and the geometry of the cell, which influences the results in the ferromagnetic as well as in the anti-
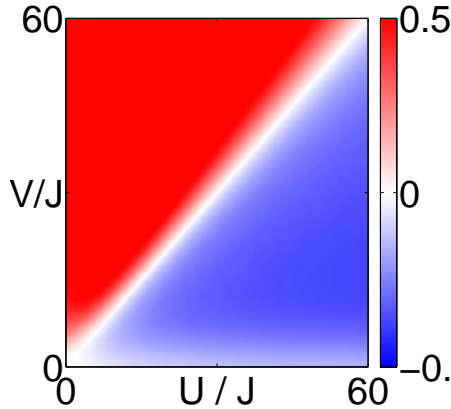
Figure 4.7: The phase-diagram in case of four sites, the sharp transition is caused by the the small cell size: There are only a few possibilities to occupy the sites. The anti-ferromagnetic correlations are extraordinarily high. In a small cell with four sites the quantum-fluctuations are reduced.

ferromagnetic regime. Classically, one would expect an a staggered ground state independent of the size and geometry of the unit cell in the regime for $V_{AB} < U$. But as the quantum fluctuations vary with an increasing number of lattice sites the ground state varies with the cell size also in the anti-ferromagnetic regime. Parts of the wavefunction occur where triples or dimers of the same sort of atoms are embedded in the alternating structure.

4.3.1 The four sited cell

A cell with four sites, as depicted in Fig. 4.9 a, has been introduced in Chapter 3 where it has been shown, that the basic features like fluctuations and ,especially, the jump in the energy gap are not reflected very well because of the small number of sites. A similar problem arises considering the 'magnetic behavior'. Regarding the phase diagram in this case (Fig. 4.7), it stands out, that the transition from the ferro- to the anti-ferromagnetic regime is very sharp and it is situated along the straight line $U = V_{AB}$. In the Mott insulator regime are only six possibilities to distribute two A- and two B-particles on four sites without a double occupation: Two times a staggered lattice (see Fig 4.8 a), two times the chains (see Fig 4.8 b), and two times the dimers (see Fig 4.8 c). Therefore the transition from the ferro- to the anti-ferromagnetic regime is very sharp. Additionally the anti-ferromagnetic correlation is much stronger than in cases of increasing number of sites. This is also caused by the fact, that there are only a few configurations for the atoms to occupy the sites, and hence much less quantum-fluctuations occur (see Fig. 4.9). In the case of $V_{AB} > U$, where $g_{i,i+1}$ has positive values (red regime), the best configuration for half filling are chains of A and B-bosons along the zig zag pattern, see Fig. 4.9 b. Be reminded, that the requirement of zero total polarisation (equal numbers of A- and B-bosons) does not allow for a single monodomain. In this
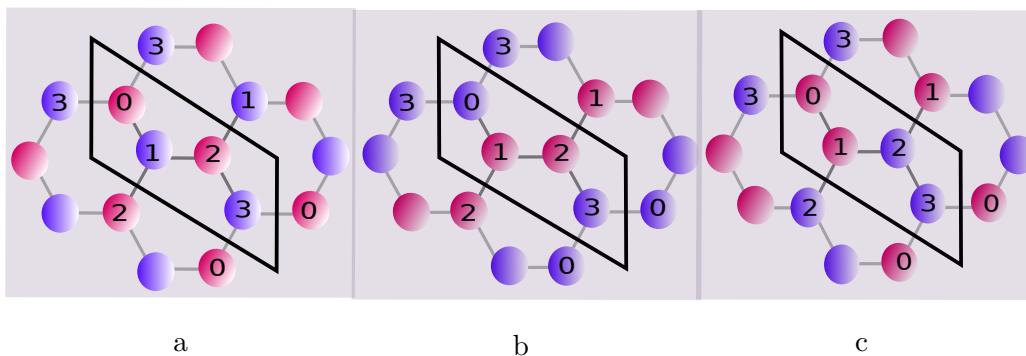
Figure 4.8: Depicted here are the three possibilities in the Mott insulator phase to distribute two A- and two B-bosons at four sites without a double occupation. The staggered (a) and the dimers (c) correspond to the anti-ferromagnetic regime, whereas the chains of A- and B-bosons along the zig-zag pattern (b) correspond to the ferromagnetic regime.

regime the ground state, deep in the Mott phase is given by the superposition of

$$|\Psi\rangle \approx \frac{1}{\sqrt{2}} |1001\rangle_A |0110\rangle_B + \frac{1}{\sqrt{2}} |0110\rangle_A |1001\rangle_B . \qquad (4.10)$$

In the regime $V_{AB} < U$, where the values of $g_{i,i+1}$ are negative (blue regime) one would naively expect an staggered ordered ground state. As this is not possible due to quantum fluctuations the presence of non staggered parts of the ground state wavefunction is given by a configuration of dimers (see Fig. 4.8 c) which are embedded in the alternating structure. As it is shown in Fig. 4.10, this configuration is important in the anti-ferromagnetic regime, providing nearly half of the weight of the anti-ferromagnetic wave function. This will be increasingly important for growing cell sizes. The four sited cell is the only one, where, in the anti-ferromagnetic Mott insulator phase, the staggered parts of the wavefunction provide about 50 %. This contribution decreases for increasing lattice cells. This all shows that the four sited cell reflects insufficiently the behavior of a big sample. Keep in mind that these contributions only consider states with single occupied sites, which means this results are not valid in the superfluid regime.

4.3.2 The six sited cell

The six sited cell (see Fig. 4.12 a) has to be considered separately. Here two special features occur because of its special geometry. First, it is not possible to cluster more than three atoms in a chain. Second, occupation with dimers is also impossible because of the odd particle number (three A- and three B-atoms). Due to this properties some abnormalities occur in the $g_{i,i+1}$-correlation diagram (see Fig. 4.11). Overall, the ferromagnetic correlations are smaller, than for any
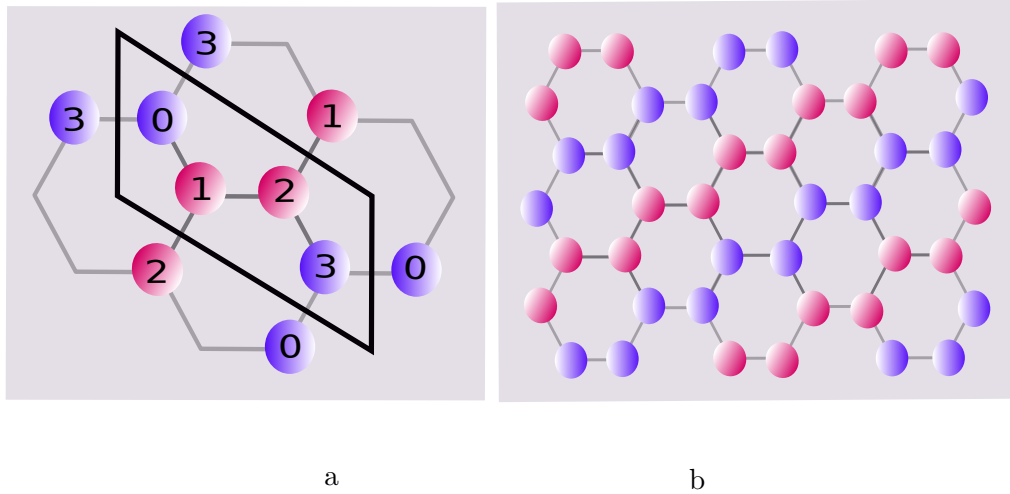
Figure 4.9: Shown here is the unit cell with four sites with its nearest next neighbors (a) and the lattice configuration in the ferromagnetic 'phase' (b).
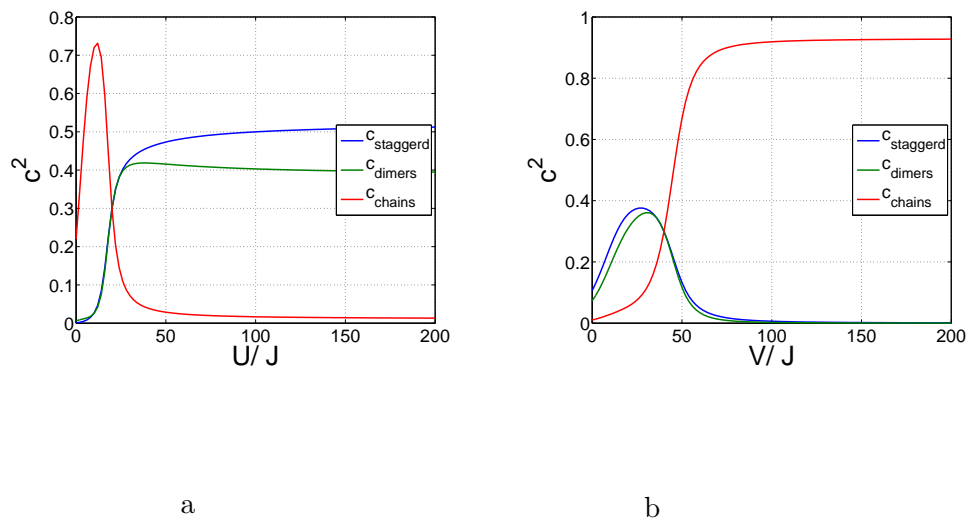

Figure 4.10: (a) Shown here are the weights of the different contributions to the wavefunction of the four sited cell during the transition to the anti-ferromagnetic Mott insulator for $V_{AB} = 20J$, (b) and to the ferro-magnetic Mott insulator for $U = 20J$. As one can easily see, the contributions with dimers are very important in the anti-ferromagnetic regime, in ferromagnetic regime the groundstate is mainly given by the ferromagnetically ordered chains.
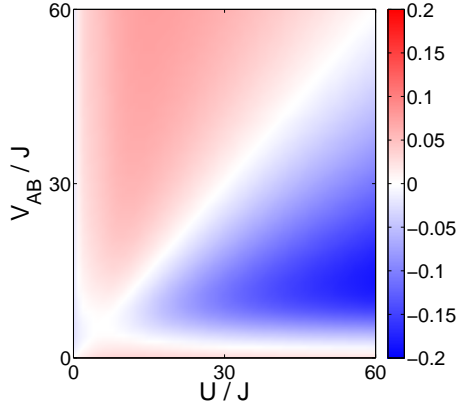
Figure 4.11: The phase-diagram in case of six sites. It is striking that there are ferromagnetic correlations in the regime for $V_{AB} << U$ and anti-ferromagnetic correlations in the regime $U << V_{AB}$. This occurs due to the special geometry and the filling with three A- and three B-bosons.

other cell size. This is caused by the triple structure. In the ferromagnetic regime ($V_{ab} > U$), a configuration is favored where the atoms arranged in triples of the same sorts as the best ferromagnetic configuration in this parameter regime and half filling. This is depicted in Fig. 4.12 b. The six sited cell is the smallest one, which build laminar domains of A- and B- bosons, see Fig 4.11 a and Fig. 4.13 b. The ratio of the lengths of the domain wall and the domain bulk is so huge, that the anti ferromagnetic correlations overbalance the ferromagnetic correlations. Therefore, in average, the triple structure provides more next neighbors of the other particle sort, than of its own sort. Two A-bosons are doubly neighbored by B-bosons and single neighbored by their own kind (A-boson). Only one A-boson is double neighbored by A-bosons and single neighbored by B-boson and vice versa. In case of a pure domain structure, the correlations are FM$= \frac{8}{3}$ and AF$= \frac{10}{3}$, normalized this gives a z-correlation of $g_{i,j}^z \approx 0.093$, which fits well to the numerical results. Beneath the overall small ferromagnetic correlations in the Mott insulator, also the correlations in the superfluid regime are particular. In the ferromagnetic correlated superfluid, for $U = 0$ and $V > 2J$, the next-neighbor correlations are rather anti-ferromagnetic and in the anti-ferromagnetic correlated superfluid, for $V < 3J$ and $U > 2$, the next-neighbor correlations are rather ferromagnetic. One has to remind, that in the superfluid regime configurations with multi occupied sites are favored. For small U/J, atoms of the same kind favor to sit on the same site, but this contributions will not be counted within the next-neighbor correlations, although this would mean a ferromagnetic correlated superfluid. In almost the same manner, the correlations in the superfluid regime for small V neglect the AB-onsite correlations. This onsite correlations will be evaluated in the case of an eight sited cell in chapter 5. The anti-ferromagnetic correlations in the ferromagnetic regime appear due to the fact, that no chains can be build. Therefore ferromagnetic correlations are missing to compensate the reduction caused by multi-occupied sites, which are not "counted" to be ferromagnetic. In the other regime, ferromagnetic in the anti-ferromagnetic regime one

has to consider that it is not possible to have dimers of A- and B-atoms. It will be shown in the next subsection (eight sited cell) that this contribution is very important in the antiferromagnetic regime (see Fig. 4.16 a). The groundstate in the anti-ferromagnetic regime in a cell with six sites consists only of the triple and the staggered structure (see Fig. 4.13 a), whereas the staggered structure is turned into the triple one by one single flip-flop jump in the case of a six sited cell. At least, this explains the high occupation of the triple order even in the anti-ferromagnetic case as well as the low ferromagnetic correlations in the regime of $V_{AB} > U$. The contribution of the domain structure to the groundstate in the deep ferromagnetic Mott insulator amounts to 95% (see Fig. 4.13).
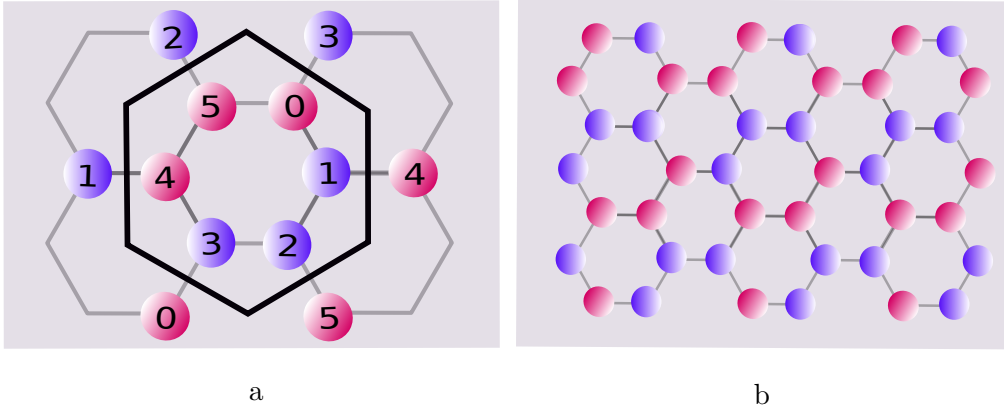
Figure 4.12: The six sited unit-cell (a) and the special triple order in the ferromagnetic 'phase' (b). In this triple order, the neighboring sites are, on average, rather occupied with the other atoms of the other kind and it is reached from the staggered order by one single flip-flop jump. This explains the high occurrence of this state even in the antiferromagnetic regime (see Fig. 4.13) and the weak ferromagnetic correlations in the regime for $V_{AB} > U$
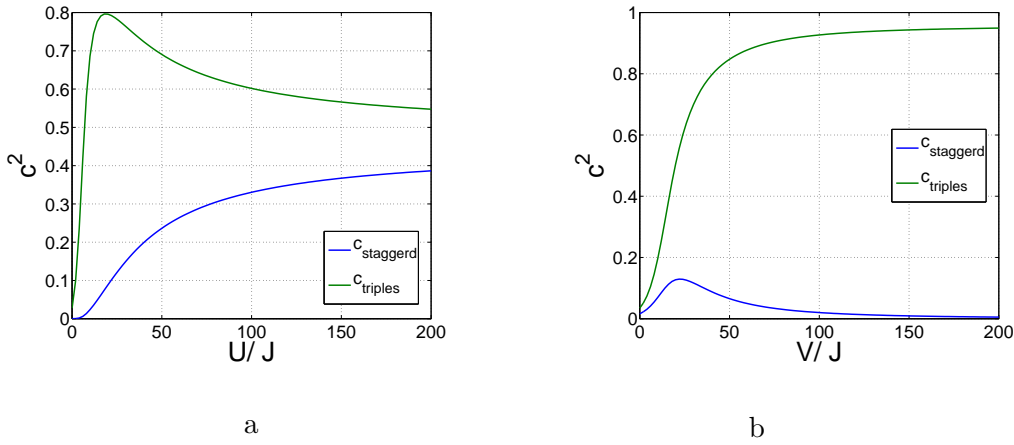

Figure 4.13: Shown here are the weights of the different contributions to the wavefunction in the antiferromagnetic regime for increasing values of U and $V_{AB} = 20J$. These contributions are given by the staggered structure and the triple structure (a). Depicted in (b) are the weights of the different contributions to the wavefunction in the ferromagnetic regime for increasing V and $U = 20J$. It can easily be seen, that the triple structure provides a contribution to the deep anti ferromagnetic regime, as well as to the ferromagnetic regime. It is highly noticeable that the sum of both weights stays much smaller than 1 in the superfluid. This means, that in this regime other contributions, namely multi occupied states, dominate the wave function, see chapter 5.

4.3.3 The eight sited cell

The cell with eight sites has been evaluated more deeply, being a reasonable compromise between the cell size and numerical effort. On the one hand, the eight sited cell gives feasible results, since the finite size effects decrease and, unlike the six sited cell, no special geometrical issues occur. On the other hand, the system has a reasonable basis size of dimension $d = 108900$.
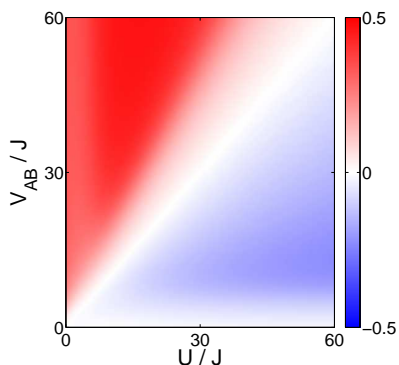

Figure 4.14: The phase-diagram for an eight sited cell. The light colored stripes for small V and increasing values of U and for small U and increasing values of V are caused by the high on-site correlations in this superfluid regime. The multiple occupation of one site reduces the site to site correlations. This feature will be picked up in the discussion of the correlations in the superfluid regime, and we will get access to the configuration in this regime by other correlation functions.

Shown in Fig 4.14 are the nearest neighbor z-correlations for the eight sited cell. It shows high ferromagnetic correlations in the regime $V > U$ as one would expect and anti ferromagnetic correlations in the regime $U > V$. In contrast to the six sited cell no abnormalities occur due to the geometry, which allows to build larger domains (chains), like we will see in the following. In the ferromagnetic regime ($V_{ab} > U$) a configuration is favored where the atoms are arranged in chains, along the three cristallographic axes (see Fig. 4.15). A real phase separation in laminar domains is not yet possible, because the cell is to small. However, these three kinds of chains along the different axes represent a separation into two distinct domains. The corresponding contributions of these states to the groundstate in the ferromagnetic regime is depicted in Fig. 4.16 b. They tend to nearly one in the deep Mott insulator phase. The anti-ferromagnetic order consists not only of the staggered ordered groundstate, but also of an admixture of dimers and triples. The different contributions to the groundstate wavefunction in the anti-ferromagnetic regime is shown in Fig. 4.16 a. It seems astonishing, that the structure which includes triples of same atoms the "claw"-ordering, provides the highest contribution to the wavefunction in the anti ferromagnetic regime. This can be explained by Fig. 4.17 a,b, and c. By one single flip-flop hopping the dimer structure and the staggered structure is transferred to the "claw"-structure. In the anti ferromagnetic regime, the prefactor is negative, therefore a flip-flop hopping lowers the energy. That is the reason for the ground-state structure, consisting of a staggered contribution, the dimers, and the "claw"-structure. In chapter 5.2.1 it will be shown, that for this groundstate the next neighbor in-plane correlations are maximal, revealing an in-plane state. It has to be considered, that there are
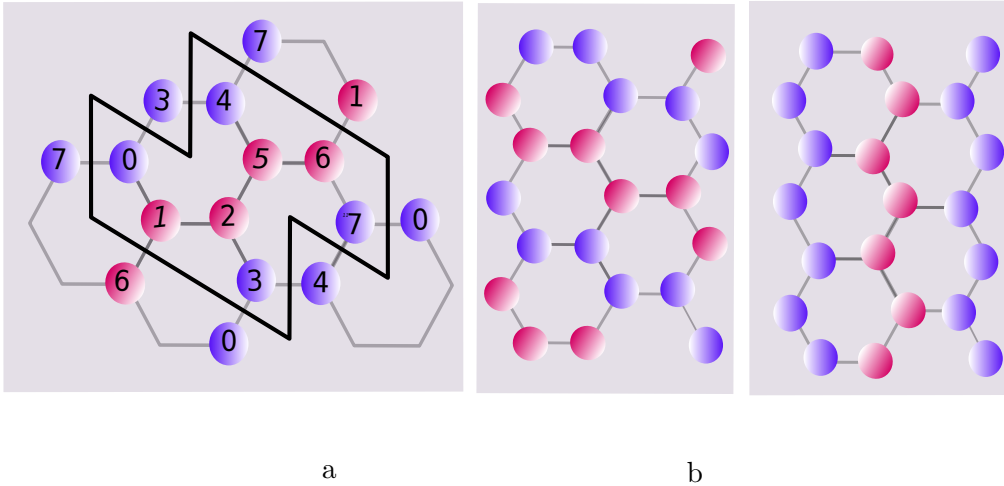
Figure 4.15: The unit-cell with eight sites (a) and two of three possible lattice configurations in the ferromagnetic regime (b). The chains of A- and B- bosons along the three axes denote a spatial separation in A- and B-areas for increasing cell sizes.

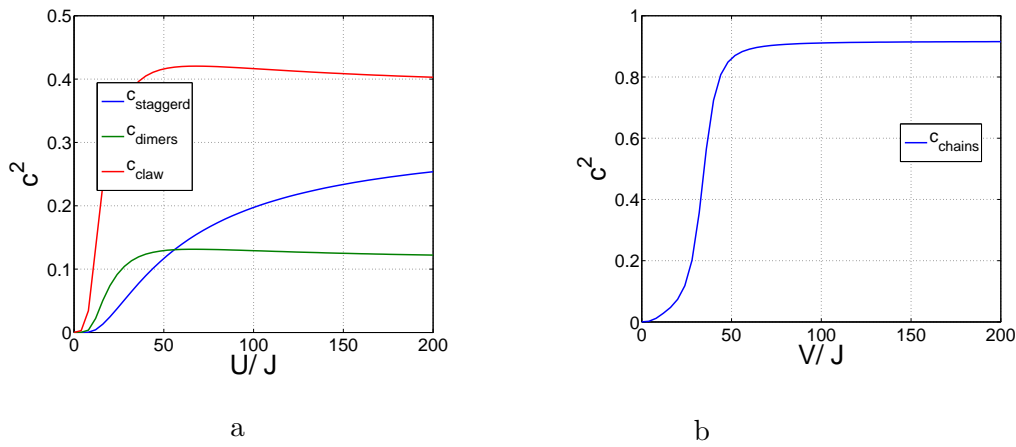Figure 4.16: Shown here are the weights of the different contributions to the wavefunction in the antiferromagnetic regime for $V_{AB} = 20J$ (a), and in the ferromagnetic regime for $(U = 20J)$ where the contribution of the chains tend to more than 90% (b). Keep in mind, that this contributions only consider states with single occupied sites, what means, this is not valid in the superfluid regime.

six possibilities to build the chains in the ferromagnetic regime. 24 possibilities to build the "claw"-configuration with triples and alternating areas. And six possibilities to build up dimers and two of a pure staggered structure. Additionally there are also contributions of four atoms in a chain, called the "bowl" (see Fig. 4.17 d) or four atoms ordered like stars, "stars" (see Fig. 4.17 e), and even a small contribution of chains in the anti-ferromagnetic regime occur (see Fig. 4.17 f). This three additional parts supply the missing 20% of the contribution to the groundstate wave function (Fig 4.16 a). Shown in Fig. 4.18 are all important contributions during the crossing from the anti ferromagnetic to the ferromagnetic regime in the Mott insulator phase (see Fig. 4.18 a) and in the crossover from the ferromagnetic to the anti-ferromagnetic regime (see Fig. 4.18 b). As described above, it is obvious, that the ferromagnetic order is robust in contrast to the anti ferromagnetic order, which always contains ferromagnetic contributions. For an eight-site unit-cell the number of possibilities to occupy the sites increases again, therefore more quantum-fluctuations are generated and the heights of the anti-ferromagnetic correlations decrease compared to the four sited cell.
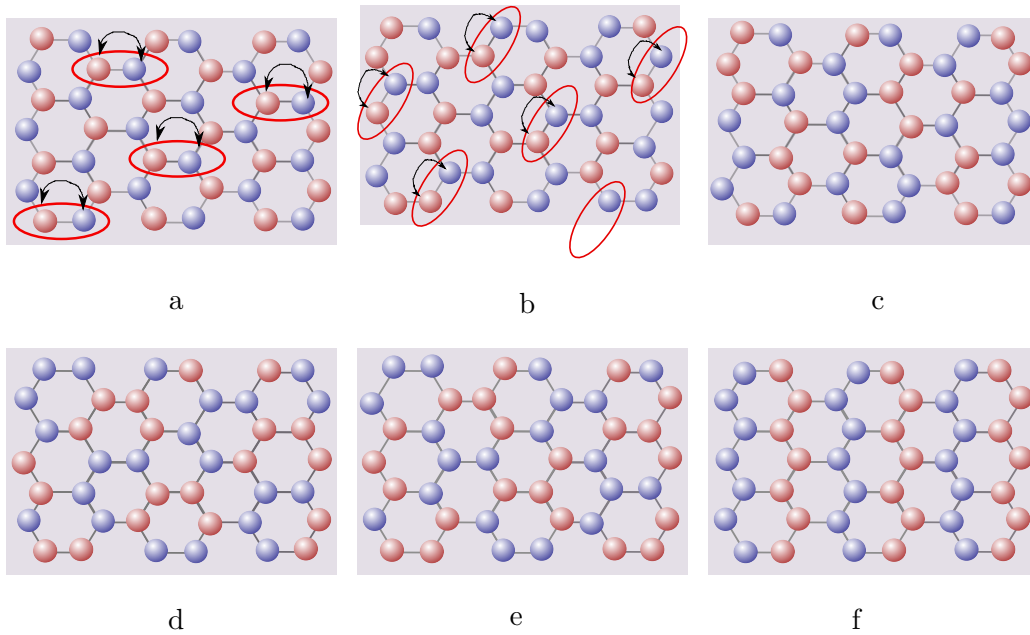
Figure 4.17: Depicted here are the admixtures to the groundstate in the anti-ferromagnetic regime in case of eight sites in the cell: a) staggered, b) dimers, c) claws, d) bowls , e) stars, and f) chains. Like depicted by circles and arrows, one single flip-flop- hopping transfers the staggered- or the dimer-structure in the claw-structure, which provides the highest contribution to the wavefunction in the antiferromagnetic regime. This is consistent with an in-plane state, which includes many contributions linked by one AB flip-flop. (see Fig. 4.16 a).
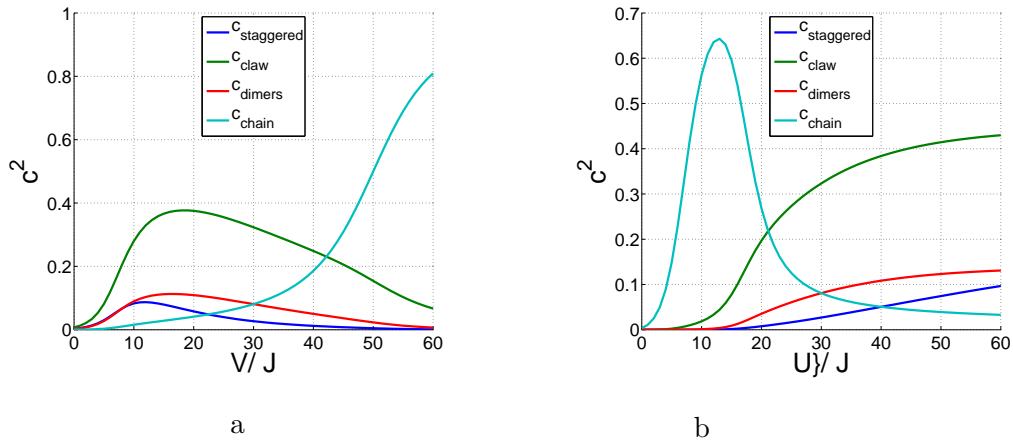

Figure 4.18: Depicted here are the different contributions to the groundstate for $V_{AB} : 0...60J$ and $U = 30J$ (a) and the corresponding contributions for $U : 0...60J$ and $V_{AB} = 30J$ (b). The ferromagnetic groundstate is dominated by the chain formation. Whereas the anti-ferromagnetic groundstate never assume a Neél-state, see Fig. 4.17.

4.3.4 The ten sited cell

In the case of ten sites per unit cell the phase-diagram looks similar to the one of the eight sited cell, but with stronger correlations and a reduce of finite size effects. The influence of the quantum fluctuations in the anti-ferromagnetic regime is stabilized, this is reflected by an enhancement of the anti-ferromagnetic correlation, see Fig. 4.19. Giving attribute to the computational effort, the calculations are performed with a truncated basis including only those Fock states with a maximum of two atoms of the same sort per site. This specifically enhances the ferromagnetic correlation for $U = 0$ and increasing values of V. Since states with more than 2 atoms of one kind per site are forbidden the site-to-site correlation are higher in the feromagnetic superfluid regime. Consequently, the correlations deep in the Mott insulator regime ($U/J > 15$) are authentic, where higher occupations of one site are avoided by high on-site interaction anyway. The absence of the light colored stripe in case of $U = 0$ is noticeable. In case of small V and increasing U, which allows one A- and one B-atom per site, this is not the case. The light colored stripe, which arises due to multi occupied sites, is visible. The on site correlations, which examine the physics in this superfluid regime will be discussed in the next chapter.
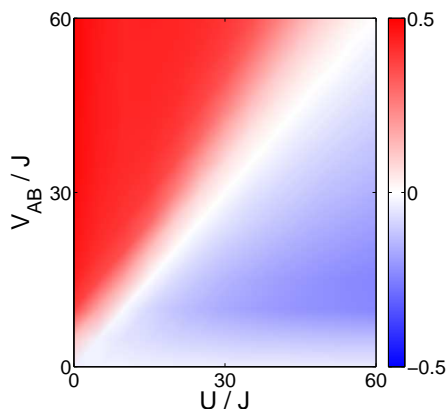

Figure 4.19: The phase-diagram in the case of ten sites. The magnetic correlations become stronger again and the transition from the ferro- to the anti-ferromagnetic regime is pinched compared to the eight sited cell. In the regime for small U and increasing V there is no light colored stripe because multi-occupied sites are avoided by a truncated basis.

For the ten-site sized unit cell a real separation of the two sorts of atoms can be observed (connected areas of A- and areas of B-atoms occur, see Fig. 4.20). In contrast to the eight sited cell the transition from the ferro- to the anti-ferromagnetic regime is more restricted towards the $U = V$-line. This could not be caused by the truncated basis, considering, that in the crossover to the Mott insulator phase higher occupations are rather avoided. Therefore, we could assume, that for increasing cell sizes the transition from the ferromagnetic to the anti-ferromagnetic regime will become sharper and quantum-fluctuations in the anti-ferromagnetic regime will be stabilized.
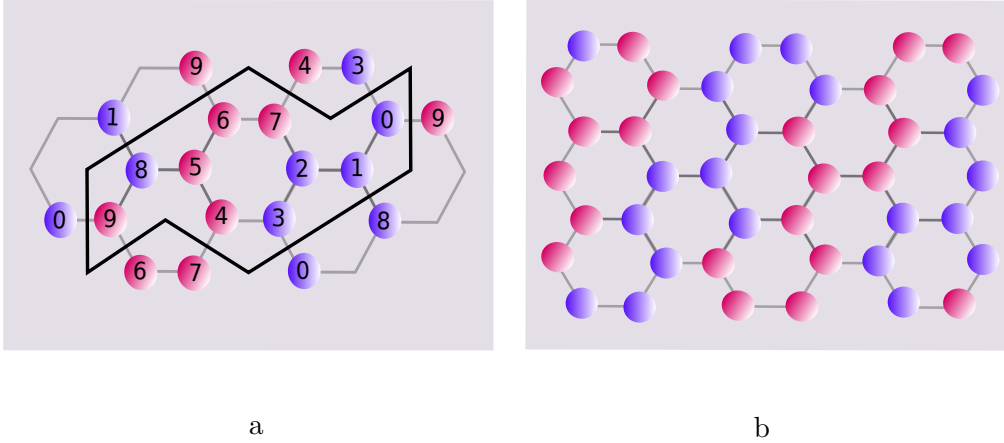
Figure 4.20: The unit unit-cell with ten sites (a) and the configurations in the ferromagnetic regime (b). The ten sited cell is the first one with an areal separation of A- and B-atoms.

For further increasing cell sizes, in the ferromagnetic regime a spatial separation of A- and B- atoms will occur for every cell size and the size of the domain will increase. The ratio between domain wall and domain bulk in contrast will become smaller what enhances the ferromagnetic correlations. Additionally it must be considered, that the correlation function 4.8 only include next neighbor correlations. If more than one atom occupy a site, in the superfluid regime, states with two or more atoms of the same sort (or different sorts) at one site would rather indicate ferromagnetic (anti-ferromagnetic) z-correlations. These on-site correlations are not considered within our correlation function, it will be disscussed in Chapter 5.

4.4   Conclusions

In Chapter 4 I investigated the short ranged 'magnetic z-correlations' of the honeycomb lattice filled with two sorts of bosons. In the limit of of $U, V_{AB} >> J$ the system has been mapped onto a spin-$\frac{1}{2}$-system in second-order perturbation theory in the tunneling. As this is only valid in the deep Mott phase, I developed a 'magnetic' correlation function for finite sized systems which can be applied to the whole parameter regime. After an examination of the fluctuations of a Bose-Bose mixture in an eight sited cell to determine the superfluid and the Mott insulating regimes a phase-diagram was presented. I identified ferro- and anti-ferromagnetic regimes in the Mott insulator as well as ferro- and anti-ferromagnetic correlations in the superfluid phase, which will be investigated in more detail in the next chapter. Furthermore I focused on finite size effects, by evaluating the 'magnetic' correlations for different sized unit cells: the four, the six, the eight sited, and

the ten sited sized cell. I found, that there is a ferromagnetic ground state for $V_{AB} < U$ which depends on the cell size but is robust against increasing cell sizes and represents clearly the ferromagnetic regime with a domain structure. In the case of the four sited cell and the eight sited cell, the A- and B-bosons are arranged in chains along the different axes. Cells with six sites are the first one which allow the creation of closed domains of one particle sort. Due to the huge ratio between domain wall and domain bulk the ferromagnetic correlations are very small. In case of the ten sited cell, the ratio of domain wall and bulk increases, therefore high ferromagnetic correlations arise. The anti-ferromagnetic groundstate in contrast is not staggered (there is no Neél-state as a ground state) but always contains claws, dimers, bowls, or stars of the same sort which are embedded in the staggered pattern. This is caused by quantum fluctuations which also depend on the size of the considered cell and it is consistent with the theoretical predictions, e.g. [53]. For increasing cell sizes with ten or more sites the growth of the quantum fluctuations seems to be stabilized and the transition between the two 'magnetic' regimes is pinched to the $V_{AB} \approx U$-line.

Chapter 5

Unconventional magnetic order in the Superfluid regime

The results of this chapter have been achieved in collaboration with M. Prada [63]. In the previous chapter I analyzed the phase diagram distinguishing the ferro- and anti-ferromagnetic z-correlations in the Mott insulator phase and could identify a correlated superfluid. In this chapter we will evaluate this superfluid regime, expecting a phase, which is characterized by the co-existence of the off-diagonal-long-range superfluid order and a solid order, what means a density imbalance, i.e. a supersolid (2.7). Compared to the investigations in the previous chapter, two characteristics have to be considered. First, multiple occupied states are not considered sufficiently in the nearest-neighbor correlation function, although they play a key role in the regime for small V or small U. Second, in a homogeneous honeycomb lattice filled with A- and B-bosons ($\eta_A = 0.5$ and $\eta_B = 0.5$), the average fillings per site are $\bar{n}_A = 0.5$ and $\bar{n}_B = 0.5$, in this case the population imbalance from site to site vanishes in every case, due to the high symmetry of the system. In experiments which deal with huge systems in contrast to our eight or ten sited cell, a spontaneous symmetry break can easily be done. Even in a mean-field approach, the symmetry break is given by dealing with a nonlinear differential equation where the nonlinear part is just given by the density of the system. In contrast, by performing exact diagonalization we do not have a spontaneous symmetry break. Apparently the density is not a good quantity to analyze superfluid states, therefore we investigate the magnetic ordering in the superfluid phase by means of different inter-site correlation functions which we define below.

5.1 Distance-correlation functions

To investigate the iso spin correlations in the superfluid regime, I introduce distance correlation functions, which do not refer to a special site, but only consider the distance, i.e. the number of sites between two bosons. Therefore the symmetry

becomes irrelevant and we understand how the atoms arrange themselves due to the interaction. The correlation functions can be defined in terms of the general pair-correlation function:

$$g_{i,j}^{\alpha\beta} = \left\langle \Psi | a_{i,\alpha}^\dagger a_{j,\beta}^\dagger a_{j,\beta} a_{i,\alpha} | \Psi \right\rangle. \tag{5.1}$$

The lattice indizes are i and j and α and β are the particle sorts. To consider the weights, the correlation functions are normalized. N is given by the number of sites in the cell. N_A and N_B gives the number of A- respectively B-particles in the cell. For different particles and different lattice sites we could derive the pair correlation-functions for first nearest neighbor (NN), second NN and third NN ($j = i + 1$, $j = i + 2$ and $j = i + 3$) as:

$$g_{i,j}^{\alpha\beta} = \left\langle \Psi | a_{i,\alpha}^\dagger a_{i,\alpha} a_{j,\beta}^\dagger a_{j,\beta} | \Psi \right\rangle = \left\langle n_i^\alpha n_j^\beta \right\rangle \tag{5.2}$$

$$g_{i,i+1}^{AB} = \frac{N^2}{N_A N_B} \left\langle n_i^A n_{i+1}^B \right\rangle$$

$$g_{i,i+2}^{AB} = \frac{N^2}{N_A N_B} \left\langle n_i^A n_{i+2}^B \right\rangle$$

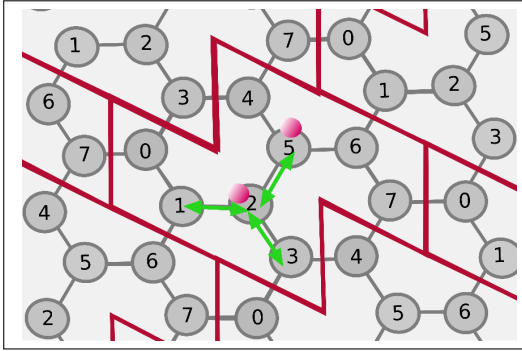$$g_{i,i+3}^{AB} = \frac{N^2}{N_A N_B} \left\langle n_i^A n_{i+3}^B \right\rangle \qquad .$$

Figure 5.1: This picture shows the first next neighbor correlations. The $g_{i,i+1}$ is unequal to zero, if the considered site i and the nearest neighbored site $i+1$ is occupied by a particle. There are three sites for every site which contribute to $g_{i,i+1}$-correlations.

For same kind of atoms but different lattice sites, the corresponding pair correlation-function *e.g.* for boson A are given by:

$$g_{i,i+1}^{AA} = \frac{N^2}{N_A(N_A - 1)} \left\langle n_i^A n_{i+1}^A \right\rangle \qquad \text{see Fig 5.1}$$

$$g_{i,i+2}^{AA} = \frac{N^2}{N_A(N_A - 1)} \left\langle n_i^A n_{i+2}^A \right\rangle \qquad \text{see Fig 5.2}$$

$$g_{i,i+3}^{AA} = \frac{N^2}{N_A(N_A - 1)} \left\langle n_i^A n_{i+3}^A \right\rangle \qquad \text{see Fig 5.3}$$
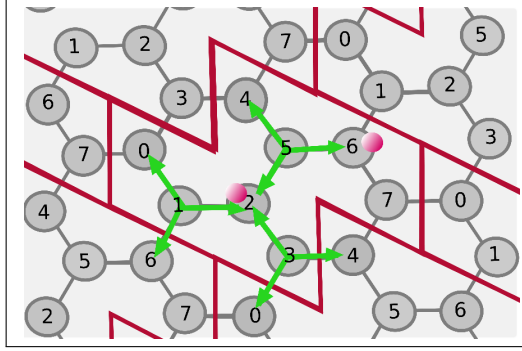
$$\tag{5.3}$$

Figure 5.2: This situation visualize second nearest neighbor correlations. The $g_{i,i+2}$- correlation would be unequal to zero if the considered site i and a site i+2, which is two sites away, is occupied by a particle. In this case (a cell with eight sites) there are also three possibilities which sites give $g_{i,i+2}$- contributions.
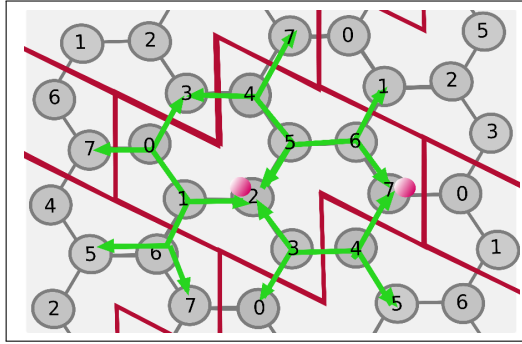

Figure 5.3: Depicted here is the situation which gives $g_{i,i+3}$-contributions. The considered site is three sites away. In every cell and for every site there is only one site which produce $g_{i,i+3}$- correlations. Keep in mind that in the eight sited cell the most possible distance is three sites.

If we consider on-site-correlation functions we end up with:

$$g_{i,i}^{AA} = \frac{N^2}{N_A(N_A - 1)} \left\langle n_i^A(n_i^A - 1) \right\rangle \qquad \text{see Fig 5.4}$$

$$g_{i,i}^{AB} = \frac{N^2}{N_A N_B} \left\langle n_i^A n_i^B \right\rangle$$

$$(5.4)$$

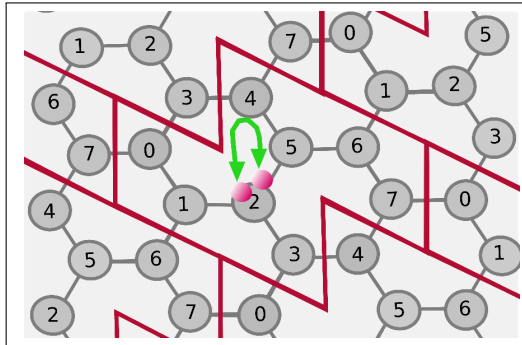For a better understanding the considered situations are illustrated in Fig. 5.1 -

Figure 5.4: : Shown here is what is meant by a distance of zero. The on-site correlation g_{ii} is unequal zero, if the considered site is occupied by more than one particle. There is one site, which gives on-site correlations: only the site itself.

Fig. 5.4.

5.2   Magnetic order in the superfluid phase

In the following chapter we will analyze the structure of the two special regimes in the superfluid phase, within the framework of distance correlation functions. In Fig. 5.5 the density fluctuations (a) and the z-correlations (b) are shown.
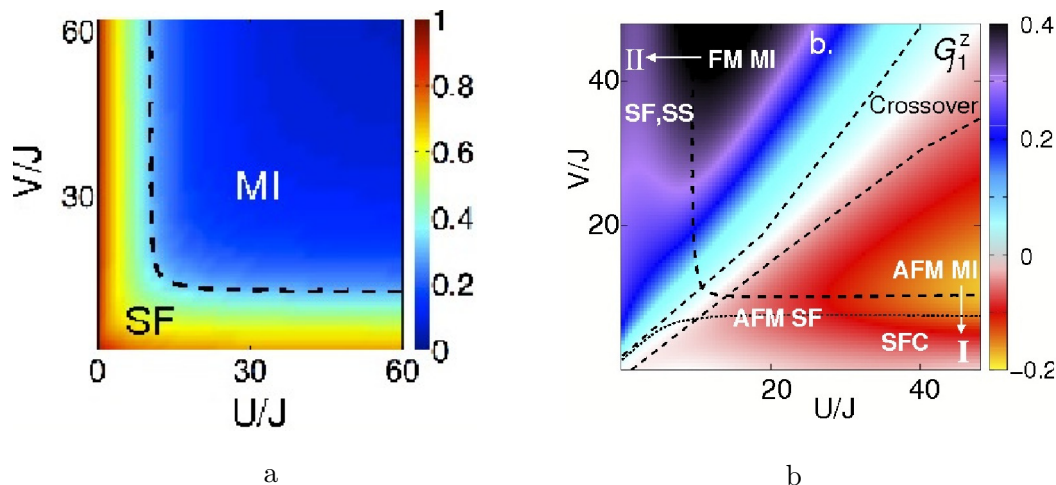

a

b

Figure 5.5: (a) Shown here are the fluctuations to illustrate the superfluid to Mott insulator transition. The deep blue colored regime corresponds to the Mott insulator ($\Delta n \leq 0.2$) and rainbow colored regime correspond to the superfluid phase. (b) Shown here are the easy-axis pair (z)-correlations for nearest neighbors which give a phasediagram we will fully examine in this chapter. As mentioned above, we do not attempt to determine a sharp well-defined boundary between the phases, as we are computationally limited to small systems.

The ferromagnetic regime in the Mott insulator phase is dominated by strong z-correlations (see section 4.3.3), the black colored area in the phasediagram. The configurations of the groundstate are given by chains of A- and B-atoms. In the anti ferromagnetic Mott insulator-regime the z-correlations are comparatively weak but negative, which means antiferromagnetic ordering (see section 4.3.3), corresponding to the yellow colored area in the phasediagram. In the regime for small on-site interaction V and strong on-site U we identify a superfluid phase with rather antiferromagnetic correlations, regime I in Fig. 5.5 b. I will demonstrate an in-plane correlated state implying superfluid counterflow. In this regime two structures of A- and B-atoms can build an anti-ferromagnetic correlated superfluid, but with small AA- and BB-fluctuations. This will be discussed in section 5.2.1. In contrast in the ferromagnetic correlated superfluid, for small onsite U and increasing onsite V (the purple area) a supersolid phase is identified, regime II in Fig. 5.5 b. This will be discussed in section 5.2.2. By applying a spin-depending lattice potential we break the symmetry in order to suggest an experimental setup,

to detect a supersolid signal, see section 5.2.3. In section 5.2.4, finite size effects are discriminated by calculating the in- and out-of-plane correlations for a ten sited cell. The in-plane-correlations (x-y) correlations ($G_{ij}^{\parallel}$) for different distances have been computed by M. Prada. They are given by a superposition of two bosonic atom sorts with the iso spin $|\uparrow>$ (boson A) and $|\downarrow>$ (boson B) in site i and j. Considering the effective Hamiltonian for the Mott insulator regime, derived in section 2.5.1, the in-plane-correlations are given by the second part of the Hamiltonian:

$$
\begin{aligned}
H_{int} &= \sum_{\langle i,j \rangle} T_{ij} \vec{S}_i \vec{S}_j \\
&= \sum_{\langle i,j \rangle} E'' (\sigma_z^i \sigma_z^j - (\sigma_-^i \sigma_+^j + \sigma_+^i \sigma_-^j)) \\
E'' &= -\frac{J^2}{2} \left(\frac{1}{U} - \frac{1}{V_{AB}} \right)
\end{aligned}
\tag{5.5}
$$

The correlations can be calculated by

$$
G_{\parallel} = \frac{1}{\Omega_n} \sum_{<ij>_n} g_{ij}^{\parallel} = \frac{1}{\Omega_n} \sum_{<ij>_n} \left\langle \hat{S}_+^i \hat{S}_-^j + \hat{S}_-^i \hat{S}_+^j \right\rangle
\tag{5.6}
$$

with

$$
\hat{S}_{\pm}^i = \hat{S}_x^i \pm i \hat{S}_y^i, \qquad \hat{S}_+^i = \hat{a}_i^\dagger \hat{b}_i \qquad \text{and} \qquad \hat{S}_-^i = \hat{b}_i^\dagger \hat{a}_i
\tag{5.7}
$$

and Ω_n being the normalization factor,

$$
\Omega_n = \eta_n \frac{(n_A + n_B)}{2}.
\tag{5.8}
$$

η_n is the number of the n-th next neighbor and the sum performed for all n-th next neighbors. For a better understanding, the "flip-flop" operator, which is used to calculate the in-plane correlations is explained in the following, restricted to single occupied sites. The "flip-flop" operator $\hat{S}_+^i \hat{S}_-^j$ is not diagonal in the basis of number states, in contrast to the z-correlation operator, I used in the previous Chapter. But if a state is given by a superposition of e.g. two number states like

$$
|\Psi\rangle = \alpha |a\rangle + \beta |b\rangle
\tag{5.9}
$$

with

$$
|a\rangle = |..., B_i, ..., A_j, ...\rangle \qquad \text{and} \qquad |b\rangle = |..., A_i, ..., B_j, ...\rangle ,
\tag{5.10}
$$

on obtain for the "flip-flop" operator $\hat{S}_+^i \hat{S}_-^j$ employed on $|b\rangle$ and $|a\rangle$

$$
\hat{S}_+^i \hat{S}_-^j |a\rangle = |b\rangle \qquad \text{and} \qquad \hat{S}_+^i \hat{S}_-^j |b\rangle = 0,
$$

$$(5.11)$$

and for the "flip-flop" operator $\hat{S}^i_- \hat{S}^j_+$ employed on $|a\rangle$ and $|b\rangle$

$$\hat{S}^i_- \hat{S}^j_+ |a\rangle = 0 \qquad \text{and} \qquad \hat{S}^i_- \hat{S}^j_+ |b\rangle = |a\rangle .$$

$$(5.12)$$

Therefore the expectation value $\left\langle \hat{S}^i_+ \hat{S}^j_- \right\rangle$ is given by:

$$\left\langle \Psi | \hat{S}^i_+ \hat{S}^j_- | \psi \right\rangle = \quad \alpha^* \beta \langle a | \overbrace{\hat{S}^i_+ \hat{S}^j_- |b\rangle}^{=0} + \beta^* \alpha \langle b | \overbrace{\hat{S}^i_+ \hat{S}^j_- |a\rangle}^{|b\rangle}$$
$$+ |\alpha|^2 \langle a | \underbrace{\hat{S}^i_+ \hat{S}^j_- |a\rangle}_{=0} + |\beta|^2 \langle b | \underbrace{\hat{S}^i_+ \hat{S}^j_- |b\rangle}_{=0} = \quad \beta^* \alpha$$

$$(5.13)$$

The expectation value in case of $\left\langle \hat{S}^i_+ \hat{S}^j_- + \hat{S}^i_- \hat{S}^j_+ \right\rangle$ then is given by

$$\left\langle \Psi | \hat{S}^i_+ \hat{S}^j_- + \hat{S}^i_- \hat{S}^j_+ | \psi \right\rangle = \beta^* \alpha + \alpha^* \beta$$

$$(5.14)$$

This implies, that a groundstate which consist mainly of superpositions of states which are linked by one $A - B$ flip-flop between site i and j produce a large contribution to the in-plane correlation function, and the iso spin lies mostly in plane. The out-of-plane correlations for different next neighbors are given by the z-correlations, derived in section 5.1. This z-correlations will be evaluate in the following. Afterwards the in-plane correlations will be analyzed. Shown in Fig. 5.6 - Fig. 5.8 is the z-component of the correlation functions for the first, the second and the third nearest neighbor.
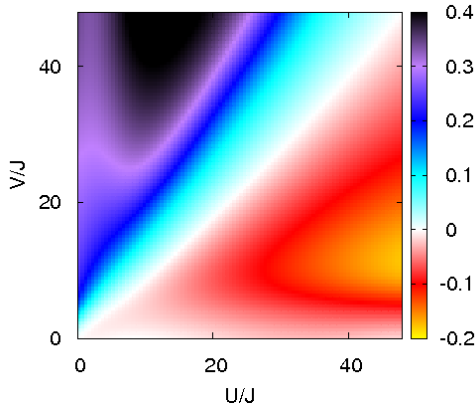

Figure 5.6: Shown here is the $g^z_{i,i+1}$. The nearest next neighbor z-correlations are definitely large and positive in the regime of small on-site U and increasing V. This indicates a ferromagnetic order in respect to the nearest next neighbor. In the regime for $V \approx 0$ and strong U, $g^z_{i,i+1} \approx 0$, this implies the entanglement of different iso spins at one site.

In the regime $V >> U$ the easy axis component of the nearest neighbor correlations (see Fig. 5.6) is very large, therefore neighboring sites are dominantly occupied by the same sort of atoms. Apart from that, the on site square of the z spin component has its maximum value, indicating multiple occupation, (see Fig. 5.12). In
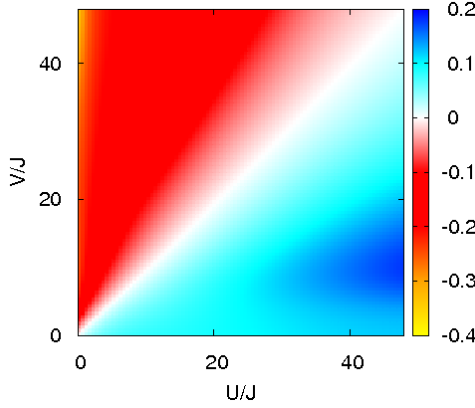
Figure 5.7: Shown here are the z-correlations for the second next neighbor, this correlation is smaller than zero in the regime of small on-site U and increasing V, since this neighboring sites are dominantly occupied with the other atom sort. In the regime $J \ll V < U$ (blue region) the groundstate is rather ordered anti ferromagnetic, see 4.3.3.

the Mott insulator regime for $J \ll U < V$ (black regime) chains of one particle sort arises, which enhances the ferromagnetic first-NN-correlations. Contrary the second and third next neighbor correlations become negative, $g^z_{i,i+2} \approx -0.35$ and $g^z_{i,i+3} \approx -0.8$ in the regime of small on-site U and increasing V, since this neighboring sites are dominantly occupied with the other atom sort, (see Fig. 5.7- Fig. 5.8). This is consistent with the supersolid state I identified in this regime, since the second but especially the third next neighbor is occupied by the other atom sort, which is in contrast to the on-site and the nearest neighbor. In the Mott insulator regime the second and the third neighbor z-correlation function is also anti ferromagnetic, because in the chain formation the second and the third neighbor is rather from the other kind of boson. In case of $U \approx V$ the z-correlations are zero, because the ferromagnetic and anti ferromagnetic contributions are equal and cancel each other. In the regime $J \ll V < U$ (blue region) the groundstate is rather ordered anti ferromagnetic, see chapter 4.3.3, therefore the second next neighbor is rather from the same kind. Considering the third next neighbor correlations in the regime $J \ll V < U$ (light blue region) the correlation are very low but also positive, keep in mind that in the anti ferromagnetic Mott insulator regime the dimer- and the claw-structure provide the highest contribution to the groundstate. Hence in the average the probability, that the third next neighbor is from the same kind is a bit enhanced. In the upper left of Fig. 5.8 the anomalous region can be identified, the $g^z_{i,i+3}$ peaks in this regime were the supersolid can be identified. For further investigation we also consider the in-plane correlations for all n-th next neighbors, see Fig. 5.9 - Fig 5.11. In the lower right of Fig. 5.9 (green regime) an SCF phase can be identified, I discuss in the next section. The second and the third next neighbor in-plane correlations in the superfluid regime in case of $V << U$ (red region in the lower right) and even the first neighbor in-plane correlations (yellow regime in the lower right) implies an entanglement of different iso spins at one site and next neighbored empty sites, see Fig. 5.10 and Fig. 5.11. Since the flip-flop between an empty site and an empty site, an empty site and a single or a double occupied site gives zero, the in-plane component is reduced to
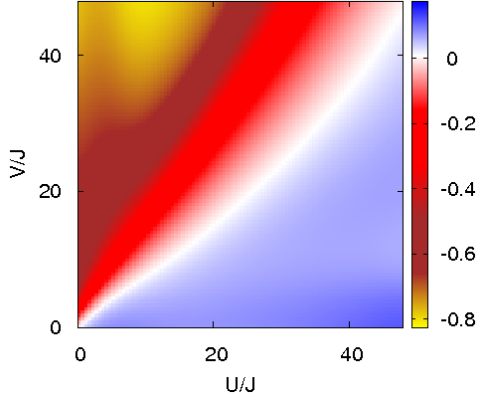
Figure 5.8: Shown here are the z-correlations for the third next neighbor, this correlation is negative but strong in the regime of small on-site U and increasing V, since the third next neighbored sites are dominantly occupied with the other atom sort, this is connected to a supersolid state, I evaluate in detail in this section.
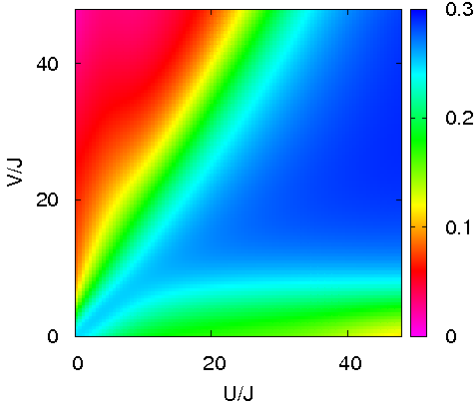

Figure 5.9: Shown here are the in plane correlations for the first nearest neighbor. In the lower right, we can confirm an easy plane state with in-plane FM ordering, see 5.2.1, which lowers the next neighbor in plane correlations. In the regime, in the regime $V \approx U$ A and B particles are indistinguishable.
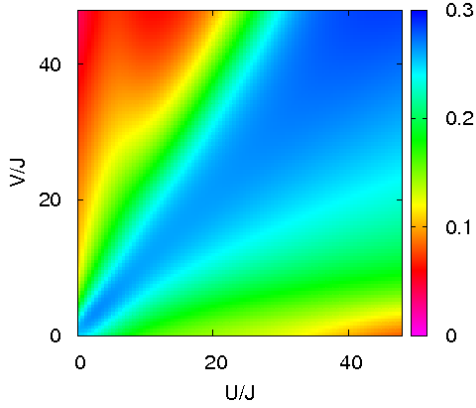
Figure 5.10: Shown here are the in-plane correlations for the second nearest neighbor, similar to the first next neighbor correlations. In the regime, where the supersolid is expected (in the upper left), the $g_{i,i+2}^{\parallel}$ shows a peak. The red region in the lower right implies an entanglement of different iso spins at one site and next neighbored empty sites.
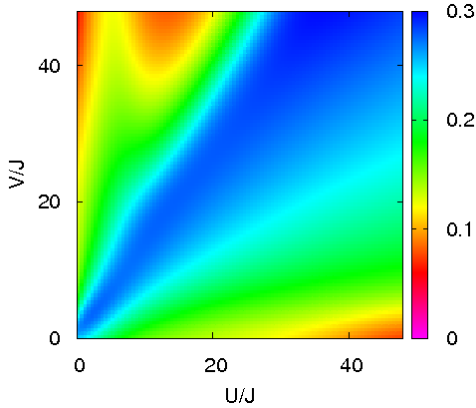

Figure 5.11: Shown here are the in-plane correlations for the third nearest neighbor. In the regime, where the supersolid is expected (in the upper left), the $g_{i,i+3}^{\parallel}$ particularly peaks, this peak is also reproduced in the $g_{i,i+3}^{z}$. The red region in the lower right indicates an entanglement of different iso spins at one site.

minimum. In the regime $U \approx V$, A and B particles are indistinguishable. The high in-plane correlations here imply that the system seems to contain only "one" particle sort. In the regime of $V > U$ the in-plane correlations in respect to the first and the second next neighbor are reduced to minimum by a ferromagnetic order. In the upper left we can denote for the first, the second and particularly for the third next neighbor correlation function an anomalous region, where especially the $g^{\parallel}_{i,i+3}$ peaks, see Fig. 5.11. This feature is reproduced in the $g^{z}_{i,i+3}$ (yellow regime) in Fig. 5.8. This is an indication of the supersolid structure I will discuss in the following.

5.2.1 The anti-ferromagnetic correlated regime

In the regime of $V/J \leq 7$ and increasing $U \geq 20$ the nearest neighbor in-plane correlations amounts to 0.5 of the absolute value. By further decreasing V/J and $U/J \geq 40$, the in-plane correlations of the second and the third next neighbor are reduced to less than 0.3 of the maximum, this implies an entanglement of different kind of bosons in one site i and an empty site j, since a flip-flop expectation value between site i and j which includes one empty site give a result equal to zero. Also the light red colored stripe in the G^{z}_{ij} for small V/J and increasing U/J is an indication for this entangled state. To investigate this further, the on-site-square of the spin components has been computed by M. Prada. In Fig. 5.12 a, is shown the on-site square of the z component $\left\langle \hat{S}^2_z \right\rangle$, in b) the on-site square of the in-plane component is shown $\left\langle \hat{S}^2_{\parallel} \right\rangle$ with

$$\left\langle \hat{S}^2_{\parallel} \right\rangle \equiv \frac{\sum_i \left\langle (\hat{S}^i_x)^2 + (\hat{S}^i_y)^2 \right\rangle}{N} \tag{5.15}$$

and

$$\left\langle \hat{S}^2_z \right\rangle \equiv \frac{\sum_i \left\langle (\hat{S}^i_z)^2 \right\rangle}{N}. \tag{5.16}$$

The on-site square of the z-component achieves its largest value in the regime of $V >> U$ and $U < 7\,J$ which is consistent with the occurrence of the superfluid-phase. In this regime, double occupancies are allowed and, in the ferromagnetic regime, where same sorts of atoms occupy one site, a large on-site spin-component out of plane is produced. In the regime for small V/J and increasing U/J the on-site square of the z-component is minimized. In contrast the in-plane-component reaches the largest value $\left\langle \hat{S}^2_{\parallel} \right\rangle = \frac{3}{4}$ for $U >> V$ and $V < 2\,J$.

For $V/J = 0$ we identify a phase, where the different iso-spins build superpositions at one lattice site, an easy-plane state with in-plane ferromagnetic ordering. Therefore the square of the on-site in-plane spin component has its maximum value. This regime is the black region in the on-site square of the easy-plane spin component (see Fig. 5.12 b).

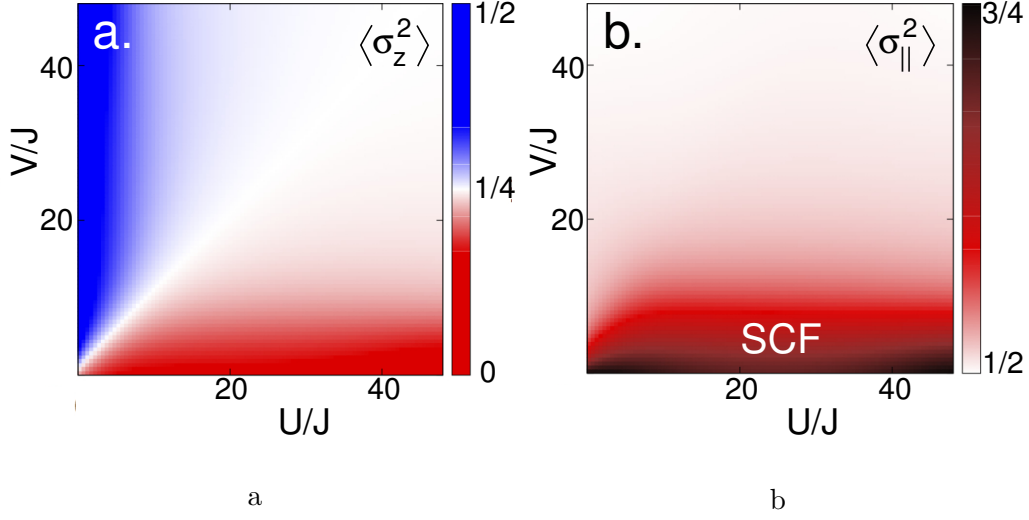a.   b.

Figure 5.12: Shown here is the on-site square of the a) z-component and b) the in-plane component. The on-site square of the in-plane-component reaches the maximum for $V \ll U$, this is the entangled state for AB-pairs on one site. The out of plane-component reaches the maximum in the regime $U \ll V$ where the same sorts of atoms rather occupy one site. This is connected to a supersolid phase we will investigate in the next section.

Since the in-plane next neighbor correlations are reduced in this regime (see Fig. 5.9, yellow regime), this implies a phase, with a huge contribution of an AB-occupied site which is next neighbored to a site which is rather not occupied. The $g_{i,i+2}^{\|}$ and the $g_{i,i+3}^{\|}$ are reduced to minimum (see Fig. 5.10 and Fig. 5.11, the red regions in the lower right) which also indicate this phase with entangled and empty sites. If a huge contribution of the ground state includes empty sites, the $\left\langle \hat{S}_+^i \hat{S}_-^j \right\rangle$ is reduced since

$$\hat{S}_+^i \hat{S}_-^j \left| ...., \underbrace{0}_{i}, ..., \underbrace{AB}_{j}, ... \right\rangle = 0 \qquad \text{and} \qquad \hat{S}_+^i \hat{S}_-^j \left| ...., \underbrace{AB}_{i}, ..., \underbrace{0}_{j}, ... \right\rangle = 0,$$

as well as

$$\hat{S}_-^i \hat{S}_+^j \left| ...., \underbrace{0}_{i}, ..., \underbrace{AB}_{j}, ... \right\rangle = 0 \qquad \text{and} \qquad \hat{S}_+^i \hat{S}_-^j \left| ...., \underbrace{AB}_{i}, ..., \underbrace{0}_{j}, ... \right\rangle = 0.$$

This could be seen as an paired superfluid vacuum (PSF phase), representing atomic (A+B) pairing at site i, neighbored to an empty site j. [37, 38, 49, 50]. A

PSF phase would require an effective attractive potential between different kinds of bosons. This could not be conclusively clarified. In any case for increasing but small V/J ($2 \leq V/J \leq 5$) this state is transferred to a super counterfluid (SCF phase) [48]. In this regime states with A and B bosons at one site are reduced due to increasing V/J and the groundstate is for simplicity given by a superposition of two states, e.g.

$$|\Psi\rangle = \alpha \, |a\rangle + \beta \, |b\rangle \tag{5.17}$$

with

$$|a\rangle = |..., B_i, ..., A_j, ...\rangle \qquad \text{and} \qquad |b\rangle = |..., A_i, ..., B_j, ...\rangle \, . \tag{5.18}$$

This results in a "flip-flop" $\left\langle \hat{S}_+^i \hat{S}_-^j + \hat{S}_-^i \hat{S}_+^j \right\rangle \neq 0$ and the n-th nearest neighbor in-plane correlations should be enhanced. This can be described by pairings of particles A and hole B in site i, and pairings of particle B and hole A in site j. This understanding is supported as the on-site square of the in-plane correlations is strongly reduced where the next-neighbor in-plane correlations are enhanced, which means the ground state involves many states which are linked by one $A - B$ "flip-flop" in respect to the first next neighbor.

For a better understanding, in order to avoid AB-on-site interaction, every second site is occupied by one kind of boson (e.g boson A) and the site between is occupied by the other kind of boson (boson B). These two structures are movable in respect to each other and to the lattice, that produces high density fluctuations, which monitor the superfluid state. The fluctuations and AB-occupations are displayed in Fig. 5.13 in case of $V = 0$ (a) and $V = 0.5J$ (b). For values of $U/J > 9$ the AA-fluctuations and the BB fluctuations are avoided due to energy cost. The part of the density fluctuations which are caused by AB-fluctuations stay unaltered high, (see Fig. 5.13, magenta line). The density fluctuations are $\Delta n \geq 0.7$, which means the system is still superfluid, but the A-particles avoid tunneling respectively to each other, just as the B-particles. One has to keep in mind, that in case of half filling, the fluctuations for the A bosons (B bosons) reach its minimum at $\Delta n_A = 0.5$ ($\Delta n_B = 0.5$). We also plotted the n-th next-neighbor z-correlation functions, see Fig. 5.15, for $0 \leq V/J \leq 50$ and $U = 50\,J$ for the same kind of bosons (a) and different kind of bosons (b). In case of $V/J = 0$ the 2nd and 3rd next-neighbor z-correlation functions for the same kind of atoms are enhanced and the first is suppressed and the on-site correlations of the same sorts are forbidden. This supports the picture of a groundstate, when the first next neighbor is not occupied by the same kind, but the second one is, apart from that there are also many empty sites. For a small increase of V the second nearest neighbor AA-correlation increases and the third- and first nearest neighbor correlations of AA and BB decreases, which reveals the configuration described in detail above when the two structures are shifted by one site. Entangled states and empty sites are
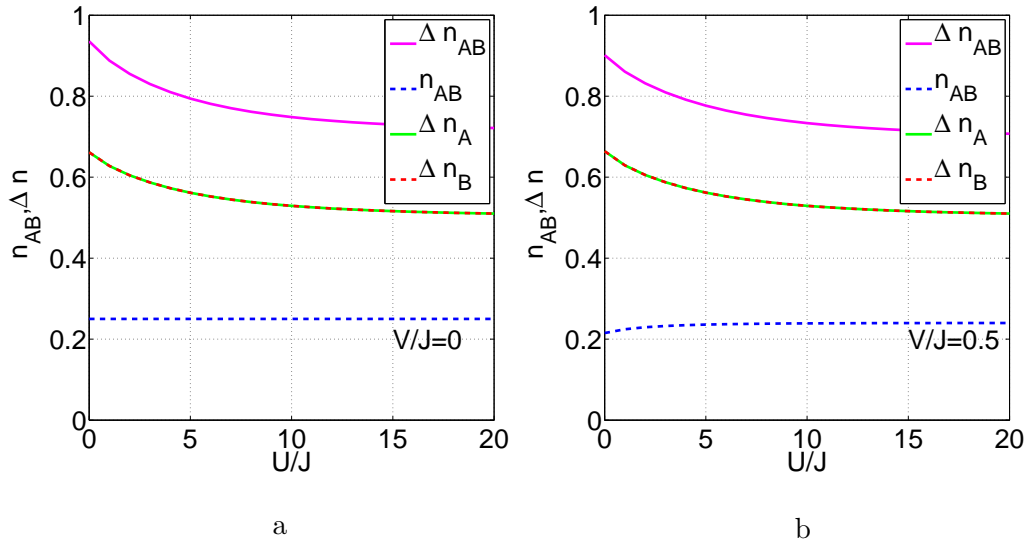
Figure 5.13: (a) The different parts of the fluctuations and occupations for $V = 0$ and the density fluctuations (magenta) are shown here. As mentioned, in contrast to the AA- (BB)- fluctuations, which are suppressed to the minimum which is possible for half filling, the fluctuations of the density never undergoes 0.7 caused by AB-fluctuations which are possible due to small interaction V between different kind of atoms. (b) Shown here are the same fluctuations, but for $V = 0.5J$. The small increase of the occupation n_{AB} for very small interaction U results from the fact, that for $U = 0$ the AB occupations are a bit suppressed, for growing U/J they increase.
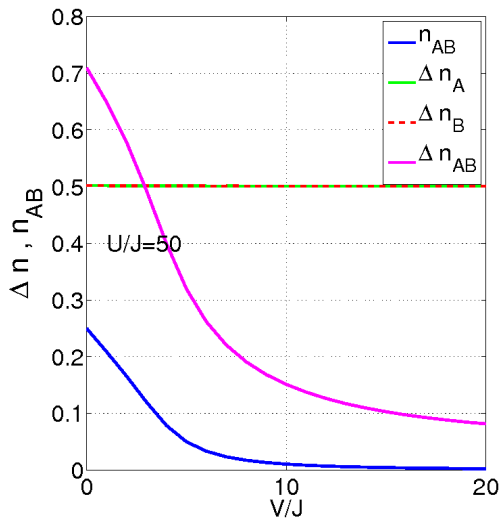
Figure 5.14: The different parts of the fluctuations and occupations for $U = 50J$ and $V = 0 - 50J$ and the density fluctuations (magenta) are shown here. Due to large on-site U there are no AA or BB fluctuations. The density fluctuations are only given by AB fluctuations, what reveals the configuration in the superfluid, see Fig. 5.16 and implies the superfluid counterflow, see Fig. 5.12. For $V > 5J$ the system is transferred to the anti ferromagnetic Mott insulator.

Figure 5.15: (a) Shown here is the z-component (out of plane component) of the n-th next-neighbor-correlations for the same sort of atoms for $U = 50J$ and increasing V. The largest probability occurs for small V for a configuration with one site spacing between two atoms of the same sort. (b) Shown here is the z-component of the n-th-next-neighbor-correlations for differ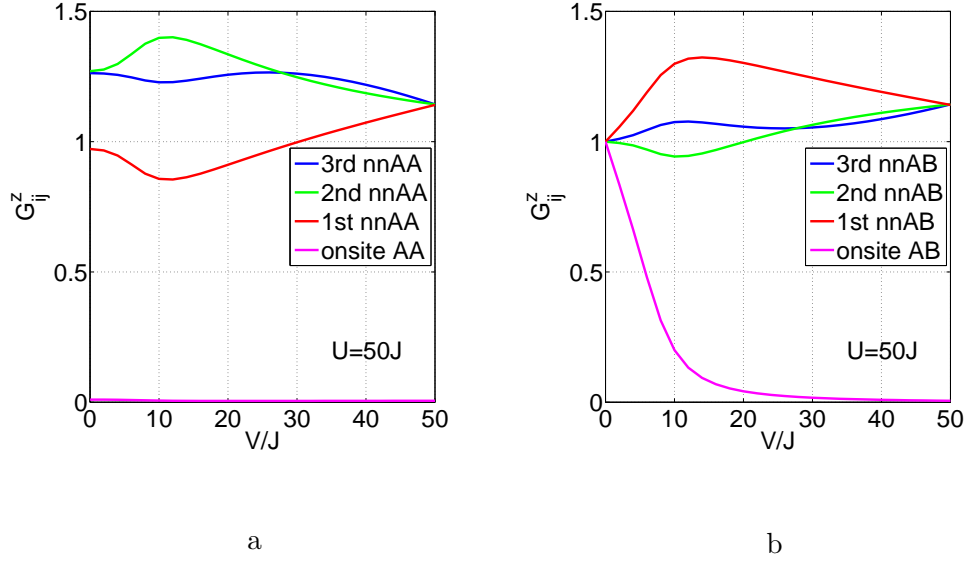ent kind of atoms, for V equals to zero the two atoms can entangled occupy the same sites. For increasing V they order themselves rather in an staggered configuration due to large on-site U which makes sure that the second next neighbor is occupied with the same sort of atoms.

reduced and different kinds of atoms occupy adjoining but not the same site. The AB-correlations show the same effect: the AB-first nearest neighbor correlation increases strongly and also the AB-3rd nearest neighbor correlation shows a small increase. The AB-2nd next neighbor correlation decreases and of course the on-site AB-correlation is more and more suppressed by increasing V, see Fig. 5.15. The fluctuations and occupations for this situation for $U = 50\,J$ and $0 \geq V/J \geq 20$ are illustrated in Fig. 5.14. The AA- and the BB-fluctuations are totally suppressed for on-site U equals to $50\,J$ but for small V the density fluctuations add up to 0.7, considering, that the Δn_A and Δn_B never undergo 0.5 due to the half filling. We stress that the density fluctuations can only consist of AB-fluctuations. To sum up we give a sketch in Fig. 5.16 of the main components of the wavefunction in the anti ferromagnetic superfluid regime. We investigated the Mott insulator phase, the contributions of the wave functions with the staggered, the dimers, and the "claw" structure have the highest weight in the groundstate, see section 4.3.3. Keep in mind, that these states are linked to each other by one AB "flip-flop", revealing an in-plane groundstate. In case of strong on site interaction U for the same kind and

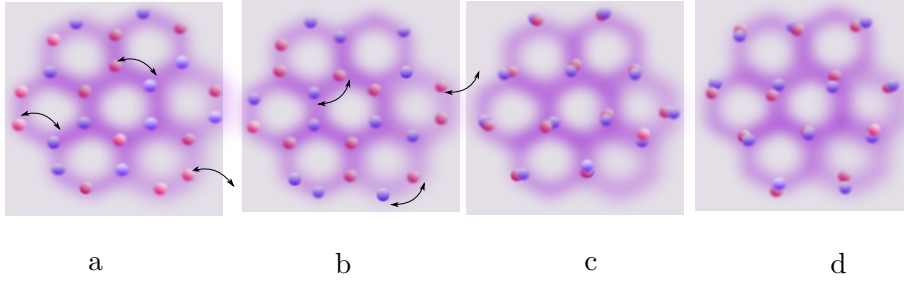<div style="text-align:center">a   b   c   d</div>

Figure 5.16: The mainly structures of an in-plane correlated superfluid in the anti ferromagnetic regime which can be derived from the correlation functions and the fluctuations. If the A- and B-structures can be regarded to be 'fix' they can tunnel without changing the distances between the same sorts (AA-fluctuations and BB-fluctuations are reduced) and therefore mainly providing AB-fluctuations. The staggered, the dimer and the claw-structure are linked to each other by one AB flip-flop, (see a) and b)). Since these states contribute the highest weight to the groundstate in the Mott insulator regime, the nn in-plane component is maximal, an in-plane state. Even in the superfluid the in-plane next neighbor correlations amounts to 0.5 of the maximum for $V \geq 2J$. For vanishing V the two structure can additionally coexist on top of each other, revealing entangled boson states, see c) and d). Therefore the in-plane next neighbor correlations are reduced and the on-site square of the in-plane component reaches maximum.

$V = 0$ for different kind of atoms, the repulsive interaction keeps the same kind of atoms away from each other, forming the "anti-ferromagnetic" groundstate for A-bosons (B-bosons), let me call it $|A_{AF}>$ ($|B_{AF}>$). But, in contrast to the Mott insulator the structures of A- and B-bosons can partly or fully coexist on top of each other. In this regime, the Hilbert space can be reduced to the subspace of all superpositions of $|A_{AF}>$ and $|B_{AF}>$. The of-site in-plane correlation is reduced by entangled AB occupations at one site and empty sites, whereas the on-site square of the in-plane spin component is maximal. For increasing but small V the Hilbert space is reduced in order to avoid A-B entangled pairs, to give a simple picture the A- and B- structures are shifted by one site, but are still movable in respected to the lattice and in respect to each other, implying superfluid counter flow. In this regime the next neighbor in-plane correlations increase and the on-site square of the in-plane spin component is reduced.

5.2.2   The ferromagnetic correlated regime

The ferromagnetic regime is characterized by a first neighbor easy axis correlation function which has values bigger than zero. This means, that neighboring sites prefer to be occupied by the same kind of atoms. If high fluctuations occur (see Fig. 5.5) combined with ferromagnetic correlations, the system is in a ferromagnetic correlated superfluid state.

Remember, that we have $N = 8$, this $d = 3$ is the maximum distance in the unitary cell, one could easily expect that for very big V/J and $U = 0$ the particles would prefer a 4-times occupation of the two sites which have the largest possible distance $d = 3$. However, we will see that this is not the case. The fluctuations for $U = 0$ and increasing V are shown in Fig. 5.17. The AA- and the BB-fluctuations are
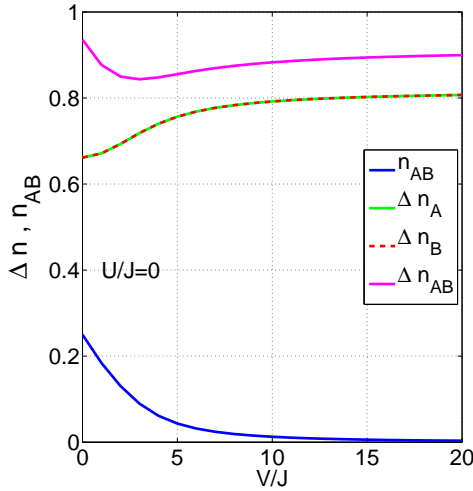

Figure 5.17: (a) The different parts of the fluctuations and occupations for $U = 0$ and the density fluctuations (magenta) are shown here. The suppressing of the AB occupation increases the AA- and BB- fluctuations, and therefore the density fluctuations increase. That is connected to a special superfluid ordering we will present in the following, where AA- and BB fluctuations are enhanced and BA fluctuations can be avoided.

enhanced in contrast to the AB-occupations, which are avoided and are reduced to half of the maximum for $V = 3J$. This is caused by high on-site-interaction V for different kind of atoms. The AA- and the BB-fluctuations increase in this region. Therefore the system stays superfluid: after a minimum at $V \approx 3J$ the density fluctuations increase again (see Fig. 5.17, magenta line) and stay robustly high even for very large V. The multiple occupation of the same sorts of atoms begin to increase only when the occupation of A and B- bosons in one site is reduced. To understand this, the basis has been truncated to single or double occupied sites for both sorts of atoms. In this case the observed anomalies do not occur. This indicates that the anomalies are linked to a supersolid formation with multi occupied sites. To investigate this effect further, in Fig. 5.18 are shown the z-component distance-correlation-functions in the superfluid regime in case of $U = 0$ and increasing V/J. For $V = 0$ all correlations are equal, for increasing V/J the 1st nn-AA and the on-site-AA increase and $2nd - nn$-AA and $3rd - nn$-AA z-correlations decrease. The system prefers a configuration where the different sorts of atoms are separated by several tunneling events. As multiple occupation
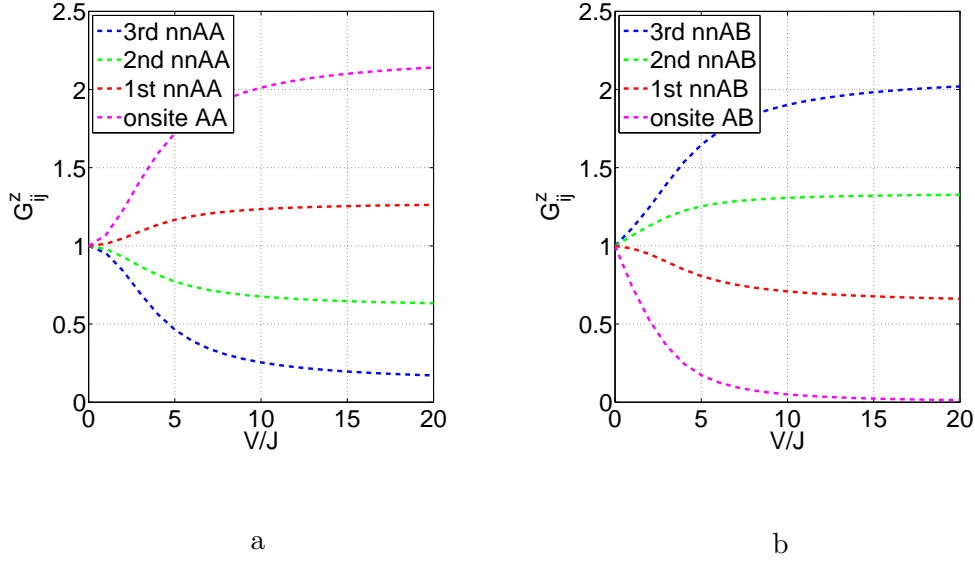
a   b

Figure 5.18: (a) Shown here are the AA correlation for different distances for $U = 0$. The g_{ii}^z gives the multiple AA occupation, $g_{1ST-NNaa}^z$-AA corresponds to the neighboring sites and so on (see 5.4-Fig. 5.3). The closer the corresponding site, the higher the AA-correlations. (b) Shown here are the AB correlations for different distances for $U = 0$. The closer the corresponding site, the smaller the AB-correlations. Note: at $V = U = 0$ all correlations are equal, owing to the fact that all particles are equal and not interacting.

is allowed for small U/J, the part of the wavefunction where a site is occupied with two or more A-bosons increases and there is a decreasing probability for the B-bosons to be nearest or second nearest neighbor and vice versa. On a fixed site of an eight sited cell, there are three sites which are two distances away, and one site which is three distances away. Atoms of one sort arrange themselves around a multi-occupied site and as far as possible away from the other atom sort. Considering the fluctuations this understanding is supported, see Fig. 5.17. In the corresponding parameter regime the atoms in the lattice are forced in a confined area in the cell to avoid interactions with the other particle sort. They can tunnel between 'their' sites and supporting multiple occupation. That enhances the AA- and BB- fluctuations and therefore also the density fluctuations, the AB on-site occupations are suppressed. To give a sketch of the supersolid configuration, which support our understanding, it is depicted in Fig. 5.19 a. The blue bubbles mean high B-boson probability and the magenta bubbles mean high A-boson probability. The density wave for the A- and the B-bosons along the path which is denoted by arrows is shown in Fig. 5.19 b. In this configuration, a multiple occupied site is surrounded by at least one particle of the same specie. Concurrently at the maximum distance, the other atom sort has 'its' multiple occupied site, surrounded
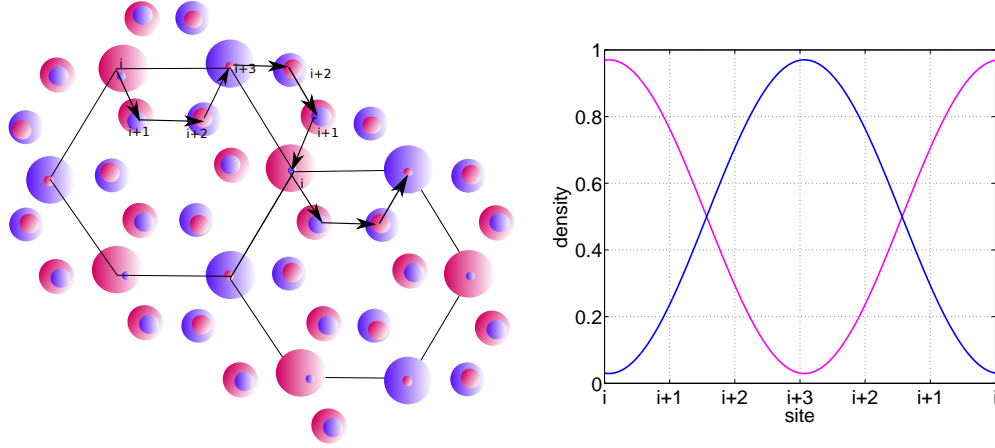
Figure 5.19: A sketch of the ferromagnetic correlated superfluid is shown in a), the atoms can fluctuate between sites which are occupied with the same sort in a high rate, supporting multiple occupation of the same sort and simultaneously avoiding the interaction with the other sort of atoms. Clusters of fluctuating A-bosons and B-bosons occur. In case of increasing U/J multi occupied sites are reduced and the supersolid formation is dissipated. In b) is shown the density wave for the A- (magenta) and the B-bosons (blue) along the path denoted by arrows in a).

by at least one particle of the same specie. Hence the particles are arranged in clusters.

Higher order correlation functions - the supersolid formation

To proof the supersolid formation, a normalized four particle correlation-function ζ_{AA-BB} is computed in case of $V/J = 50$ to demonstrate the formation of the supersolid supercell. It is given by

$$\zeta_{AA-nBB} = \frac{\left\langle n_i^A(n_i^A - 1)n_j^B(n_j^B - 1)\right\rangle - \left\langle n_i^A(n_i^A - 1)\right\rangle\left\langle n_j^B(n_j^B - 1)\right\rangle}{\Delta(n_i^A(n_i^A - 1))\Delta(n_j^B(n_j^B - 1))} \quad (5.19)$$

and it shows the correlation between an at least double occupation of boson A in site i and an at least a double occupation of boson B in site j. Site j is the first, second or third next neighbored site. It is obvious, that this correlation has its maximum value at $U = 0$ and for the third next neighbor, see Fig 5.20. This is consistent with the supersolid structure and is a good indication, since $d = 3$ is the maximum distance in an eight sited cell. The second next neighbor function is nearly uncorrelated, despite a small increase around $U/J = 2$. The first next neighbor correlation of double occupation is negative, meaning that the contribution of the wavefunction, where a double occupation of A- atoms is nearest next neighbor to a double occupation of B-atoms, is very unlikely. For very small
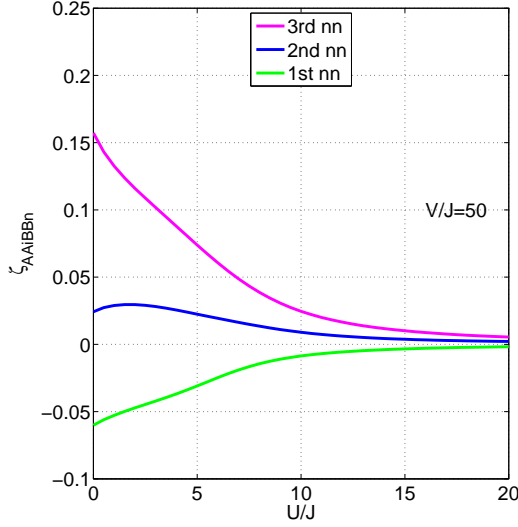
Figure 5.20: Shown is here the AA-double-occupation-BB-double-occupation correlation function for the first, the second and the third next neighbor. The third next neighbor correlation is maximum and has its maximum value at U equal to zero. The second neighbor-correlation is much lower and the first next neighbor correlation function is even anticorrelated.

U/J (nearly zero) the contribution of four- or three-occupations of one atom sort at one site has its maximum value. If U/J increases, the four-times and the three-times A- or B-occupations decrease very fast at $U/J = 1$ till $U/J = 2$. Therefore, it gets more likely that a second nearest neighbored site contains two atoms of the other specie, hopping around and in their 'supersite'. This small increase of the second next neighbor double correlation function therefore represents the broadening of the A and B- density wave and the increase of their overlap. For very small U/J the system must be arranged in a state where AA- and BB-fluctuations are supported and AB-occupation can be avoided. To get a direct proof of our picture, we finally computed a normalized six particle correlation function which indeed gives correlation of the following case: Besides an at least double AA-occupied site i, surrounded by at least one atom of the same sort at site $i+1$, we proof an at least double BB-occupied site in j, surrounded by at least one B-boson in the next neighbored site. This correlation function $\zeta_{AAiABBnB}$ is given by

$$\zeta_{AAiA-BBjB} = \frac{\left\langle n_i^{AA} n_{i+1}^A n_j^{BB} n_{j+1}^B \right\rangle - \left\langle n_i^{AA} n_{i+1}^A \right\rangle \left\langle n_j^{BB} n_{j+1}^B \right\rangle}{\Delta(n_i^{AA} n_{i+1}^A)\Delta(n_j^{BB} n_{j+1}^B)} \qquad (5.20)$$

with

$$n_i^{AA} = n_i^A(n_i^A - 1) \qquad \text{and} \qquad n_j^{BB} = n_j^B(n_j^B - 1). \qquad (5.21)$$

The data of $\zeta_{AAiA-BBjB}$ is displayed in Figure 5.21. It has its maximum value for U/J equal to zero and for the third next-neighbor and it is reduced to the half of its maximum at $U/J = 4$, where I assume the supersolid breakdown, which is
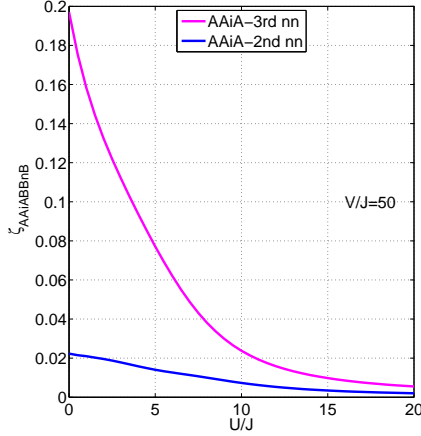
Figure 5.21: Shown here is the $\zeta_{AAiA-BBjB}$-correlation-function. It proofs an at least AA-double occupied site i, surrounded by at least one A next nearest neighbor and vice versa for the B-bosons in site i+2 and i+3. The high correlations of the third neighbor for small on-site U and $V/J = 50$ is a good proof for the described supersolid. The $\zeta_{AAiA-BBjB}$ for the second next neighbor is nearly uncorrelated.

dicussed in the following. The maximum of the corresponding correlations for the second next neighbor added only up to one-tenth of the value for the third next neighbor, this is consistent with the described supersolid.

Higher order correlation functions - the supersolid breakdown

To investigate the breakdown of the supersolid for increasing U/J we again take a look at the fluctuations and occupations in case of $V/J = 50$, i.e. the regime where I identified the supersolid. In Fig. 5.22 the fluctuations and n_{AB}-occupations are shown. As $V/J = 50$ is very large, the fluctuations are given nearly only by the AA- and BB-fluctuations. Figuratively spoken, the A- and B-bosons can, in the supersolid formation, tunnel in and around 'their' supersite. For $U/J = 4$ the n_{AB}-occupation peaks (see Fig. 5.22 b) indicating the breakdown of the supersolid. If U/J increases the A- and the B-clusters have the biggest possible overlap before the supersolid breakdown appears. To investigate this, the κ_n function is explored which can be viewed as a "flip-flop" to the n-th nearest neighbor, involving a triple occupied site with at least two bosons of the same species. The κ_n function has been computed by M. Prada.

$$\kappa_n = \frac{1}{\Omega_n} \sum_{<ij>_n} \left\langle n_i^A(n_i^A - 1)(\hat{S}_i^- \hat{S}_j^+ + \hat{S}_i^+ \hat{S}_j^-) \right\rangle \tag{5.22}$$

with Ω_n being the normalization factors,

$$\Omega_n = \eta_n \frac{(n_A + n_B)}{2} \tag{5.23}$$

, η_n being the number of the n-th next neighbor and the sum performed for the n-th next neighbor. The data of κ_n is shown in Fig. 5.23.
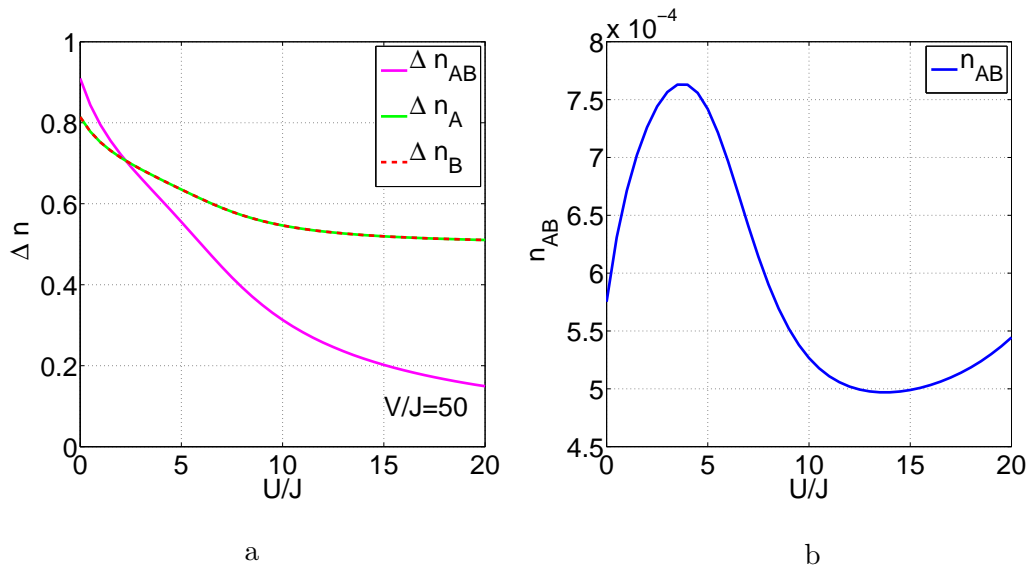
a

b

Figure 5.22: Shown here (a), are the different fluctuations Δn_{AB}, Δn_A, Δn_B and the on-site occupation of A- and B- particles n_{AB} for $V/J = 50$. As the on-site occupations of A-and B-particles are very low, the fluctuations are nearly only given by AA- and BB-fluctuations. In the region for $U/J \approx 4$ the onsite A-B-occupation-function peaks (b), which is a indication of the breakdown of the supersolid formation and a phasetransition towards the ferromagnetic 'chain'-formation.
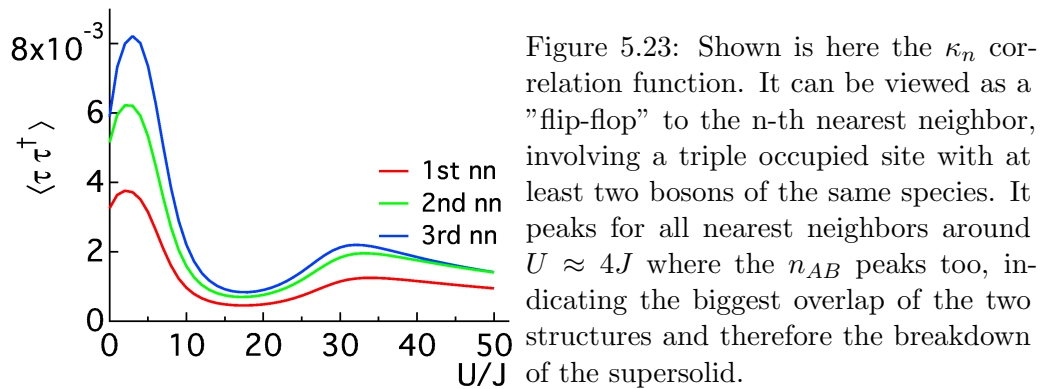
Figure 5.23: Shown is here the κ_n correlation function. It can be viewed as a "flip-flop" to the n-th nearest neighbor, involving a triple occupied site with at least two bosons of the same species. It peaks for all nearest neighbors around $U \approx 4J$ where the n_{AB} peaks too, indicating the biggest overlap of the two structures and therefore the breakdown of the supersolid.

The κ_n for the n-th nearest neighbor peaks around $U \approx 4J$, where also n_{AB} peaks, even in the same order of magnitude. The κ_3 shows the highest correlation, which is consistent with the supersolid order. One has to keep in mind that κ_n only takes

into account those contributions which involve an AB entangled flip-flop state. For simplification in case of a superposition of only two states e.g. $|\Psi\rangle = \alpha|a> + \beta|b>$ with

$$|a> = \left|....,\underbrace{AAB}_{i},....,\underbrace{A}_{j},...\right\rangle \qquad (5.24)$$

and

$$|b> = \left|....,\underbrace{AAA}_{i},....,\underbrace{B}_{j},...\right\rangle \qquad (5.25)$$

the expectationvalue of κ_n results in

$$\left\langle\Psi|(n_i^A(n_i^A - 1)(\hat{S}_i^-\hat{S}_j^+ + \hat{S}_i^+\hat{S}_j^-)|\Psi\right\rangle = 2(\alpha^*\beta + \beta^*\alpha). \qquad (5.26)$$

In the regime $V/J = 50$ these states are not very likely, since an AB occupation at one site is very improbable therefore the κ_n is very small. For increasing U/J, $(n_i^A(n_i^A - 1))$ reduces κ_n, in contrast the n_{AB} increases, the two clusters of fluctuating bosons increase their overlap. This increasing overlap enhances the n_{AB}, and therefore κ_n peaks. At this point the supersolid phase is no longer energetically convenient and the supersolid breaks down. Beyond the supersolid breakdown, increasing U/J starts to force particles of the same specie to stay one site apart and the particles begin to regroup in the 'chain' formation, which will build up the Mott insulator phase in the ferromagnetic regime. For very small U/J, the part of the four A- or four B-particle chain in the wavefunction is very small, see Fig 5.24. The increase of at least one particle-chain (A- or B-chain,
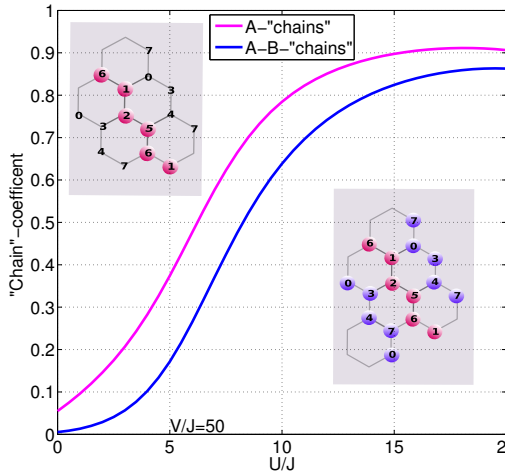
Figure 5.24: Shown here are the "chain"-formation-contributions of the ground-state. The blue line means the A- and B-"chain"-formation which gives the ferromagnetic Mott insulator state. The magenta line shows the part of the wavefunction where at least one particle sort is in the "chain"-formation. The other particle sort may be multiply occupied. The insets depict one example for an A- and B-"chain" and one example for an one-particle-"chain".

see inset upper left in Fig 5.24) has its maximum value between $U/J = 5$ and $U/J = 7$, after the maximum of the n_{AB}-occupation where the supersolid breaks

down (see Fig. 5.22). From $U/J \approx 4$ the 'chain'-formation increases fast, see Fig. 5.24. This means that the system is driven towards the Superfluid Mott insulator crossing. At $U/J = 6$, the groundstate is given by 50% of chains of one particle sort. For $U/J = 8$, the Mott insulator chain-formation (inset of Fig 5.24 lower right) supply nearly 50 % to the groundstate configuration and the increase gets weaker. In case of $U/J = 15$ the "chain" contribution amounts to more than 80%. During the Mott insulator crossing the n_{AB} is strongly reduced as well as the double occupancy. These facts causes the extinction of the doubly occupied flip-flop correlation function κ in this regime. To conclude, the z-correlations for the n-th next-neighbor (see in Fig. 5.25) and the different fluctuations and n_{AB}-occupations (see Fig. 5.26) are shown during the whole transition from the supersolid towards the ferromagnetic Mott insulator in case of $V/J = 50$ and increasing U/J. In the regime of $0 \leq U/J \leq 4$ high density fluctuation, which consist of AA- and BB-fluctuations, monitor a superfluid state, (see Fig. 5.26 a). High on-site correlations of same kind of atoms and high correlations in respect to the third next neighbor in case of different kind of atoms (see Fig. 5.25) indicate the supersolid structure, which has been examined with higher order correlation functions in the previous section. Increasing U/J leads to the breakdown of the supersolid. This can be identified by the minimum of the $3rd$-nn-AB correlation function and the increased $1st$-nn-AB correlations (see Fig. 5.25 b). The on-site AA-correlations are strongly reduced due to increasing onsite U, one site cannot be occupied by three or four atoms of same kind any more. This enhances the $1st$-nn-AA correlations as well as the $2st$-nn-AA correlations (see Fig. 5.25 a). In case of $U/J \approx 4$ the n_{AB} occupation reaches maximum (see Fig 5.26 b), this is consistent with the picture of the overlap of the A-cluster and the B-cluster. Due to the increase of the on site interaction the supersolid structure is not longer energetically convenient. The supersolid formation breaks down. In case of $U/J \geq 4$ the density fluctuations are reduced to less than 0.6 (see Fig. 5.26 a) and an increasing contribution of the groundstate wavefunction is given by the "chain" formations (see Fig. 5.24). The increase of these contributions reaches maximum in the regime of $5 \leq U/J \leq 8$. In this regime the $1st$ nn AA correlation function increase further, (see Fig.5.25 a). This is due to the Mott insulator chains which provide mostly ferromagnetic correlation for the next nearest neighbor. The probability for the same kind of boson being nearest next neighbor is two-third whereas the probability is one-third for the different kind of boson being nearest next neighbor. This is consistent with a chain formation, see inset of Fig. 5.24. In contrast the 'chains' let the $3rd$-nn- AB-correlation increase again, (see Fig.5.25 b). The $2nd$-nn-AA correlation function stay smaller, since in the chain formation the probability that the site, which is two sites away is occupied with the same kind of boson is one-third compared to the probability of two-third that it is occupied with the other kind of bosons. Additionally the $3rd - nn - AA$ z-correlation is suppressed, because of the 'chain' formation, (see Fig.5.25 a). In the regime around $U/J \approx 15$ the system is driven towards the

ferromagnetic Mott insulator, where the contribution of A and B chains amount to more than 80 % and the density fluctuations are reduce to less than 0.2, (see Fig. 5.26 a). If the system is driven to the ferromagnetic to anti ferromagnetic crossover, the correlations get assimilated, resuming, the A and B bosons to be indistinguishable.
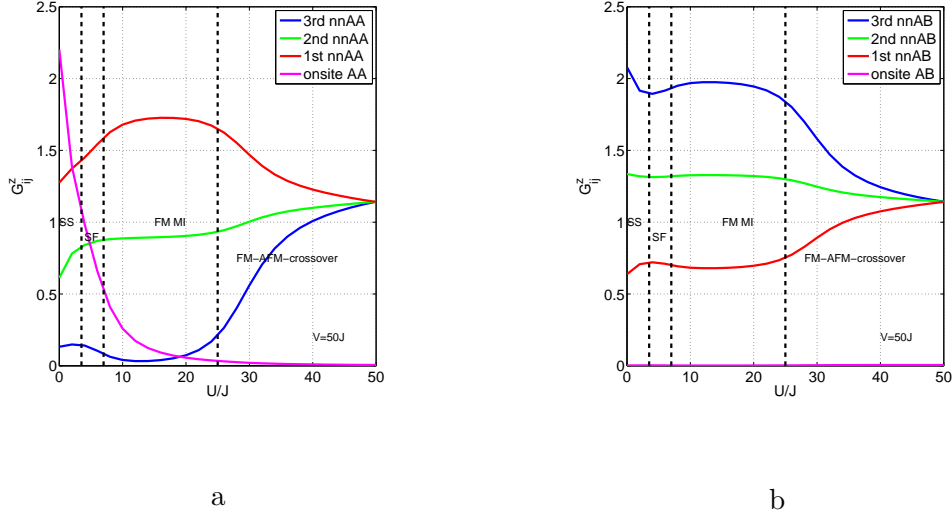
a

b

Figure 5.25: (a) Shown here are the AA correlation for different distances for $V = 50J$. The on site-AA z-correlation gives the multiple AA correlatations, the $1st - NN - AA$ corresponds to the next neighbored sites and so on (see Fig.:5.1-Fig.: 5.4). (b) Shown here are the AB correlation for different distances in case of $V = 50J$, inscribed are the different phase-transitions, the supersolid, the superfluid, where the chain formation starts, the ferromagnetic Mott insulator and, in case of similar parameter U/J and V/J, there is the ferromagnetic to anti ferromagnetic crossover, where all correlations assimilate.

a

b
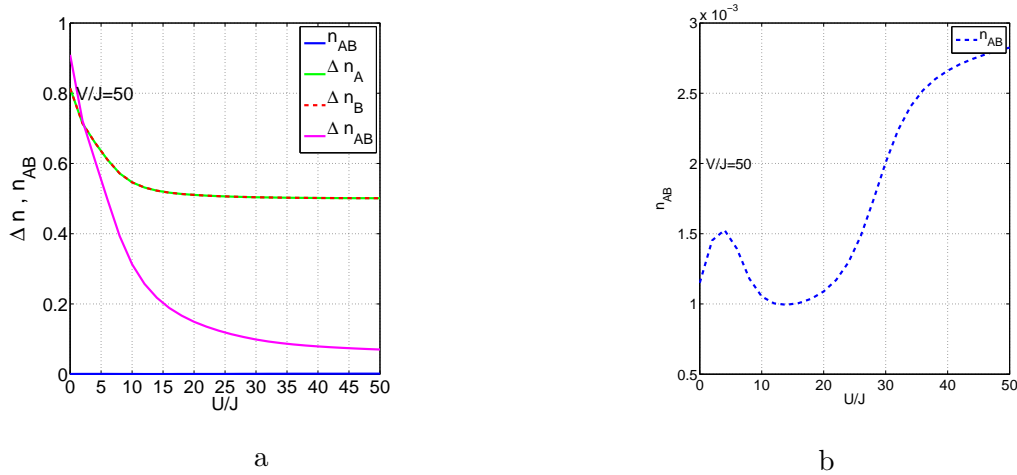
Figure 5.26: (a) Shown here are the different fluctuations for $U = 0 - 50J$ in case of $V/J = 50$. Take into account, that the lowest AA or BB-fluctuations are given by 0.5, due to half filling. (b) Shown here are the n_{AB} on-site occupations. They increase until the breakdown of the supersolid phase, then they decrease. Since the increase of the contribution of the "chains" in the wavefunction is maximum, the MI phase-transition is entered. When the system crosses the ferromagnetic to anti ferromagnetic regime, the n_{AB}-occupation increase again.
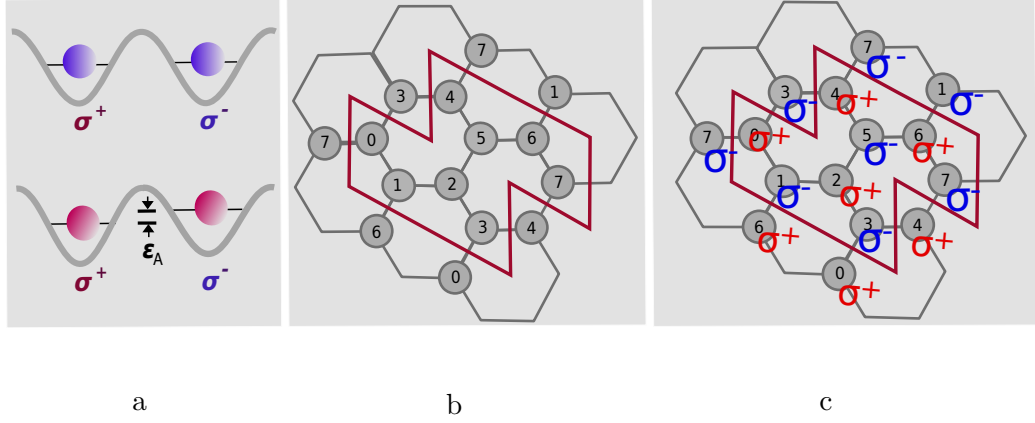
Figure 5.27: (a) To break the symmetry and investigate superfluid correlations a spindependent lattice potential is implemented for the A-bosons, two sublattices appear, characterized by σ^+- and σ^--sites (c). For the B-bosons the lattice has a homogeneous honeycomb structure (b).

5.2.3 Symmetry break

To explore the unconventional magnetic order further, I implement a small shift ϵ for one sort of atoms in one half of the lattice, this corresponds to staggered sites for the A-bosons. The B-bosons just can react on this by the interaction between different particle sorts V. The corresponding Hamiltonian is given by:

$$\mathbf{H} = -\hat{J} + \hat{U} + \hat{V} + \epsilon_{\mathbf{A},\sigma+/\sigma-}$$

This situation is shown in Fig. 5.27. For the 'blue', the B bosons, the honeycomb lattice is homogeneous (Fig. 5.27 b) and every site has equal depth, see Fig. 5.27 a (top). For the red, the A bosons two neighbored sites differ by a small additional potential ϵ_A, see Fig. 5.27 a (bottom). This ends up in a situation with two sub-lattices (Fig. 5.27 c) for the A-bosons. Experimentally this can be done by using laser beams with a defined polarization [8],[70], as it was explained in Section 2.2.2. The entire setting has been evaluated with half filling for both bosonic species in the superfluid regime and in the crossover regime. I analyze the population imbalance between two neighboring sites for both bosonic species, to determine wether a supersolid phase can be identified in our system experimentally. Shown in Fig. 5.28 are the occupation imbalance

$$\Delta n_{A,B} = \left\langle n_{A,(B),i} - n_{A,(B),i+1} \right\rangle \tag{5.27}$$

between neighboring sites for A- and B-bosons. They denote the amplitudes of the density modulation from site to site. The implemented shift between the two sub-lattices for the A-bosons is $\epsilon = 0.1J$. An occupation difference smaller than zero
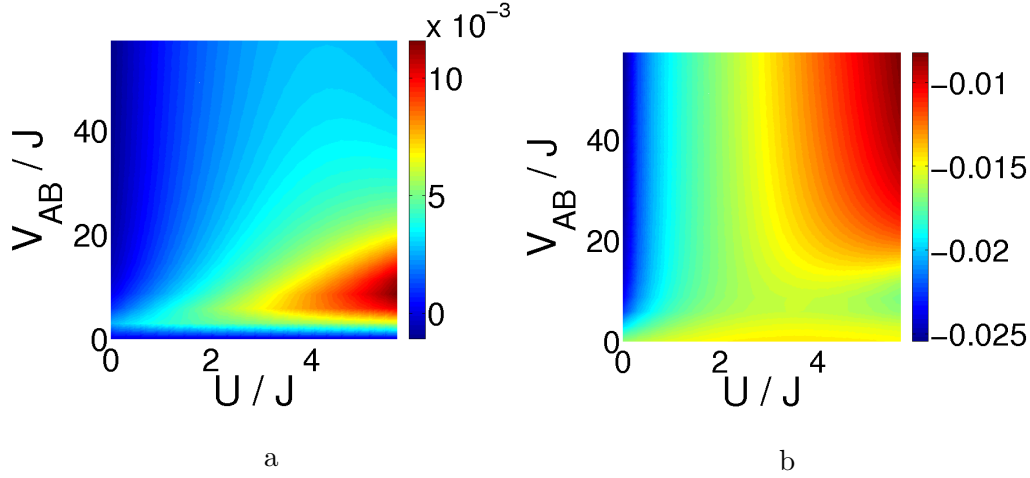
Figure 5.28: (a) Occupation-difference for neighboring sites for the B bosons, for very small on-site-interaction U B bosons occupy also predominantly σ^+ sites, due to the supersolid-formation. It peaks around $U/J \approx 4$, which denotes the breakdown of the supersolid, where the clusters of A and B bosons have the largest possible overlap. (b)Occupation-difference of neighboring sites for A bosons. In the whole regime, A bosons prefer to sit on σ^+ sites, for very small U/J they prefer the multiple occupation of one σ^+-site.

means a dominated occupation of the σ^+-site, whereas an occupation-difference which is bigger than zero means, the atoms prefer to sit at the σ^--site. On the left, the occupation difference of the B bosons and on the right the occupation difference of the A-bosons is depicted. However, the occupation difference of the B-bosons peaks at $U/J \approx 4$ due to the supersolid breakdown when the two clusters of A and B bosons are broaden which results in an increasing overlap of A and B bosons. As expected, the A bosons prefer to occupy the σ^+-site in general. For $V = 0$ no effect can be identified for the B-bosons, which are not subjected to a sublattice structure, and cannot react on the A-bosons, since the interaction between different particle sorts, V, is zero. Therefore, the occupation difference of the B-bosons starts at $V/J > 0$. If we have a closer look at the B-bosons behavior, we can identify a dark blue regime, for very small U and increasing V/J. Here the occupation difference is smaller than zero, which means, that B-bosons seem to occupy dominantly σ^+-sites. Due to the supersolid-formation, the A-bosons multiple occupy a σ^+-site and the B-bosons therefore multiple occupy the site at most distant d=3, which is a σ^--site. But, as it is surrounded by 3 dominantly B-type nearest next neighbors which are σ^+-sites, the average B-bosons favor an occupation of σ^+-sites, in case of very small U/J. This occupation reversal does not happen for the A-bosons, due to the shift which appears only to the A-bosons. They dominantly occupy σ^+-sites for very small on site U/J, see scetch in Fig.
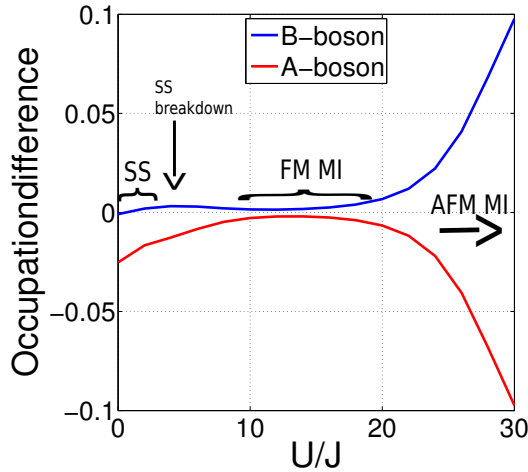
Figure 5.29: Occupation-difference for neighboring sites for the A- and B-bosons in case of $V = 50\,J$ and $U = 0 - 30\,J$. The supersolid breakdown and the occupation reversal can be detected. The occupation difference becomes symmetric and has its maximum value in the antiferromagnetic Mott insulator, where the the A bosons are pinned at the σ^+ - and the the B-bosons at the σ^- -sublattice.

5.30. For increasing U/J, the two clusters broaden and the overlap increases, the occupation difference for the B-boson increase. After the breakdown of the supersolid formation, it decrease, when the system enters the ferromagnetic Mott insulator transition and build up the A- and B- "chains". This peak in the population imbalance can be identified as the supersolid signal. We therefore propose a scheme for which a supersolid can be detected in experiments. In Fig. 5.29 the occupation imbalance for $V = 50\,J$ and $U = 0 - 30\,J$ is shown. In the regime $0 < U/J < 16$, the occupation difference decreases and later rerise for values of U/J bigger than 16, shown in Fig. 5.29. This can be explained by the fact, that for very small U the influence of the small shift ϵ_A is strong, therefore the occupation difference is remarkable. For increasing U/J the influence of ϵ_A decreases and the high occupation of more than two atoms per site is reduced, the supersolid structures are broaden and the system goes across the ferromagnetic Mott insulator phase by building the A- and B-"chains". Therefore the population imbalance vanishes in the "chain"-formation. For further increasing on site interaction U/J, the occupation difference increases due to the virtual tunneling. Neighboring sites are rather not occupied by the same atoms, thus the crossover regime is entered. In the anti ferromagnetic regime, the occupation difference is expected to be maximal as the A bosons are located in the energetically lower sublattice (σ^+-sites), see chapter 3.2. Due to $U > V/J = 50$ the B-bosons would prefer the other sublattice (σ^--sites), see Fig. 5.29. The supersolid formation in case of an energy shift would of course be nonsymmetric, the sketch in Fig. 5.30 gives an idea. The red bubbles mean predominantly occupation of A bosons and the blue bubbles mean predominantly occupation of B bosons. The A bosons accumulate a bit more in the "supersite" as they are subjected to an additional small potential.
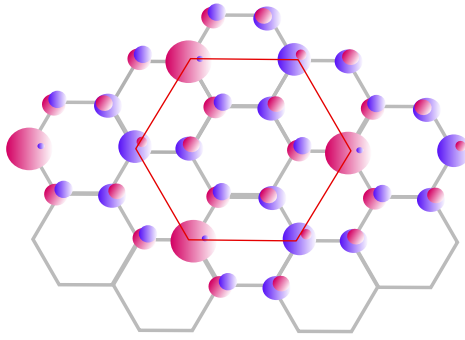
Figure 5.30: One possible structure of a ferromagnetic correlated superfluid in case of a small shift ϵ between the two sublattices. The structure is not symmetric, as the B bosons occupy dominantly σ_+-sites for vanishing U/J, the occupation difference is smaller than zero.

5.2.4 Finite-size-effects

As I evaluate finite-size effects in the Mott insulator regime I will consider now the ten sited cell, the data has been computed by M. Prada. In section 4.3.4 I found that the ferromagnetic groundstate of the ten sites cell is not given by a "chain" structure like in the eight sited case. In the ferromagnetic ground state a domain formation of the bosonic components is possible, see Fig. 5.31.
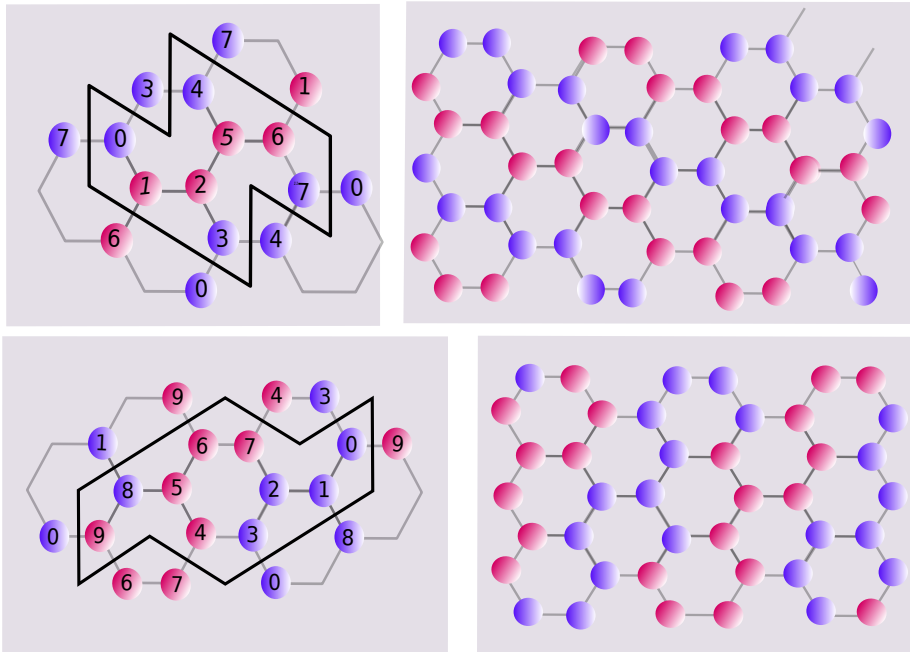
Figure 5.31: The ferromagnetic groundstate in case of unitary cell with eight sites (top left) is the "chain"-formation (top right). In case of ten sites per unitary cell (bottom left) a clear domain structure can be obtained (botton right).

The iso-magnetic correlations in the Mott insulator phase have been discussed in section 4.3.4 in case of a ten sited cell. In Fig. 5.32 left, the in-plane correlations of the n-th next neighbors are depicted. It strikes that in the superfluid regime for
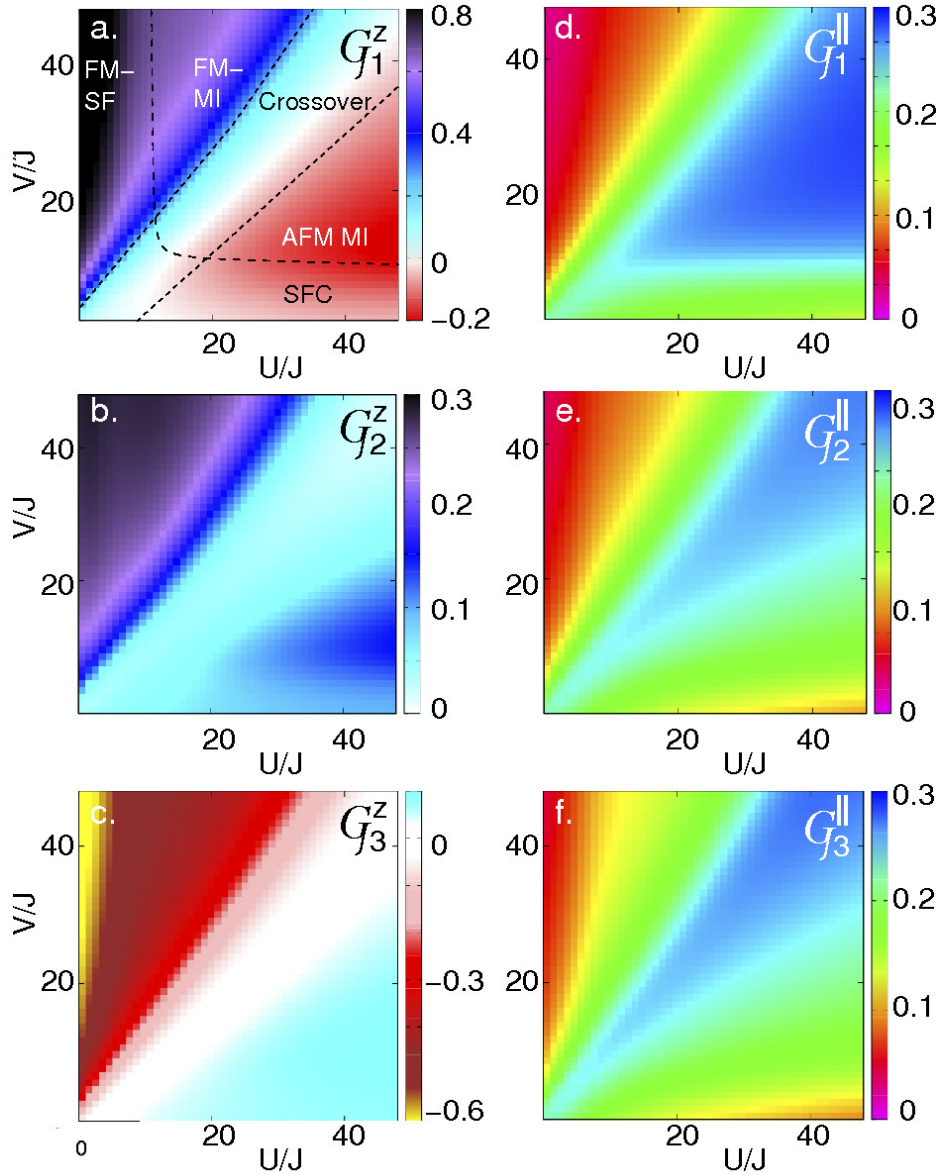
Figure 5.32: Shown on the left are the numerical results for the in-plane correlations of the first (a) the second (b) and the third(c) next neighbor. Shown on the right are the z-correlations of the first (a) the second (b) and the third (c) next neighbor. Compared to the correlations for the eight sited cell, first it strikes also the absence of the supersolid-peak and second the ferromagnetic correlations for the second next neighbor. The first is due to the fact, that $N = 10$ is not commensurate with the supersolid structure and the second is due to the domain formation in the ferromagnetic Mott insulator. In the domain formation, the second next neighbor is dominated by the same kind of atom, providing ferromagnetic correlations.

small U and increasing V the "supersolid"-peak, is absent for all next neighbors. Apart from that, the correlations are similar to the corresponding in plane correlations of the eight sited cell. In Fig. 5.32 right, the z-correlations for the ten sited cell are shown. We stress, that the supersolid formation can not occur, because the cell with ten sites is incommensurate with the supersolid structure. It is striking, that the second nearest neighbor correlation-function is ferromagnetic, which is consistent with the phase separation of the two bosonic species, see Fig. 5.31. Concerning the nearest next neighbor correlations, there the absence of the supersolid formation is reflected in an enhancement of the ferromagnetic correlations in the deep superfluid regime for small U and increasing V/J. Additionally the ferromagnetic correlations in the Mott insulator are stronger, due to the domain structure of the ten sites system.

5.3 Conclusions

In the last chapter I investigated the superfluid regime of the honeycomb lattice filled with two sorts of bosons. I obtained a rich phase diagram which has been evaluated further by developing in-plane- and out-of-plane pair correlation functions to explore the correlations in respect to the first, the second and the third nearest neighbor. In the superfluid regime in case of $V = 0$ and strong U/J, a phase has been identified where the particles of different sorts show high entanglement and the on-site square of the in-plane spin has its maximum value. The reduce of the in-plane next neighbor correlation in this regime suggests that there is an huge contribution of double (AB) occupied sites, next neighbored with empty ones. For increasing but small V this is transferred to an SCF-phase. In the superfluid regime where U is very small and V/J is large, I evaluate the ground state as supersolid, meaning that a density modulation exist simultaneous with a superfluid state. The supersolid formation lowers the translational symmetry. A unit cell with eight sites is necessary to represent this supersolid, in contrast to a unit cell of two sites for the honeycomb lattice. We get a direct proof of the supersolid formation and the supersolid breakdown by computing three-, fourth- and six-operator correlation-functions. We further explore the supersolid breakdown and its phase transition to the Mott insulator. Furthermore, we break the symmetry with a spin-dependent lattice, therefore we could identify a supersolid signal in the population imbalance from site to site. Hence, we suggest an experimental method to detect a supersolid phase by implementing a spin depending lattice potential. To conclude, finite size effects were explored in case of a ten sites cell expecting the absence of a supersolid-signal due to the fact, that the N=10 cell is incommensurate with the supersolid-formation. The in-plane and out-of plane correlations show the absence of this special phase. Apart from that, the important features of the phase diagram were reproduced also for the ten sited cell. This suggests that the results of the pair-correlation functions and the different isomagnetic phases even are valid for larger systems.

Chapter 6

Summary

In this work, one and two-component ultracold quantum gases in optical lattices has been studied in the superfluid and in the Mott insulator phase in an exact diagonalization framework by computing particle occupations, fluctuations, site-to-site, and higher order correlation functions for commensurate and incommensurate fillings. In doubly filled systems, the superfluid to Mott insulator crossing is shifted to higher values of U/J in agreement with mean-field calculations. For incommensurate fillings no Mott insulator can be reached in a homogeneous lattice. Criteria were established to identify whether our system is in the superfluid or in the Mott insulator state. In order to estimate finite size effects, we investigated different sized lattice cells. For increasing cell sizes, the fluctuations and the on site correlations decrease stronger in the regime of the Mott-insulator crossing. This is in agreement with mean field calculation where the superfluid to Mott transition is prompt at the critical value U/J. In contrary to the infinite case our system showed gapped excitations even in the superfluid phase, however this gap decreases for increasing cell sizes. The level crossing of the first and the second exited state could be identified as a clear indication for the superfluid to Mott insulator transition. This crossing is the reason for a kink in the energy gap. In the case of the eight sited cell, in the regime above $U/J \approx 20$, a Mott insulating phase is observed which implies low particle fluctuations, low on-site-correlations and a "Mott"-characteristic groundstate with excitations, linear in U. In this groundstate every lattice site is occupied with one single atom in the case of a filling $\eta = 1$. Contrarily the super fluid regime, which is assumed for $0 \leq U/J \leq 5$ implies high particle fluctuations, high on-site correlations, and a "Mott"-characteristic state with high energy. As one main issue the groundstate of a bipartite honeycomb lattice with a triangular sub-lattice structure and a variable shift ϵ between the two sub-lattices is studied. This has been studied for different fillings from $\eta = 0.5$ up to $\eta = 2$ and detail-rich phase-diagrams could be archived. By changing the ratio of U/ϵ the system can be driven into the Mott insulator phase even for incommensurate fillings. The particles occupy the energetically lower sublattice with a filling of $2 \cdot \eta$. The energetically higher sublattice is depleted. For increasing U/ϵ it

is repopulated with a repopulation rate which depends on the ratio of U/ϵ. Therefore two different Mott insulators could be observed in the lattice simultaneously. In Chap. 4 we investigated the short ranged 'magnetic correlations' of the honeycomb lattice filled with two sorts of bosons. The system has been mapped onto a spin-$\frac{1}{2}$-system in second-order perturbation theory in the tunneling in the limit of $U, V_{AB} >> J$. To explore the magnetic order in any regime we introduced the z-correlation function. Depending on the ratio of interaction between same kind and different kind of bosons the phase diagram shows both anti-ferro-magnetic and ferro-magnetic correlations. First we focused on the Mott insulator regime. In the anti-ferromagnetic regime the groundstate of the system never assumes the Neél state, which is in agreement with theoretical predictions. Due to quantum fluctuations the anti-ferromagnetic ground state always contains, besides the staggered order, contributions where two (dimers) or even three (triples) adjoining lattice site are occupied with the same kind of atoms. These structures are related by one flip-flop hopping, revealing an in-plane (xy) groundstate. The ground state in the Mott insulator regime for $V_{AB} < U$ is ferromagnetic. In this regime the system builds two different domains each with one particle sort, independent on the cell size. In the case of the four sited cell and the eight sited cell, the A- and B-bosons are arranged in chains along the different symmetry axes. Cells with six sites and ten sites allow the creation of enclosed domains. As the ratio of domain wall and bulk increases for increasing cell sizes, increasing ferromagnetic correlations are provided.

In Chap. 5 the superfluid regime is focused, where detail-rich phase diagrams are obtained. This regime is investigated further by developing in-plane- and out-of-plane pair correlation functions to explore the correlations with respect to the first, the second, and the third nearest neighbor. In the superfluid regime for vanishing V and strong on-site U/J a phase could be identified, where the different iso-spins build up superpositions at one lattice site and the on-site square of the in-plane correlations has its maximum value. This implies a phase, where double occupied (AB)-sites alternate with empty sites, reducing the in-plane next neighbor correlations. Whether this is a precursor for a paired superfluid vacuum (PSF phase) could not be conclusively clarified. For increasing but small V/J this entangled state is transferred to the super counter fluid phase (SCF) which describes pairings of particles A and hole B in site i and pairing of particle B and hole A in the nearest neighbored site. The on-site square of the in-plane correlations is strongly reduced whereas the next-neighbor in-plane correlations are enhanced, this supported the assumption of a super counter fluid.

In the superfluid regime where U is very small and V/J increases, the ground state is found to be supersolid. In this phase, the system can be described by a non-trivial density-modulation which lowers the symmetry. The superlattice period is four times bigger than the primary unit cell and includes simultaneous solid and superfluid qualities and the on-site square of the easy-axis spin component has it maximum value. We computed three-, four- and six-operator correlation func-

tions to get a direct proof of the supersolid formation. The development of these correlation functions also allows to monitor the breakdown of the supersolid. The transition to the ferromagnetic Mott-insulator is explored, where the groundstate of the system is given by domains each with one particle sort. Hence, an experimental method is suggested to detect a supersolid phase by implementing a spin depending lattice potential. Finite size effects are discriminated by calculating the in- and out-of-plane correlations for a ten sited cell, which is incommensurate with the supersolid supercell and remark the absence of the supersolid features. Apart from that, the phase diagram was reproduced also for the ten sited cell. This suggests that the correlation functions allow to distinguish the different quantum phases which also occur in macroscopic systems.

Bibliography

[1] The cold atom hubbard toolbox. *Ann. Phys. (N.Y.)*, 315(1):52 – 79, 2005. ISSN 0003-4916. doi: 10.1016/j.aop.2004.09.010. Special Issue.

[2] Ehud Altman, Walter Hofstetter, Eugene Demler, and Mikhail D Lukin. Phase diagram of two-component bosons on an optical lattice. *New Journal of Physics*, 5(1):113, 2003.

[3] M. H. Anderson, J. R. Ensher, M. R. Matthews, C. E. Wieman, and E. A. Cornell. Observation of bose-einstein condensation in a dilute atomic vapor. *Science*, **269**:198, 1995.

[4] P.W. Anderson. *Science*, 235, 1987.

[5] Daniel P. Arovas and Assa Auerbach. Functional integral theories of low-dimensional quantum heisenberg models. *Phys. Rev. B*, 38:316–332, Jul 1988. doi: 10.1103/PhysRevB.38.316. URL `http://link.aps.org/doi/10.1103/PhysRevB.38.316`.

[6] Sébastien Balibar. How could a solid be superfluid? *Physics*, 1:16, Aug 2008. doi: 10.1103/Physics.1.16. URL `http://link.aps.org/doi/10.1103/Physics.1.16`.

[7] C. Becker. Multi component bose-einstein condensates.

[8] C Becker, P Soltan-Panahi, J Kronjäger, S Dörscher, K Bongs, and K Sengstock. Ultracold quantum gases in triangular optical lattices. *New Journal of Physics*, 12(6):065025, 2010. URL `http://stacks.iop.org/1367-2630/12/i=6/a=065025`.

[9] I. Bloch. Quantum gases. *Science*, 2008.

[10] Immanuel Bloch, Jean Dalibard, and Wilhelm Zwerger. Many-body physics with ultracold gases. *Rev. Mod. Phys.*, 80: 885–964, Jul 2008. doi: 10.1103/RevModPhys.80.885. URL `http://link.aps.org/doi/10.1103/RevModPhys.80.885`.

[11] Massimo Boninsegni and Nikolay V. Prokof'ev. *Colloquium* : Supersolids: What and where are they? *Rev. Mod. Phys.*, 84: 759–776, May 2012. doi: 10.1103/RevModPhys.84.759. URL http://link.aps.org/doi/10.1103/RevModPhys.84.759.

[12] S. N. Bose. Plancks Gesetz und Lichtquatenhypothese. *Z. Phys.*, **26**(178), 1924.

[13] G. Grynberg C. Cohen-Tannoudji, j.Dupont-Roc. *"Atom Photon interaction"*. John Wiley and Sons Inc., 1992.

[14] H. Smith C. J. Pethick. *"Bose Einstein Condensation in Dilute Gases"*. Cambridge university Press, 2001.

[15] Andrey V. Chubukov, Subir Sachdev, and Jinwu Ye. Theory of two-dimensional quantum heisenberg antiferromagnets with a nearly critical ground state. *Phys. Rev. B*, 49:11919–11961, May 1994. doi: 10.1103/PhysRevB.49.11919. URL http://link.aps.org/doi/10.1103/PhysRevB.49.11919.

[16] F. Cinti, P. Jain, M. Boninsegni, A. Micheli, P. Zoller, and G. Pupillo. Supersolid droplet crystal in a dipole-blockaded gas. *Phys. Rev. Lett.*, 105:135301, Sep 2010. doi: 10.1103/PhysRevLett.105.135301. URL http://link.aps.org/doi/10.1103/PhysRevLett.105.135301.

[17] Ph. Courteille, R. S. Freeland, D. J. Heinzen, F. A. van Abeelen, and B. J. Verhaar. Observation of a feshbach resonance in cold atom scattering. *Phys. Rev. Lett.*, 81:69–72, Jul 1998. doi: 10.1103/PhysRevLett.81.69. URL http://link.aps.org/doi/10.1103/PhysRevLett.81.69.

[18] Gerd Czycholl. *"Theoretische Festkörperphysik"*. vieweg, 2000.

[19] K. B. Davis, M.-O. Mewes, M. R. Andrews, N. J. van Druten, D. S. Durfee, D. M. Kurn, and W. Ketterle. Bose-einstein condensation in a gas of sodium atoms. *Phys. Rev. Lett.*, **75**:3969, 1995.

[20] Demtröder. *Experimentalphysik 2*. Springer.

[21] S. Diehl, M. Baranov, A. J. Daley, and P. Zoller. Observability of quantum criticality and a continuous supersolid in atomic gases. *Phys. Rev. Lett.*, 104:165301, Apr 2010. doi: 10.1103/PhysRevLett.104.165301. URL http://link.aps.org/doi/10.1103/PhysRevLett.104.165301.

[22] L.-M. Duan, E. Demler, and M. D. Lukin. Controlling spin exchange interactions of ultracold atoms in optical lattices. *Phys. Rev. Lett.*, 91:090402, Aug 2003. doi: 10.1103/PhysRevLett.91.090402. URL http://link.aps.org/doi/10.1103/PhysRevLett.91.090402.

[23] A. Einstein. Quantentheorie des einatomigen idealen Gases: Zweite Abhandlung. *Sitzungsber. Preuss.Akad. Wiss.*, (3), 1925.

[24] T. Esslinger. Fermi-Hubbard Physics with Atoms in an Optical Lattice. *Annual Review of Condensed Matter Physics*, 1:129–152, April 2010. doi: 10.1146/annurev-conmatphys-070909-104059.

[25] Andreev A. F. and Lifshitz E. M. *Sov. Phys. JETP*, 29, 1969.

[26] Matthew P. A. Fisher, Peter B. Weichman, G. Grinstein, and Daniel S. Fisher. Boson localization and the superfluid-insulator transition. *Phys. Rev. B*, 40 (1):546–570, Jul 1989. doi: 10.1103/PhysRevB.40.546.

[27] Fabrice Gerbier, Artur Widera, Simon Fölling, Olaf Mandel, Tatjana Gericke, and Immanuel Bloch. Interference pattern and visibility of a mott insulator. *Phys. Rev. A*, 72:053606, Nov 2005. doi: 10.1103/PhysRevA.72.053606. URL http://link.aps.org/doi/10.1103/PhysRevA.72.053606.

[28] Fabrice Gerbier, Artur Widera, Simon Fölling, Olaf Mandel, Tatjana Gericke, and Immanuel Bloch. Phase coherence of an atomic mott insulator. *Phys. Rev. Lett.*, 95:050404, Jul 2005. doi: 10.1103/PhysRevLett.95.050404. URL http://link.aps.org/doi/10.1103/PhysRevLett.95.050404.

[29] Daniel Greif, Leticia Tarruell, Thomas Uehlinger, Robert Jördens, and Tilman Esslinger. Probing nearest-neighbor correlations of ultracold fermions in an optical lattice. *Phys. Rev. Lett.*, 106: 145302, Apr 2011. doi: 10.1103/PhysRevLett.106.145302. URL http://link.aps.org/doi/10.1103/PhysRevLett.106.145302.

[30] Markus Greiner, Olaf Mandel, Tilman Esslinger, Theodor W. Hänsch, and Immanuel Bloch. Quantum phase transition from a superfluid to a mott insulator in a gas of ultracold atoms. *Nature*, 415(6867):39–44, 2002. doi: 10.1038/415039a. URL http://dx.doi.org/10.1038/415039a.

[31] Rudolf Grimm, Matthias Weidemüller, and Yurii B. Ovchinnikov. Optical dipole traps for neutral atoms. volume 42 of *Advances In Atomic, Molecular, and Optical Physics*, pages 95–170. Academic Press, 2000. doi: http://dx.doi.org/10.1016/S1049-250X(08)60186-X. URL http://www.sciencedirect.com/science/article/pii/S1049250X0860186X.

[32] E. P. Gross. Hydrodynamic of a Superfluid Condensate. *J. Math Phys.*, **4**: 195–207, 1963.

[33] E.P Gross. Classical theory of boson wave fields. *Annals of Physics*, 4(1): 57–74, 1958. ISSN 0003-4916. doi: 10.1016/0003-4916(58)90037-X. URL http://www.sciencedirect.com/science/article/pii/000349165890037X.

[34] Eugene P. Gross. Unified theory of interacting bosons. *Phys. Rev.*, 106:161–162, Apr 1957. doi: 10.1103/PhysRev.106.161. URL `http://link.aps.org/doi/10.1103/PhysRev.106.161`.

[35] Kenneth Günter, Thilo Stöferle, Henning Moritz, Michael Köhl, and Tilman Esslinger. Bose-fermi mixtures in a three-dimensional optical lattice. *Phys. Rev. Lett.*, 96:180402, May 2006. doi: 10.1103/PhysRevLett.96.180402. URL `http://link.aps.org/doi/10.1103/PhysRevLett.96.180402`.

[36] Liang He, Yongqiang Li, Ehud Altman, and Walter Hofstetter. Quantum phases of bose-bose mixtures on a triangular lattice. *Phys. Rev. A*, 86:043620, Oct 2012. doi: 10.1103/PhysRevA.86.043620. URL `http://link.aps.org/doi/10.1103/PhysRevA.86.043620`.

[37] Anzi Hu, L. Mathey, Ippei Danshita, Eite Tiesinga, Carl J. Williams, and Charles W. Clark. Counterflow and paired superfluidity in one-dimensional bose mixtures in optical lattices. *Phys. Rev. A*, 80:023619, Aug 2009. doi: 10.1103/PhysRevA.80.023619. URL `http://link.aps.org/doi/10.1103/PhysRevA.80.023619`.

[38] Anzi Hu, L. Mathey, Eite Tiesinga, Ippei Danshita, Carl J. Williams, and Charles W. Clark. Detecting paired and counterflow superfluidity via dipole oscillations. *Phys. Rev. A*, 84: 041609, Oct 2011. doi: 10.1103/PhysRevA.84.041609. URL `http://link.aps.org/doi/10.1103/PhysRevA.84.041609`.

[39] A. Hubener, M. Snoek, and W. Hofstetter. Magnetic phases of two-component ultracold bosons in an optical lattice. *Phys. Rev. B*, 80:245109, Dec 2009. doi: 10.1103/PhysRevB.80.245109. URL `http://link.aps.org/doi/10.1103/PhysRevB.80.245109`.

[40] S. Inouye, M. R. Andrews, J. Stenger, H.-J. Miesner, D. M. Stamper-Kurn, and W. Ketterle. Observation of feshbach resonances in a bose-einstein condensate. *nature*, 392:151−+, March 1998. doi: 10.1038/32354.

[41] D. Jaksch, C. Bruder, J. I. Cirac, C. W. Gardiner, and P. Zoller. Cold bosonic atoms in optical lattices. *Phys. Rev. Lett.*, 81: 3108–3111, Oct 1998. doi: 10.1103/PhysRevLett.81.3108. URL `http://link.aps.org/doi/10.1103/PhysRevLett.81.3108`.

[42] Gyu-Boong Jo, Jennie Guzman, Claire K. Thomas, Pavan Hosur, Ashvin Vishwanath, and Dan M. Stamper-Kurn. Ultracold atoms in a tunable optical kagome lattice. *Phys. Rev. Lett.*, 108: 045305, Jan 2012. doi: 10.1103/PhysRevLett.108.045305. URL `http://link.aps.org/doi/10.1103/PhysRevLett.108.045305`.

[43] Strohmaier N. Gunter K. Moritz H. Esslinger T. Jordens, R. A mott insulator of fermionic atoms in an optical lattice. *Nature*, 455:204–207, 2008/09/11/print.

[44] Tassilo Keilmann, Ignacio Cirac, and Tommaso Roscilde. Dynamical creation of a supersolid in asymmetric mixtures of bosons. *Phys. Rev. Lett.*, 102:255304, Jun 2009. doi: 10.1103/PhysRevLett.102.255304. URL `http://link.aps.org/doi/10.1103/PhysRevLett.102.255304`.

[45] E. Kim, J. S. Xia, J. T. West, X. Lin, A. C. Clark, and M. H. W. Chan. Effect of ^{3}He impurities on the nonclassical response to oscillation of solid ^{4}He. *Phys. Rev. Lett.*, 100:065301, Feb 2008. doi: 10.1103/PhysRevLett.100.065301. URL `http://link.aps.org/doi/10.1103/PhysRevLett.100.065301`.

[46] Alexei Kitaev. Anyons in an exactly solved model and beyond. *Annals of Physics*, 321(1):2–111, 2006. ISSN 0003-4916. doi: http://dx.doi.org/10.1016/j.aop.2005.10.005. URL `http://www.sciencedirect.com/science/article/pii/S0003491605002381`. January Special Issue.

[47] Walter Kohn. Theory of the insulating state. *Phys. Rev.*, 133: A171–A181, Jan 1964. doi: 10.1103/PhysRev.133.A171. URL `http://link.aps.org/doi/10.1103/PhysRev.133.A171`.

[48] A. B. Kuklov and B. V. Svistunov. Counterflow superfluidity of two-species ultracold atoms in a commensurate optical lattice. *Phys. Rev. Lett.*, 90:100401, Mar 2003. doi: 10.1103/PhysRevLett.90.100401. URL `http://link.aps.org/doi/10.1103/PhysRevLett.90.100401`.

[49] Anatoly Kuklov, Nikolay Prokof'ev, and Boris Svistunov. Superfluid-superfluid phase transitions in a two-component bose-einstein condensate. *Phys. Rev. Lett.*, 92:030403, Jan 2004. doi: 10.1103/PhysRevLett.92.030403. URL `http://link.aps.org/doi/10.1103/PhysRevLett.92.030403`.

[50] Anatoly Kuklov, Nikolay Prokof'ev, and Boris Svistunov. Commensurate two-component bosons in an optical lattice: Ground state phase diagram. *Phys. Rev. Lett.*, 92:050402, Feb 2004. doi: 10.1103/PhysRevLett.92.050402. URL `http://link.aps.org/doi/10.1103/PhysRevLett.92.050402`.

[51] Anatoly B. Kuklov, Nikolay V. Prokof'ev, and Boris V. Svistunov. How solid is supersolid? *Physics*, 4.

[52] A. J. Leggett. Can a solid be "superfluid"? *Phys. Rev. Lett.*, 25:1543–1546, Nov 1970. doi: 10.1103/PhysRevLett.25.1543. URL `http://link.aps.org/doi/10.1103/PhysRevLett.25.1543`.

[53] M. Lewenstein. Ultracold atomic gases in optical lattices: Mimicking condensed matter physics and beyond, 2007.

[54] D.-S. Lühmann. Multiorbital physics in optical lattices.

[55] Dirk-Sören Lühmann, Kai Bongs, Klaus Sengstock, and Daniela Pfannkuche. Localization and delocalization of ultracold bosonic atoms in finite optical lattices. *Phy. Rev. A*, 77(2):023620, 2008. doi: 10.1103/PhysRevA.77.023620. URL `http://link.aps.org/abstract/PRA/v77/e023620`.

[56] Dirk-Sören Lühmann, Kai Bongs, Klaus Sengstock, and Daniela Pfannkuche. Self-trapping of bosons and fermions in optical lattices. *Phys. Rev. Lett.*, 101:050402, Jul 2008. doi: 10.1103/PhysRevLett.101.050402. URL `http://link.aps.org/doi/10.1103/PhysRevLett.101.050402`.

[57] L. Mathey, Ippei Danshita, and Charles W. Clark. Creating a supersolid in one-dimensional bose mixtures. *Phys. Rev. A*, 79:011602, Jan 2009. doi: 10.1103/PhysRevA.79.011602. URL `http://link.aps.org/doi/10.1103/PhysRevA.79.011602`.

[58] H.J. Metcalf and P. van Straten. *Laser Cooling and Trapping*. Springer, 2002.

[59] K. I. Petsas, A. B. Coates, and G. Grynberg. Crystallography of optical lattices. *Phys. Rev. A*, 50:5173–5189, Dec 1994. doi: 10.1103/PhysRevA.50.5173. URL `http://link.aps.org/doi/10.1103/PhysRevA.50.5173`.

[60] L. P. Pitaevskii. Vortex lines in an imperfect Bose Gas. *Sov. Phys. JETP*, **13**:451, 1961.

[61] L. Pollet, N. V. Prokof'ev, B. V. Svistunov, and M. Troyer. Absence of a direct superfluid to mott insulator transition in disordered bose systems. *Phys. Rev. Lett.*, 103:140402, Sep 2009. doi: 10.1103/PhysRevLett.103.140402. URL `http://link.aps.org/doi/10.1103/PhysRevLett.103.140402`.

[62] Stephen Powell. Magnetic phases and transitions of the two-species bose-hubbard model. *Phys. Rev. A*, 79:053614, May 2009. doi: 10.1103/PhysRevA.79.053614. URL `http://link.aps.org/doi/10.1103/PhysRevA.79.053614`.

[63] Marta Prada, Eva-Maria Richter, and Daniela Pfannkuche. Isospin correlations in two-partite hexagonal optical lattices. *Phys. Rev. A*, 90:013613, Jul 2014. doi: 10.1103/PhysRevA.90.013613. URL `http://link.aps.org/doi/10.1103/PhysRevA.90.013613`.

[64] Nikolay Prokof'ev. Waht makes a crystal supersolid. *Advances in Physics*, 56:381–402.

[65] D. Sorensen C. Yang R. Lehoucq, K. Maschhoff. *Arnoldi Package (ARPACK)*.

[66] John D. Reppy. Nonsuperfluid origin of the nonclassical rotational inertia in a bulk sample of solid ^{4}He. *Phys. Rev. Lett.*, 104: 255301, Jun 2010. doi: 10.1103/PhysRevLett.104.255301. URL `http://link.aps.org/doi/10.1103/PhysRevLett.104.255301`.

[67] Subir Sachdev. Kagome- and triangular-lattice heisenberg antiferromagnets: Ordering from quantum fluctuations and quantum-disordered ground states with unconfined bosonic spinons. *Phys. Rev. B*, 45: 12377–12396, Jun 1992. doi: 10.1103/PhysRevB.45.12377. URL `http://link.aps.org/doi/10.1103/PhysRevB.45.12377`.

[68] Subir Sachdev and Jinwu Ye. Universal quantum-critical dynamics of two-dimensional antiferromagnets. *Phys. Rev. Lett.*, 69: 2411–2414, Oct 1992. doi: 10.1103/PhysRevLett.69.2411. URL `http://link.aps.org/doi/10.1103/PhysRevLett.69.2411`.

[69] Pinaki Sengupta, Leonid P. Pryadko, Fabien Alet, Matthias Troyer, and Guido Schmid. Supersolids versus phase separation in two-dimensional lattice bosons. *Phys. Rev. Lett.*, 94: 207202, May 2005. doi: 10.1103/PhysRevLett.94.207202. URL `http://link.aps.org/doi/10.1103/PhysRevLett.94.207202`.

[70] D.-S.; Struck J. Windpassinger P.; Sengstock K Soltan-Panahi, P; Luehmann. Quantum phase transition to unconventional multi-orbital superfluidity in optical lattices. *Nature Physics*, 8:71–75, 2012.

[71] Struck J.-Hauke P. Bick A. Plenkers W. Meineke G. Becker C. Windpassinger P. Lewenstein M. Soltan-Panahi, P. and K. Sengstock. Multi-component quantum gases in spin-dependent hexagonal lattices. *Nat Phys*, 7:434–440, 2011. doi: http://dx.doi.org/10.1038/nphys1916.

[72] David J. Tannor. *Introduction to Quantum Mechanics*. 2007.

[73] N. Teichmann, D. Hinrichs, and M. Holthaus. Reference data for phase diagrams of triangular and hexagonal bosonic lattices. *EPL (Europhysics Letters)*, 91(1):10004, 2010. URL `http://stacks.iop.org/0295-5075/91/i=1/a=10004`.

[74] L. Tisza. Transport Phenomena in Helium II. , 141:913, May 1938. doi: 10.1038/141913a0.

[75] I. Titvinidze, M. Snoek, and W. Hofstetter. Supersolid bose-fermi mixtures in optical lattices. *Phys. Rev. Lett.*, 100: 100401, Mar 2008. doi: 10.1103/PhysRevLett.100.100401. URL `http://link.aps.org/doi/10.1103/PhysRevLett.100.100401`.

[76] D. van Oosten, P. van der Straten, and H. T. C. Stoof. Quantum phases in an optical lattice. *Phys. Rev. A*, 63(5):053601, Apr 2001. doi: 10.1103/Phys-RevA.63.053601.

[77] Wilhelm Zwerger. Mott–hubbard transition of cold atoms in optical lattices. *Journal of Optics B: Quantum and Semiclassical Optics*, 5(2):S9, 2003. URL `http://stacks.iop.org/1464-4266/5/i=2/a=352`.

Danksagung

An dieser Stelle möchte ich mich ganz herzlich bei allen Personen bedanken, die mich in der Zeit meiner Doktorarbeit unterstützt haben. Vor allem möchte ich Frau Professor Daniela Pfannkuche danken, zuerst einmal für die Möglichkeit, diese Doktorarbeit anfertigen zu können und nicht zuletzt auch für den sicheren Arbeitsplatz in ihrer Arbeitsgruppe. Außerdem danke ich ihr für die ermutigende Betreuung, ihr großes Interesse an meiner Arbeit und das mir, trotz der langwierigen Entstehung der Arbeit, entgegengebrachte Vertrauen.
Ich danke Herrn Professor Michael Potthoff für die Übernahme des Zweitguachtens der Dissertation.
Ich danke auch besonders Herrn Professor Klaus Sengstock für seine Unterstützung und die Übernahme des Zweitgutachtens der Disputation.
Ich danke Dirk Sören Lühmann, der mich, vor allem im ersten Teil meiner Arbeit kompetent betreute. Desweiteren möchte ich besonders Holger Niehus und Marta Prada für ihre Unterstützung und ihr Mitwirken bedanken. Für die Korrekturarbeiten danke ich ebenfalls Marta Prada und vor allem auch Lars-Hendrik Frahm!
Ich danke der gesamten Gruppe für euren Zuspruch und eure Unterstützung, und wünsche Euch alles erdenklich Gute für die weitere Forschung und den Rest des Lebens.
Ich danke meiner ganzen Familie, vor allem Henning, meinen Kinder Merlin Paul und Elisabeth Marie, meinem Vater Wolfgang, meinen Geschwistern Bernadette und Johannes, meinem Opa Helmut, Hildegard und Thomas. Ich danke all meinen Freunden, die mich während dieser Zeit immer unterstützt haben. Außerdem danke ich dem SFB 925, dem GRK 1355, der Landesexzellenzinitiative Hamburg und der Joachim Herz Stiftung für die finanzielle Unterstützung bei der Erstellung meiner Dissertation.